Hydrodynamic behaviour of silica-DNA microparticles in surface water

A systematic laboratory-based understanding of SiDNA(Fe) tracers

Tang, Yuchen

DOI
10.4233/uuid:7c8e98e0-21ab-4f6c-9de3-8acf8d899e88

Publication date
2023

Document Version
Final published version

Citation (APA)
Tang, Y. (2023). *Hydrodynamic behaviour of silica-DNA microparticles in surface water: A systematic laboratory-based understanding of SiDNA(Fe) tracers*. [Dissertation (TU Delft), Delft University of Technology]. https://doi.org/10.4233/uuid:7c8e98e0-21ab-4f6c-9de3-8acf8d899e88

Hydrodynamic behaviour of silica-DNA microparticles in surface water

A systematic laboratory-based understanding of SiDNA(Fe) tracers

Hydrodynamic behaviour of silica-DNA microparticles in surface water

A systematic laboratory-based understanding of SiDNA(Fe) tracers

Proefschrift

ter verkrijging van de graad van doctor
aan de Technische Universiteit Delft,
op gezag van de Rector Magnificus prof. ir. T.H.J.J. van der Hagen,
voorzitter van het College voor Promoties,
in het openbaar te verdedigen op woensdag 8 november 2023 om 10:00 uur

door

Yuchen Tang

Master of Science in Water Environment and Management,
University of Bristol, the United Kingdom,
born in Panzhihua, China.

Dit proefschrift is goedgekeurd door de

Dr. T.A. Bogaard, promoter
Dr. J.W. Foppen, copromotor

Samenstelling promotiecommissie:

Rector Magnificus,	voorzitter
Dr. T.A. Bogaard,	Technische Universiteit Delft
Dr. J.W. Foppen,	Technische Universiteit Delft
Onafhankelijke leden:	
Prof. dr. ir. M.K.de Kreuk,	Technische Universiteit Delft
Prof. dr. S. Krause,	University of Birmingham, UK
Prof. dr. H. Gao,	East China Normal University, China
Dr. ir. C. Chassagne,	Technische Universiteit Delft
Dr. L. Pang,	Institute of Environmental Science and Research, New Zealand

Keywords: Microparticle tracer; River water; Transport behaviour; DNA

Printed by: proefschrift-aio.nl

Front & Back: By Yuchen Tang

ISBN 978-94-6366-767-8

An electronic version of this dissertation is available at
http://repository.tudelft.nl/.

to my family

Contents

Summary

Rivers are vital for maintaining freshwater ecosystems as they distribute nutrients as well as dilute and transport anthropogenic pollution. Tracers provide direct empirical data on complex waterflows and reveal transport processes of waterborne substances. Recent advances in material engineering and biomolecular technology have made it possible to tag material with unique synthetic DNA sequences. Synthetic DNA sequences can be encapsulated or bound to desired material and accurately quantified by quantitative Polymerase Chain Reaction (qPCR). This DNA-tagging technique has enormous potential for river tracing purposes. No systematic research has been conducted and more knowledge is required with regard to the transport behaviour and fate of such DNA-tagged material in surface water hydrology. Therefore, the objective of this research was to understand the transport behaviour of such DNA-tagged materials in river waters, evaluate their applicability as tracers for studying surface water transport processes such as advection and dispersion, and investigate their transient interactions. This dissertation utilized two types of such DNA-tagged microparticles. The first type was non-magnetic silica-encapsulated DNA-tagged microparticles with a silica core (Si-DNA). The second type was superparamagnetic silica-encapsulated DNA-tagged microparticles with a iron oxide core (SiDNAFe). Collectively, these two types were referred to as SiDNA(Fe) throughout this dissertation.

This dissertation first examined the transport behaviour of Si-DNA in laboratory injection experiments without mass loss. The results indicated that Si-DNA was comparable to conventional NaCl tracer behaviour, with similar hydrodynamic dispersion coefficient (D_L) in various surface water qualities.

Potential particle settling due to hetero-aggregation and homo-aggregation has the potential to reduce the transport distance of DNA-tagged microparticles. Therefore, SiDNAFe was tested for settling potential in the presence of natural organic matter and suspended particulate matter in river waters. The similar settling behavior of SiDNAFe observed in different river water qualities, as well as MilliQ water, suggested that SiDNAFe was generally colloidally stable and its hetero-aggregation with suspended particulate matter was negligible in natural river water environments. SiDNAFe settling in quiescent conditions can be adequately mimicked by a first-order decay process, and thus I recommend to include a predefined first-order decay coefficient for transport modelling of SiDNAFe in tracing experiments in natural streams and rivers.

Furthermore, this dissertation investigated the potential mass loss of SiDNAFe in river bed sediment, a well-recognised accumulation hotspot for nano/micro particles in streams and rivers. SiDNAFe mass recoveries exhibited a wide range, varying from 50% to 120 % from sediment-free conditions to fine sediment and to coarse (coated) sediment conditions. Retention of SiDNAFe was 1 - 2 orders of magnitude greater than gravitational settling rates, which might associate with grain-scale hyporheic flows and coupled water-sediment-particle interactions. In small-scale laboratory set-up, SiDNAFe exhibits similar dispersion behaviour as solute NaCl tracers. SiDNAFe can be reliably and reproducibly utilized

in tracing experiments, as evidenced by the complete mass recoveries observed in 6 out of 8 cases. However, caution must be exercised when transitioning from water quality of lower complexity to a more complex water type, as changes in water qualities and sediment characteristics may be coupled to affect the fate of SiDNAFe in streams and river environments.

This dissertation has established a reliable methodology for applying two types of DNA-tagged microparticles, i.e., SiDNA(Fe). Obviously, for potential applications of SiDNA(Fe) in natural steams and rivers, centrifugation and magnetic separation can facilitate easy and quick sample up-concentration, which is prerequisite from large volumes of environmental waters to micro-litre volumes of samples for DNA analysis by qPCR. While SiDNA(Fe) generally shows a comparable dispersion behaviour as to solute tracer NaCl, a pre-defined first-order mass loss term due to gravitational settling and other environmental factors, e.g., particle-sediment interactions, should be considered in advance case by case for transport modelling in streams and rivers. We acknowledge that our results and current protocol are based on laboratory-scale findings, and field trials are warranted to validate the capability of SiDNA(Fe). Moreover, to improve the accuracy of SiDNA(Fe) mass balance accounting, further research is required to assess factors including flow velocity variations, seasonal water hydro-chemical changes, and the impact of anthropogenic pollution.

Preface

As a fresh graduate with a master's degree in 2017, I found myself lost in the direction of my future. Little did I know that a midnight interview (due to the time difference) during my trip to Brisbane, Australia, would alter the course of my life for the next five years, and perhaps even longer. The Netherlands, a country renowned for its tulips, was not even on my itinerary during my travels in Europe. Yet, it entered my life unexpectedly and transformed my trajectory in ways I could never have imagined. Such unpredictable twists and turns, coupled with delightful surprises, are the very essence of the life I strive for.

Just as I had not anticipated pursuing a PhD in the Netherlands, I also had not foreseen the many challenges and obstacles I would face over the course of five years. Fortunately, luck was on my side, and I was blessed with supportive friends, helpful colleagues, encouraging mentors, and most importantly, a life partner. Along this journey, I have encountered beautiful serendipitous moments and emotions that transcend linguistic expressions.

I am exceedingly fortunate to have everything that I possess: a loving partner who stands by me through thick and thin, a healthy and happy family, and a bright future ahead of me, regardless of which path I may take. I am ready to face whatever comes my way, embrace it all, and look forward to what the future holds.

Yuchen Tang
Delft, January 2023

Acknowledgements

I would like to express my deep gratitude to my promoter, Dr. Thom Bogaard, and my co-promoter, Dr. Jan Willem Foppen, for their invaluable support, guidance, and encouragement throughout my PhD journey. Dr. Bogaard, thank you for giving me the opportunity to pursue this PhD position and for your unwavering support and supervision. Your mentorship has been instrumental in shaping my research and personal growth. Dr. Foppen, thank you for your critical feedback, insightful comments, and inspiring research ideas. Your contribution and supervision have helped me push my boundaries and strive for excellence. Once again, I would also like to express my gratitude towards both of them for having faith in my abilities and allowing me to explore my potential during this significant journey. I recognize that my accomplishment would not have been possible without their unwavering support and encouragement.

I would like to express my sincere gratitude to Dr. Sulalit Bandyopadhyay for his invaluable contributions to my research. Dr. Sulalit's work on the production of DNA tracers was indispensable for my research, and his insightful comments and guidance on enhanced my understanding of the engineered particle field. I am also grateful to Dr. Anuvansh Sharma and PhD student Zeeshan Ali for their help in producing the DNA tracers for my experiments.

I would also like to acknowledge the invaluable support of Dr. Ahmed Abdelrady, who patiently answered my queries and provided technical support in the laboratory. My heartfelt thanks go to my PhD colleagues, Swagatam Chakraborty and Bahareh Kianfar, for their teamwork and camaraderie in the WaterTagging group. I would like to express my gratitude to WaterTagging lab technician Bright Namata, who provided invaluable assistance during the pandemic period in the qPCR lab. During my PhD research, I have been working in two separate labs - the IHE lab and the TUD lab. This has necessitated frequent travel between the two locations and has required me to carefully coordinate my schedule with the operational hours of both labs. I would also like to thank lab technicians Armand Middeldorp at TUD WaterLab, and Peter Heerings, Ferdi Battes, Berend Lolkema, and Zina Al Saffar at IHE lab for their support and assistance. I appreciate their ability to bring a sense of enjoyment and resilience to the laboratory when faced with difficult situations.

I would like to thank my Master's student, Fay van Rijh and Fengbo Zhang and for their camaraderie and collaboration in experiments. I learned a great deal from them, and I am grateful for the opportunity to work with them. I would also like to thank my colleagues, also my dear friends, Dengxiao Lang, Shuo Zhang, Dr. Xin Tian, Dr. Zhengwu Wang, Dr. Mingyan Fu, Dr. Xueqin Chen, Qin Ou, and Yanghui Xu for their encouragement, support, and camaraderie during this journey.

My gratitude extends to my beloved husband, who has been my unwavering source of emotional support, encouragement, and love. His selfless sacrifice to resign from his job and accompany me to the Netherlands during this journey is immeasurable. I cannot thank him enough for being my solid rock, especially during the challenging times.

Finally, I would like to express my heartfelt appreciation to my parents, whose unwavering support and encouragement made it possible for me to pursue my research career. I am grateful for their love, guidance, and unwavering belief in me. Thank you all for your unwavering support, encouragement, and friendship. Your contributions have made this journey unforgettable, and I am grateful for everything.

致谢

我想对我的导师，Thom Bogaard博士，以及我的共同指导老师，Jan Willem Foppen博士，表示深深的感谢，感谢他们在我博士研究期间所给予的宝贵支持、指导和鼓励。Bogaard博士，感谢您给我这个攻读博士的机会，以及您坚定不移的支持和监督。您的指导对于塑造我的研究和个人成长起到了关键的作用。Foppen博士，感谢您的批判性反馈、有见地的评论和鼓舞人心的研究想法。您的贡献和指导帮助我突破了自己的界限，追求卓越。我想对Sulalit Bandyopadhyay博士表示衷心的感谢。Sulalit博士在DNA追踪剂的制造对我的研究起到至关重要的作用。我也感谢Anuvansh Sharma博士和博士生 Zeeshan Ali在我的实验中帮助制造DNA追踪剂。我还想感谢Ahmed Abdelrady博士，在实验室对我的指导和帮助。我想感谢我的硕士学生，Fay van Rijh和张丰博，感谢他们的友情和实验合作。我从他们那里学到了很多，我很感激有机会和他们一起做实验。

由于我的研究需要，我需要在两个实验室工作——IHE实验室和TUD实验室，甚至疫情期间的第三个实验基地，TUD植物园。因此，我频繁地在此之间来回辗转，并且仔细协调时间安排，以配合实验室的工作时间。这样的辗转使得我在疫情期间的工作更加困难。在此，我想向WaterTagging的同事Swagatam Chakraborty和Bahareh Kianfar和实验室技术员Bright Namata表示感谢。我还要感谢TUD WaterLab的实验室技术员Armand Middeldorp，以及IHE实验室的Peter Heerings, Ferdi Battes, Berend Lolkema和Zina Al Saffar，感谢他们的支持和帮助。

我还想感谢我的同事，也是我亲爱的朋友，郎登潇, 张硕, 田欣博士, 王正午博士, 付明岩博士，陈学勤博士，欧芹，徐仰辉。感谢他们在这段旅程中的鼓励、支持和友谊。我们的周末娱乐活动对于排解疫情带来的困难、寂寞和思乡情绪起到了至关重要的作用。特别是在疫情期间以及疫情后的种种，让我意识到我们俨然已经相处成为在荷兰的家人。

我要感谢我亲爱的丈夫，杨博雄先生，他一直是我情感上的支柱，给予我持续的支持、鼓励和爱。他为了陪伴我，毅然辞职北京的工作来到荷兰攻读硕士并留在荷兰工作。在无数个为了实验而痛苦的日夜，他一直是我坚强的后盾。认识他伊始到现在我们已经结婚快一年，我们一起携手走过了我的整个博士生涯。我希望我们未来的生活也能如同过去以及现在一样甜蜜如初、情比金坚。正因为有了杨博雄先生的余生陪伴，我才相信我有勇气和信念迎接任何未来的挑战。谢谢你，杨先生。

最后，我想向我的父母和外婆表示由衷的感谢，是你们坚定不移的支持和爱护，使我得以快乐成长，无忧无虑，并追求我想追求的生活和事业。我想感谢我的父亲，是他对于我的鼓励和情感支持，让我得以不容怀疑地开始我的博士生涯。也感谢他在我成长道路上每一个至关重要的关头都能给予我指导和帮助。我想感谢我的母亲，是她对我无限的关爱和无私地照顾，让我能寻找自己，相信自己，并突破自我。我感激你们的爱、指导和对我坚定不移的信念。

感谢大家的坚定支持、鼓励和友谊。你们的贡献使这段旅程难以忘怀，我为此感激不尽。

1

Introduction

1

Rivers are a vital component of Earth's freshwater resources, serving as a complex network of "blood vessels" that facilitate the transfer and exchange of nutrients between terrestrial and marine ecosystems. Rivers are not only integrators of evolving geological and ecological processes, but also bear the imprint of human activities, which has led to an increasing role for rivers in the transport of anthropogenic contaminants from fluvial habitats to marine environments. These contaminants include pesticides, medicines, personal care products, and plastics, with waste water treatment plants estimated to discharge up to 520,000 tons per year of microplastics to rivers in Europe (Horton et al., 2017; Frei et al., 2019). To assess the impact of human activity on fluvial ecosystems and plan for their restoration, a thorough understanding of mass transport in rivers is crucial, particularly regarding dissolved and/or particulate contaminants. However, characterizing mass transport processes in rivers is a challenging task due to their spatiotemporal heterogeneity and multiscale interactions between flowing water and waterborne substances. Tracer methods that combine observation and modeling represent an effective approach for hydrologists to decipher the riverine mass transport puzzle.

1.1. Tracers and tracer tests

Tracers play a crucial role in hydrology as they allow for the detection and tracing of water flows. They serve as proxies for phenomena of interest that are not easily observable due to inaccessibility or long timescales. Initially, tracers such as wooden balls, salts, urine, and bacteria were used to locate underground waterways and spring sources (Werner, 1998). Tracers and tracing technology have advanced tremendously over decades, as was seen in a proliferation of hydrological and biogeochemical studies using tracers. In these studies, tracers are generally divided into two categories: environmental tracers which are naturally occurring, and artificial tracers which are introduced for experimental purposes (Leibundgut et al., 2009). Isotopic tracers, such as the stable isotopes of water (18O/16O and 2H/1H), are considered ideal tracers for water because they are water itself (Becker and Coplen, 2001). Environmental tracers are commonly used to understand physical mixing processes of large timescales in hydrological systems, such as river basin flushing time, residence time estimation, and water balance (Michel, 2005). In contrast, artificial tracers, such as chemical tracers (e.g., fluorescent dyes & salts), and micro-size particles, are typically used to obtain detailed information at a local temporospatial scale, such as river discharge, velocity, direction, mean residence time, and transport behaviour. These tracers are preferred because they are cost-effective, easy to handle, and sensitive. The use of tracers has thus enabled hydrologists to reveal how waterborne substances behave in various hydrological and geographical environments, including groundwater aquifers, karst water, polluted rivers and streams, and coastal sewage dispersion.

Tracer tests are a commonly used method to investigate mass transport processes in streams and rivers. Usually, tracers are injected at an upstream location, and their movement is monitored at one or more downstream sites. The data collected from these observations is represented by the concentration-time history of the tracers, known as the breakthrough curve (BTC). The BTC provides valuable insights into the transport mechanisms, such as advection and dispersion, which can be used to estimate mass transport-related parameters. These parameters can be estimated by fitting the observed BTC with appropriate models. For example, in a deterministic transport model, the governing advection and dispersion

equation is as follows:

$$\frac{\partial C}{\partial t} = -u\frac{\partial C}{\partial t} + D\frac{\partial^2 C}{\partial x^2} \tag{1.1}$$

Where C is the solute concentration [g/m^3], t the time [s], u the mean flow velocity [m/s], x the distance [m], and D_L the dispersion coefficient [m^2/s]. On the right-hand site, the first term accounts for the majority of the mass transported by the mean velocity, known as the advection transport, whereas the second term represents the mixing of mass due to velocity variations in water flows, known as the mass dispersion.

This advection-dispersion equation (ADE) provides a theoretical framework for understanding the transport of solute tracers in hydrogeological systems. However, the ADE is limited to the assumption of ideal mass transport, neglecting sources and sinks of tracer mass in the system. Furthermore, the BTCs observed in the field often exhibit pronounced tailing behaviour, which cannot be fully explained by the ADE alone. This tailing effect is primarily caused by the accumulation of tracer mass in stagnant areas where water flows at a slower rate than the main stream. To address these limitations, the Transient Storage Model (TSM) was introduced, which includes a first-order transient exchange term accounting for mass exchange between fast-flowing mainstream and slow-flowing or stagnant storage zones (Workshop, 1990). Although the TSM approach can be appropriate for hydrological systems that have a single storage zone with an exponential frequency distribution of residence time, in some other cases, multiple storage zones should be considered (Choi et al., 2000), or non-exponential residence time distributions should be used to provide more accurate predictions that are consistent with experimental data (Haggerty et al., 2002; Wörman et al., 2002).

To accurately model tracer BTCs, it is crucial to consider a comprehensive subset of interactions, prioritizing those most influential in the context of the specific system under investigation. Consequently, incorporating the most relevant interactions into the governing equations becomes imperative to interpret modeling results effectively and to achieve a balance between model complexity and feasibility.

Dissolved salts are commonly used in benchmarking studies as conservative tracers to evaluate newly introduced tracers. However, it is important to note that dissolved salts with different molecular diffusion coefficients may behave differently under certain conditions, such as low flow rates in porous media where molecular diffusion predominates. For instance, higher diffusion coefficients can result in lower peak concentration and mass recovery due to more diffusive mass exchange into the immobile zone (Knorr et al., 2016). Fluorescent dyes, such as Rhodamine WT, have been reported to sorb onto various surfaces, including suspended sediments, porous media, biofilms, and detritus, with sorption increasing with increasing organic matter content (Smart and Laidlaw, 1977). Mass recovery checks and conjecturing with conservative salts are frequently employed to examine the behaviour of fluorescent dyes in hydrodynamics investigations of rivers and streams. When advection dominates, fluorescent dyes show conservative transport characteristics with high mass recovery (Stern et al., 2001; Cox et al., 2003), due to their limited interactions with the solid surface of the streambed. However, in conditions where substantial mass loss of the dye occurs in wetlands, accurate estimates of travel times and hydraulic parameters can still been obtained, as these determinations are largely based on parts of the BTC preceding the tail (i.e., the bulk of the tracer mass) (Runkel, 2015). This portion of the tracer has been

transported by the main advective flow, and is thus less affected by sorption. Therefore, travel-time and other quantities based on the bulk of the tracer mass may be less sensitive to mass loss than parameters based on the tracer tail.

In the case of particle tracers, such as fluorescent microspheres, the discrete nature of these tracers may lead to discrepancies in transport behaviour from solute tracers. While micro-size particles are found to mostly travel no later than or faster than dissolved salts in surface fast-flowing environments and in groundwater of porous media, they often have lower mass recoveries than solute tracers due to aggregation, sedimentation, and transient interactions with the bed metrics (e.g., deposition and resuspension) (J. Drummond et al., 2014). Once particles enter the hyporheic zone, they tend to penetrate less deep and are retained more compared to conservative solute tracers (Harvey et al., 2012).

In order to accurately characterize transient storage and hyporheic exchange, it is essential to account for mass loss in the governing equations. To achieve this, extended terms such as retardation factor (Haggerty et al., 2002), first-order decay and dilution factors (Gooseff et al., 2003), and mass loss factors (Gooseff et al., 2007) can be used. However, it is important to note that storage exchange occurring over time or length scales longer than that of the tracer test may not be properly represented (Harvey et al., 1996). From a practical standpoint, the detection limit of a conventional tracer is a critical limitation when characterizing flows returning from the hyporheic exchange to the stream. In particular, small fluxes of hyporheic water returning to the channel after most of the tracer mass has passed may not provide enough signals to be observed (Bencala et al., 2011).

1.2. DNA-based tracing framework

Despite the tremendous development of artificial tracers, our knowledge of riverine environments is limited by the inadequate spatial coverage of available tracer tools. This limitation hinders the sensitive quantification of temporal-spatial exchange dynamics. To address this issue, more sensitive and versatile tracer methods are required to quantify heterogeneous mass transport dynamics in streams and rivers, such as the quantification of multi-scales of surface storage zones and hyporheic transient storage. In addition, studies requiring multi-tracing experiments, such as river pollution source tracking, can greatly benefit from an easy-to-handle and quantitatively accurate tracing technique. While not imperative, employing tracers that are bio-physio-chemically identical could furnish additional benefits by ensuring experimental consistency, although they must remain distinguishable from each other and the environment throughout the experiment.

Synthetic DNA tracers have the potential to fill the gap. The DNA strands are designed in short lengths, with single-stranded (ssDNA) or double-stranded (dsDNA) molecules ranging from $\sim$ 50 - 500 bases or base pairs, respectively (Foppen, 2023). To ensure specificity, DNA sequences are screened with gene screening software (i.e., BLAST) to avoid any genetic background DNA in the environment (Liao et al., 2018). Quantification of DNA templates is achieved by targeting the DNA with specially designed primers and exponentially amplifying the DNA replicates through a series of thermal cycles until a sufficient number of DNA molecules are reached, using the quantitative Polymerase Chain Reaction (qPCR) technique (Watson et al., 1992). The working principle of the technique involves denaturation of the DNA template by heating, followed by annealing of primers that are specific to the target DNA sequence, and then then extension where a new DNA strand

is synthesised in the reaction. The fluorescent dyes or probes which are introduced in the reaction emit fluorescence in the presence of amplified DNA, enabling real-time tracking of the DNA amplification process. The emitted fluorescence is directly proportional to the quantity of the target DNA present in the reaction, providing a quantitative measure of DNA's initial concentration. The qPCR technique theoretically allows the amplification of as few as one DNA molecule per reaction well, increasing the detection limit down to μg/mL in a quantitative manner. This makes synthetic DNA strands a prominent tagging agent for tracing virtually any material.

Since Mahler and co-workers first used DNA-labeled clay particles for sediment tracing (Mahler et al., 1998), the use of DNA-based tracers for hydrology studies has flourished. Depending on the experimental conditions, DNA tracers can be used as naked DNA molecules or DNA-tagged microparticles. Studies using naked DNA tracers typically use ssDNA (see the detailed comparison in Foppen (2023)), as dsDNA synthesis with the same length costs twice as much as ssDNA, despite its greater chemical and structural stability (Lindahl, 1993). In surface water environments, naked DNA tracers were reported to travel similarly or faster (e.g., McCluskey et al. (2021)) than conventional chemical solute tracers in sharp pulses. A plausible explanation for these earlier and sharper BTCs, as provided by experimental authors, is that naked DNA tracers selectively engaging with fewer, and predominantly wider, flow paths, which naturally sustain swifter fluid flow velocities. However, it's noteworthy that the use of naked DNA tracers often results in much lower mass recoveries, as reported in various studies (Foppen et al., 2011; Foppen et al., 2013; Dahlke et al., 2015; Pang et al., 2020). Lower mass recoveries of free DNA tracers also applied to cases in porous media (Pang et al., 2017; Pang et al., 2020; McCluskey et al., 2021; Y. Zhang et al., 2021), except the one in Aquilanti et al. (2013). Such naked DNA tracers were concluded to be suitable for flowpath investigations, particularly in karst systems and fissured rocks, providing qualitative presence/absence data for previously unknown interwell connections (Aquilanti et al., 2013; Aquilanti et al., 2016). However, naked DNA tracers are subject to adsorption/attachment to mineral surfaces, degradation due to pH and elevated temperatures, and microbial consumption (Sabir et al., 2000; Foppen et al., 2013; Pang et al., 2017). These intrinsic physio-chemical properties of naked DNA tracers make them more suitable to be used in clean water, e.g., glacial water (Dahlke et al., 2015; Liao et al., 2018). In complex water or environments, e.g., high concentrations of catabolic enzymes, acidic pH levels, ultraviolet radiation, and abundant microorganism activity, naked DNA tracers are too fragile to survive long enough or travel long enough (the highest tracing record is 1 km) for a standard field tracing experiment, evident by low mass recoveries (Foppen et al., 2011; Foppen et al., 2013; McCluskey et al., 2021; Pang et al., 2020; C. Wang et al., 2022).

DNA-tagged microparticles, an innovative advancement in DNA-based tracing frameworks for stream and river tracing, hold significant promise. To ensure the resilience of tracers against complex biophysiochemical conditions they may encounter, the incorporation of a protective shell becomes imperative. Currently, six types of DNA-tagged microparticles were used for hydrological investigations. These include: 1) a silica core, surrounded by a layer of DNA, and protected by an outer cover of silica (Paunescu et al., 2013; Mikutis et al., 2018); 2) a few superparamagnetic iron cores bounded by a layer of DNA and protected by an outer silica cover; 3) a core of iron oxide nanoparticle combined with DNA and encapsulated by polylactic acid (A. N. Sharma et al., 2012; Dahlke et al., 2015; McNew et al.,

2018); 4) mixture of DNA with chitosan with an alginate cover (Pang et al., 2020); 5) a core of superparamagnetic iron and plasmid DNA, encapsulated by poly lactic-co-glycolic acid (Liao et al., 2020); and 6) condensed DNA stabilized by a self-assembling system consisting of poly-amidoamine, a cationic homopolymer, and a PEG-PAA-PEG copolymer (Garnett et al., 2009). Notably, incorporating iron cores offers the advantage of magnetic separation and enables up-concentration, making them suitable for applications involving larger water volumes (Puddu et al., 2014; A. Sharma et al., 2021). Foppen (2023) gave a more detailed summary on these six types of DNA-tagged microparticles for hydrological applications.

Compared to naked DNA tracers, DNA-tagged microparticles are much larger (typically in 100 – 1000 nm) and either lighter or denser than water depending on the carrier's density (e.g., SiO_2 > 1 (Paunescu et al., 2013), polylactic acid < 1 (Liao et al., 2020). As their finite size falls within the size spectrum of colloids, their behaviour in aquatic environments is primarily determined by the microparticles (Pang et al., 2020). Field applications have shown that DNA-tagged microparticles are detectable for a further 5 hours after the main flow peak has passed (Garnett et al., 2009) and survive significantly longer with less mass reduction than naked DNA tracers (Pang et al., 2020), though mass recoveries vary depending on field conditions (A. N. Sharma et al., 2012; Dahlke et al., 2015; Mikutis et al., 2018; Pang et al., 2020).

A mass balance is necessary to account for possible sinks of DNA-tagged microparticles and understand their behaviour and fate in large-scale environmental applications. A few possible reasons for mass losses were listed in the literature, e.g., adsorption to sediment and clay particles (Dahlke et al., 2015; Pang et al., 2020), instantaneous losses or unprecised DNA detection which was caused by divalent cation bridging effect with natural organic matter (NOM) (Foppen et al., 2013; Liao et al., 2018; Pang et al., 2022; Foppen, 2023; poor design of injection and sampling schemes (A. N. Sharma et al., 2012), improper sample storage resulting in biofilm growth which engulfs particles (Mikutis et al., 2018). DNA-tagged microparticles may undergo physical and/or chemical reactions such as aggregation, adsorption, sedimentation, redox reactions, dissolution, speciation, and bio-transformation when they coexist with bio- and geo-colloids and suspended particulates in river water environments (Petosa et al., 2010; Shevlin et al., 2018). Hetero-aggregation is an aggregation process between particles of different types. Hetero-aggregation with natural colloids and suspended sediment is the main reason for rapid settling and sedimentation of engineered nanomaterials in natural waters (Quik et al., 2012; Velzeboer et al., 2014). Additionally, this may alter the surface properties of DNA-tagged microparticles and affect downstream sample processing, particularly qPCR quantification (e.g., in the case of the aforementioned cation bridging effect with NOM).

Finally, up-concentration of DNA-tagged microparticles is essential for DNA quantification in large-scale tracing experiments. The up-concentration protocol and sample processing protocol must be well-designed and verified to be workable without compromising the accuracy of DNA quantification.

1.3. Research Questions

The overarching research question is: "Can we use DNA-tagged microparticle as a hydrological tracer for mass tracing in river systems?" Hereto the following sub-questions need to be addressed:

"1) How to optimise the experimental protocol, including sampling schemes, sample storage and sample analysis?" The effect of river substances on qPCR efficiency is uncertain. This holds both for free particulates and heteroaggregated to SiDNA(Fe). This is especially relevant as qPCR analysis of DNA to quantify tracer mass requires several pre-treatment steps.

Additionally, a second important sub-question is: "2) Which environmental factors cause their mass loss in natural surface water conditions and what is the expected magnitude?" Furthermore, if the mass loss is inevitable, how would this mass loss affect the determination of hydrodynamical parameters of advection and dispersion?

1.4. Research Objective and Outline

This dissertation utilized two types of such DNA-tagged microparticles. The first type was non-magnetic silica-encapsulated DNA-tagged microparticles with a silica core, referred to as Si-DNA. The second type was superparamagnetic silica-encapsulated DNA-tagged microparticles with an iron oxide core, referred to as SiDNAFe. Collectively, these two types were referred to as SiDNA(Fe) throughout this dissertation.

Therefore, the objective of this research was to understand the transport behaviour of SiDNA(Fe) in river waters, evaluate their applicability as tracers for studying surface water transport processes such as advection and dispersion, and investigate their transient interactions. The rest of this dissertation is organized as follows:

Chapter 2 outlines the development of a reliable workflow for sample pre-treatment, including sample-taking, sample up-concentration, and sample analysing of SiDNA(Fe).

Chapter 3 compares the hydrodynamic dispersion behaviour of Si-DNA with that of a solute tracer NaCl in controlled open channel injection experiments with no mass loss. A series of open channel injection experiments were conducted in six different, environmentally representative water types to obtain tracer BTCs. Hereafter, the BTCs were simulated using a 1-D advection-dispersion model with one transient storage zone (OTIS) by calibrating the hydrodynamic dispersion coefficient D_L and a storage zone exchange rate coefficient α.

Chapter 4 presents the settling and aggregation behaviour of SiDNAFe in three river waters. Thirty-hour quiescent settling experiments of SiDNAFe were conducted with the presence and absence of various particulate matter in river waters, as well as in MiiliQ water (MQ), to evaluate the aggregation and settling potential of SiDNAFe. The assessment of the aggregation and settling potential of SiDNAFe in river waters is a prerequisite for modeling SiDNAFe in future large-scale field tracing applications.

Chapter 5 builds on the previous chapters and further evaluates the effect of bed characteristics on the transport behaviour and especially the mass loss of SiDNAFe in open channel injection experiments. Four channel bed conditions were selected: no sediment, fine river sediment, coarse sand, and goethite-coated coarse sand, with two water qualities: tap water and Meuse river water. Following the conclusion of Chapter 4, which is that the settling could be described as an exponential decay process, the mass loss was accounted for as a first-order process.

Chapter 6 summarizes the contributions of this dissertation in river water application of SiDNA(Fe). Limitations and potential future research and applications of DNA-tagged microparticles in surface water tracing are discussed and highlighted.

2

Sample processing and analysis

2

This chapter presents sample processing and analysis protocols that were used in this PhD study, focusing on the development of sample washing and up-concentration techniques prior to DNA analysis.

The quantification of DNA concentrations in surface water samples using qPCR analysis presents challenges primarily due to the presence of natural inhibitors, such as humic and fulvic acid, polysaccharides, bacterial debris, metal ions, and nucleases (Gibson et al., 2012; I. G. Wilson, 1997). Humic substances, in particular, are widely recognized as the main inhibitors affecting PCR application in environmental samples (I. G. Wilson, 1997; Rådström et al., 2004). Preliminary tests conducted also confirmed the severe inhibition and occurrence of false negatives when directly assaying river water samples, hindering further meaningful data evaluation. Consequently, it becomes crucial to address the inhibitory effects encountered when working with surface water samples abundant in humic substances. Various mechanisms can be employed to mitigate inhibition, including improving sample concentrations (e.g.,Gibson et al., 2012), utilizing filtration resins to remove inhibitors (e.g., Schriewer et al., 2011), incorporating PCR facilitators to bind inhibitory substances (e.g., Pang et al., 2020), and diluting the effect of inhibitors (e.g., Gibson et al., 2012; Foppen et al., 2013).

Furthermore, once DNA-tagged microparticles are released into large volumes of surface water bodies for tracing experiments, they would undergo significant dilution, resulting in extremely low DNA concentrations. Field tracing experiments often require hundreds of millilitre or a litre of volume to be sampled. Despite the theoretical capability of qPCR to quantify DNA molecules through multiple amplification rounds, the low DNA concentration becomes highly susceptible to error propagation during practical operations, from sample collection to the final qPCR assay. Therefore, achieving up-concentration of DNA-tagged microparticles in river waters becomes vital for obtaining robust and reliable quantification outcomes, facilitating meaningful data evaluation. This up-concentration process involves the separation of DNA-tagged microparticles from the aqueous media, followed by re-suspension in a smaller volume of the desired fluid.

Hence, in this dissertation, we have designed and implemented sample washing and up-concentration techniques as crucial pre-qPCR sample processing steps to ensure robust and reliable quantification outcomes for meaningful data evaluation. The subsequent sections will delve into the detailed methodologies and procedures employed, providing a comprehensive understanding of the sample analysis process for DNA-tagged microparticles in this dissertation.

2.1. SiDNA(Fe) and DNA analysis

As mentioned in Chapter 1, this dissertation utilized two types of DNA-tagged microparticles. The first type was non-magnetic silica-encapsulated DNA-tagged microparticles with a silica core, referred to as Si-DNA, which were the same as those used in a study conducted by Mikutis et al. (2018) and provided by ETH Zurich. The second type was superparamagnetic silica-encapsulated DNA-tagged microparticles, referred to as SiDNAFe, which were prepared by the Norwegian University of Science and Technology in Trondheim, Norway. Collectively, these two types are referred to as SiDNA(Fe) throughout this dissertation. Table 2.1 shows the features of the given two types of DNA-tagged microparticles (i.e., SiDNA(Fe)). The surface of SiDNA(Fe) reflects SiO_2 properties, and no interference with

Table 2.1: Features of SiDNA(Fe) used in this PhD dissertation.

	Hydrodynamic diameter [nm]	PDI [-]	Zeta Potential [mV]	Detection limit [mg/mL]
Si-DNA	200 - 300	0.1 - 0.2	-38	1e-08
SiDNAFe	400 - 500	0.3 - 0.4	-24	1e-06

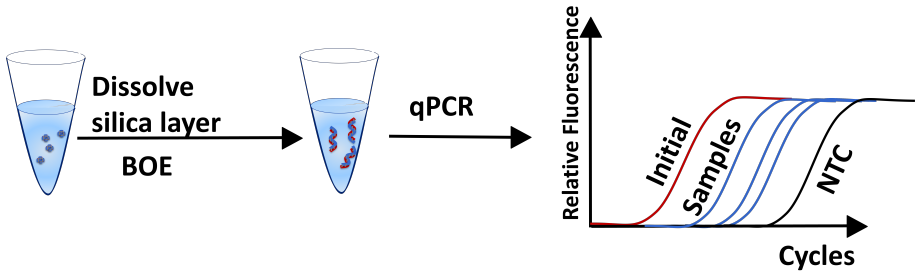

Figure 2.1: Schematic figure of the DNA analysis.

DNA chemistry is expected (Paunescu et al., 2013; Puddu et al., 2014). The synthesized Si-DNA microparticles are spherical in shape with a narrow and unimodal size distribution. The synthesis of SiDNAFe was described in detail by A. Sharma et al. (2021). In brief, SiDNAFe is synthesized by silica encapsulation of iron oxide nano-particles which have been previously bound to dsDNA. The nucleotide sequence of the dsDNA and primer sequences are provided in the Appendix A.

As shown in Fig. 2.1, to quantify SiDNA(Fe), dsDNA was released by dissolving the protective silica shell followed by DNA quantification using qPCR. Firstly, the silica shell of SiDNA(Fe) was dissolved by a buffered oxide etch solution (BOE, 2.3 g of NH_4FHF (Sigma Aldrich) and 1.9 g of NH_4F (J.T.Baker)). After pH adjusted with 0.1 M Tris-HCl, 5 μL of sample mixture was added to 15 μL PCR mix which consisted of 10 μL SYBR green master mix (KAPA SYBR FAST qPCR MasterMix (2X) Universal, Kapa Biosystem), 1 μL 10 μM Forward Primer, 1 μL 10 μM Reverse Primer (Biolegio B.V, Nijmegen, the Netherlands), and 3 μL qPCR water. For contamination control and to avoid manual pipetting errors, all mixing was carried out by a QIAgility high-precision automated PCR setup (QIAgility System HEPA/UV, Cat No. /ID: 9001532).

The released and intact dsDNA was quantified using qPCR on a Bio-Rad CFX96 Touch System (96 wells), whereby the amplification of dsDNA was initiated by one-time heating at 95 °C for 6 min and 40 s and followed by 42 cycles of a three-step thermal profile (20 s at 95 °C, 40 s at 58 °C, 35 s at 72 °C).

2.2. Standard Curves and Mass Calculation

The qPCR technique relies on the detection of fluorescent amplicon label intensity, which is directly proportional to the DNA concentration, assuming similar amplification efficiencies across all samples, thereby enabling comparison of DNA concentrations across different samples (S. Zhao and Fernald, 2005). To ensure that comparisons are accurate, it is crucial to set the same threshold fluorescence level for all samples. This allows for the measurement of the number of amplification cycles (Cq) by identifying the crossing point at the same fluorescence level. In this dissertation, we use the algorithm developed by S. Zhao and Fernald (2005) to determine Cq, which was also employed by Foppen et al. (2013) in an earlier research on the application of naked DNA in stream tracer injection experiments.

To quantify the concentrations of SiDNA(Fe), Cq values were converted from a logarithmic scale to a linear scale (mg/mL) based on 10-fold dilution curves (i.e., the standard curves) of SiDNA(Fe), which ranged in concentrations from 0.01 mg/mL to 0.000001 ng/mL in MQ. For each qPCR run, a standard curve in MQ was included in duplicate to extrapolate sample concentrations in the same assay. The mass conversion equation used for this purpose was:

$$C_m = 10^{(\frac{Cq - int}{slope})} \tag{2.1}$$

Where C_m (mg/mL) represents the mass concentration of samples, Cq is the threshold cycle, int and $slope$ are the intercept and slope of the log-transformed standard curve.

However, this logarithmic-to-linear conversion would magnify small variations in Cq values. For example, a mere 0.2 difference in Cq values between replicates could result in a concentration difference of ~ 15% (calculated as $2^{0.2}$). Such variations in Cq values are inherent to qPCR and can arise from factors like pipetting errors, intrinsic variances of enzymatic efficiency due to minor temperature difference in the qPCR apparatus (Foppen et al., 2013), and/or variations in water quality (Gibson et al., 2012; Zipper et al., 2003).

Furthermore, subsampling is required when transferring millilitre-sized samples into microlitre-size for qPCR analysis (i.e., 20 μL by manual pipetting in our protocol). During subsampling, it is essential to ensure that the subsample contains a sufficient number of particles to minimize statistically significant variations (Crowe et al., 2011). In the case of diluted SiDNA(Fe) samples, even a slight difference of a few particles between two samples can lead to a particle concentration difference of up to 20%, resulting in variations in the qPCR signals observed in subsamples and replicates during the qPCR assay (Kittilä et al., 2019).

In this dissertation, the SiDNA(Fe) mass recovery in an injection experiment was calculated by numerical integration according to Eq. A.1 in the Appendix A. However, attention should be paid to potential errors induced from numerical integration of concentration BTC based on discrete samples using Eq. A.1. To do so, in the injection experiments conducted in this dissertation, discharge between samples was collected. This allowed the determination of the SiDNA(Fe) mass at those intermediate time intervals and subseuqnetly compare the numerical integrated mass calculation with the one derived from the sum of mass obtained from the discrete samples and discharge samples. The averaged difference between these two methods was found to be less than 5%. In practice, especially in stream or river tracing experiments, it's unfeasible to collect data on all discharges between samples due to logisti-

cal constraints. Given this consideration, I made a deliberate choice to maintain consistency in my approach by relying on the numerical integration method to calculate SiDNA(Fe) mass recovery.

Considering these factors, a mass variation of 20% was anticipated and accepted in this dissertation based on the variations observed in Cq values.

2.3. Centrifugation protocol development for Si-DNA

Centrifugation is the easiest and most straightforward method to up-concentrate Si-DNA. However, extensive testing of the original Paunescu et al. (2013) centrifugation protocol for washing samples revealed a substantial number of particles remained in the supernatant. Thus, optimizing the centrifugation protocol for Si-DNA is crucial to ensure no mass loss of Si-DNA during sample washing and up-concentration. In a general centrifugation protocol, particles are first spun down under a specific centrifugal force and duration. The fluid above the particles or pellet, referred to as supernatant, is then removed by careful pipetting, and a desired volume of intended fluid is added to resuspend the pellets. When designing a centrifugation protocol for Si-DNA microparticles, the centrifuge force and duration are the primary considerations.

2.3.1. Centrifuge force and duration

In this dissertation, a High Speed Table Centrifuge Machine (Z36HK, rotor No. 221.23 V01, HERMLE Labortechnik GmbH) was employed to develop the centrifugation protocol. This particular machine has the capability to apply centrifugal forces of up to 65,000 g, offering a wide range of possibilities for experimentation. The simplified centrifugation process used in this study is illustrated in Fig. 2.2.

For a successful centrifugation, particles should settle under a certain centrifuge force until it reaches the bottom of the tube before the centrifuge duration ends. To estimate the least duration required for particles to settle, settling velocity of particles can be calculated by the Stokes's law:

$$v_s = \frac{\rho_p - \rho_f}{\mu} \frac{g_R d^2}{18} \tag{2.2}$$

Where v_s [m/s] is the settling velocity, ρ_p and ρ_f the density of the particles and the fluid [kg/m^3], respectively, μ the dynamic viscosity of the fluid [kg/(m·s)], g_R the acceleration generated by the relative centrifuge force (RCF) [m/s^2], and d the particle diameter [m]. Subsequently, the centrifuge duration can be calculated:

$$t_c = \frac{l_t}{v_s} \tag{2.3}$$

Where t_c is the centrifuge duration [s], l_t the tube length [m].

To design the appropriate RCF and centrifuge duration for the Si-DNA used in this dissertation, calculations were performed as a guideline. The mean diameter of the Si-DNA ranged from 140 to 260 nm, and to ensure that all particles were effectively spun down, the duration required for the smallest particle must be considered. For the smallest particles, the calculated duration was approximately 8 minutes under a 5,000 g RCF. Ideally,

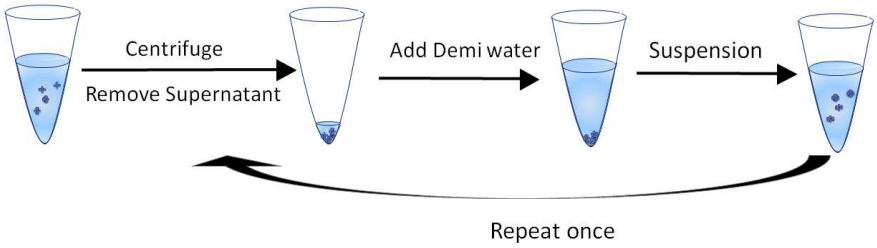

Figure 2.2: Schematic figure of the centrifugation protocol.

each centrifuge force should correspond to a specific duration to achieve optimal particle separation. However, in practice, the duration often exceeds the theoretical calculation. In our centrifugation tests, the duration used was at least two times longer than the estimated duration. To compare the effects of different centrifuge forces and durations, we tested a full range of forces from 5,000 g up to 65,000 g. This wide range of forces allowed us to determine the most suitable force and duration for Si-DNA.

2.3.2. Separation efficiency and mass balance

In evaluating the effectiveness of a centrifugation protocol, the separation efficiency is a crucial metric. By defining the separation efficiency, it is possible to assess the overall performance of the centrifugation protocol. This efficiency is determined by calculating the percentage mass recovery, which is the ratio of the recovered Si-DNA mass to the initial input mass:

$$S_E = \frac{M_a}{M_0} = \frac{C_{mixa} \times V_{mixa}}{C_{mix0} \times V_{mixa0}} \tag{2.4}$$

Where M_a, C_{mixa}, and V_{mixa} are the recovered Si-DNA mass[mg], the recovered Si-DNA concentration of the re-dispersed suspension in the test tube [mg], and the volume of the suspension in the tube [mL], respectively; M_0, C_{mix0}, and V_{mix0} the initial Si-DNA mass (mg), the initial Si-DNA concentration of the test suspension in the tube [mg/mL], and the volume of the initial test suspension [mL], respectively.

The overall mass balance of every test was determined and used to rule out any test with the recovered mass less than 80 % due to improper suspension or pipetting operations. Two times of centrifugation (i.e., spinning down the particle, removing the supernatant, adding Demi, and re-suspending the pellets) were performed for one combination of RCF and duration. Mass balance is expressed as:

$$M_B = \frac{C_{mixa} \times V_{mixa} + C_{su1} \times V_{su1} + C_{su2} \times V_{su2}}{C_{mix0} \times V_{mixa0}} \tag{2.5}$$

Where C_{su1} and C_{su2} are the concentrations of the first removed supernatant and the second removed supernatant [mg/mL], respectively; V_{su1} and V_{su2} are their volumes [mL], respectively.

To prepare for the tests, 500 μL aliquots of Si-DNA suspension with a concentration of ~ 1.5×10^{-4} [mg/mL] were utilized. Prior to each test, sonication was performed for 30 seconds

in order to prevent any particle clumping (Hielscher UP200St, ~ 12 W/S). A control sample of 100 μL was taken prior to the experiment to assess the initial concentration. Thereafter, an equal volume of demineralized water (Demi), i.e., 400 μL, was added to the same tube. The centrifugation tests, which were designed to apply specific RCFs and durations, were carried out at room temperature (20 °C).

Following the first centrifugation, 700 μL of the supernatant was removed using a 1000-μL pipette, and the remaining supernatant was removed using a 100-μL pipette. As previously mentioned, it is important to carefully avoid the pellet location during this step, particularly when using a 100-μL pipette in close proximity to the pellet. The supernatant that was removed was kept aside for later qPCR analysis, referred to as "wash 1". The pellet was then re-suspended by adding 800 μL Demi and subjected to several 'rack shakes' and vortexing. Rack shakes involved firmly holding the bottom of a microtube, such as a 1.5 or 2 mL tube, and swiftly rubbing it horizontally against the opening side of a tube rack designed for holding 1.5 or 2 mL tubes. This motion was repeated from one end to the other end of the rack, causing the bottom of the tube to be struck by each consecutive opening. The purpose was to efficiently achieve intense and thorough mixing of the liquid contained within the tube in a short period. Afterwards, the process was repeated with a second centrifugation, and the resulting supernatant from this step was referred to as "wash 2." Finally, the pellet was re-suspended in Demi water to achieve the same volume as the initial sample volume, after which a 100 μL sample was taken for qPCR analysis.

The overall performance of a centrifugation protocol was evaluated based on separation efficiency, which increased with increasing RCF while the mass in the wash (supernatant) dropped correspondingly (Fig. 2.3). For RCF less than 10,000 g, the separation efficiency remained lower than 40% even with centrifuge durations that were more than double the minimum duration calculated by Stokes' law. Between 10,000 g and 20,000 g, the average separation efficiency was higher, but with substantial variation ranging from ~ 40% to ~ 100%. For RCFs between 20,000 g and 40,000 g, there was a slight increase in separation efficiency with little variation, of which half were acceptable levels around 80% to 100%. For RCFs of 40,000 g and higher, the separation efficiencies were stable between 80% and 120%.

In addition, Fig. 2.4 shows the distribution of separation efficiency over the range of the RCF, which was divided into three groups: RCF < 20,000 g; 20,000 g – 35,000 g; 40,000 g - 65,000 g. The standard deviations in Group 3 (40,000 g to 65,000 g) were the lowest of the three groups. Student's T tests showed that there was a statistically significant difference between each group at the 0.05 level ($p < 0.05$). Moreover, the variances of the three groups decreased with increasing RCF from Group 1 to Group 3. In Group 3, the lowest variance was obtained at 60,000 g with 6 minutes (Fig. 2.5). Therefore, the protocol of 60,000 g with 6 minutes was considered to be the best combination of RCF and duration.

2.3.3. Separation operations

Pipetting separation

Centrifugation has two important steps, namely the spinning process and the separation operation. When it comes to separating the pellet from the fluid, the operator should have an idea of the approximate location of the pellet. The position of the pellet strongly depends on the angle of the tube during spinning, and different centrifuge rotors have varied angles

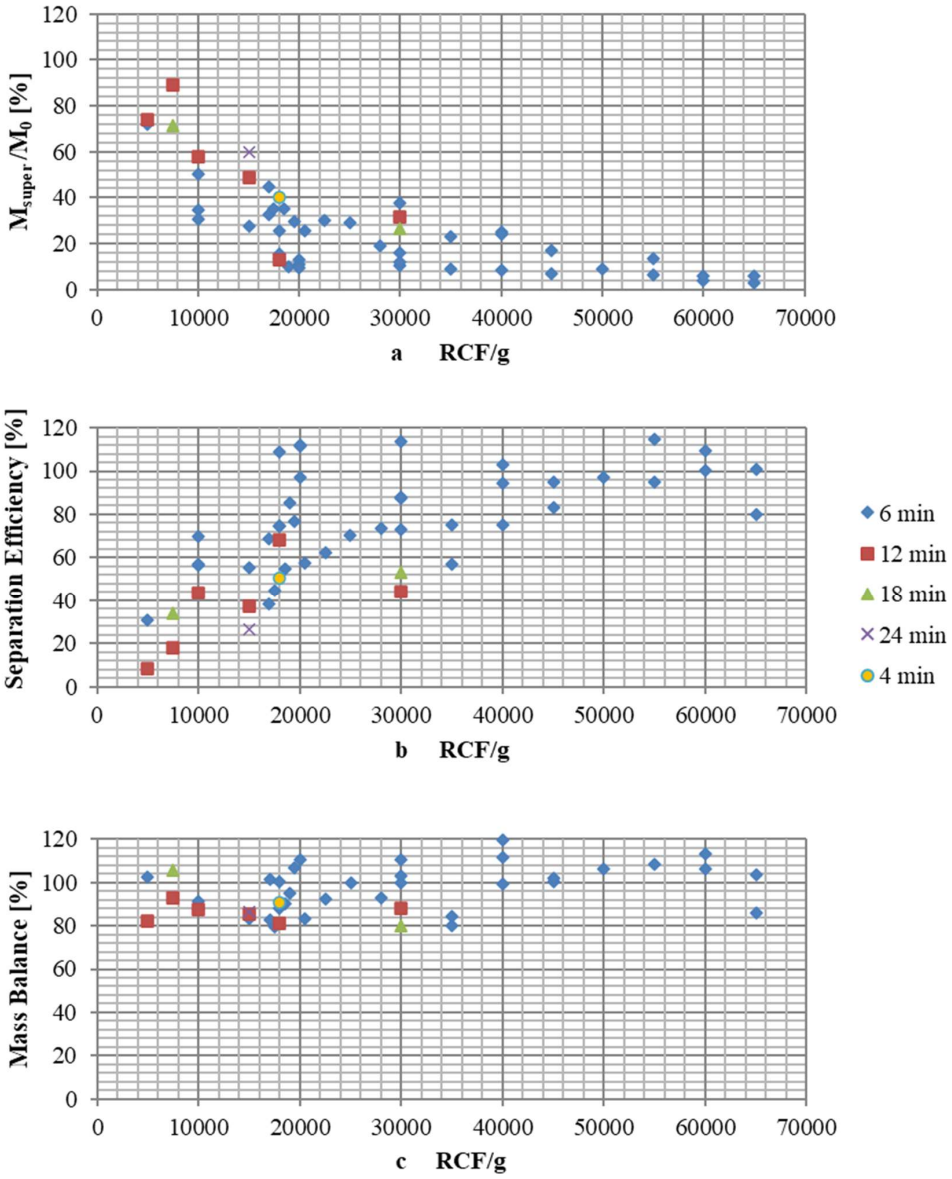

Figure 2.3: Overview of the separation efficiency with varied combinations of duration and the relative centrifuge force (RCF). Panel a: M_{super}/M_0 [%] represents the ratio of Si-DNA mass (M_{super}) in the supernatant (both wash 1 & wash 2) over the initial Si-DNA mass (M_0); panel b: Separation Efficiency [%] represents the ratio of the Si-DNA mass in the final sample after centrifugation over the initial Si-DNA mass; panel c: Mass Balance [%] represents a mass balance of an individual sample, which is the sum of M_{super}/M_0 and Separation Efficiency.

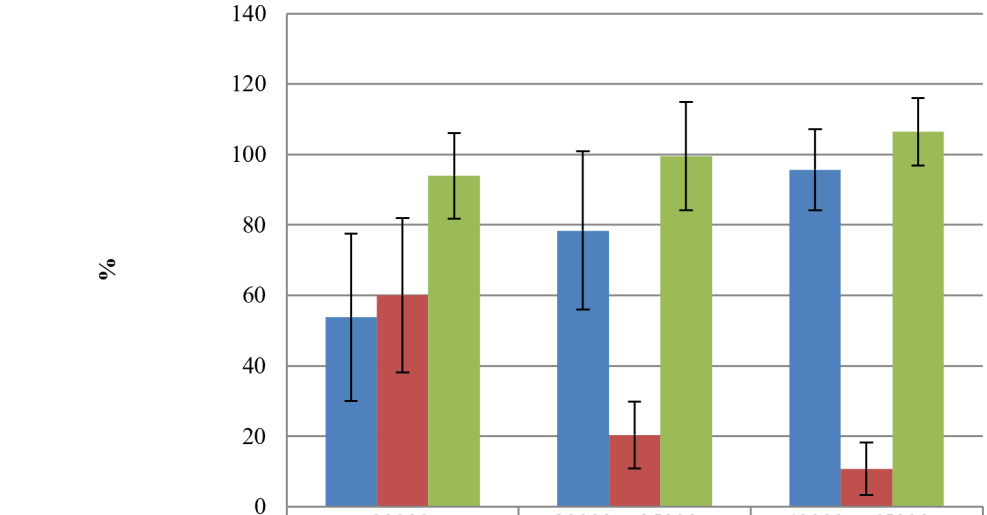

	<20000 g	20000 g-35000 g	40000 g-65000 g
Separation Efficiency [%]	54	78	96
M_{super}/M_0 [%]	60	20	11
Mass Balance [%]	94	100	106

Figure 2.4: An overview of Separation efficiency, the ratio of Si-DNA mass in the supernatant over initial Si-DNA mass (M_{super}/M_0 [%]), and total mass balance over 3 groups of RCF. Error bars represent standard deviations.

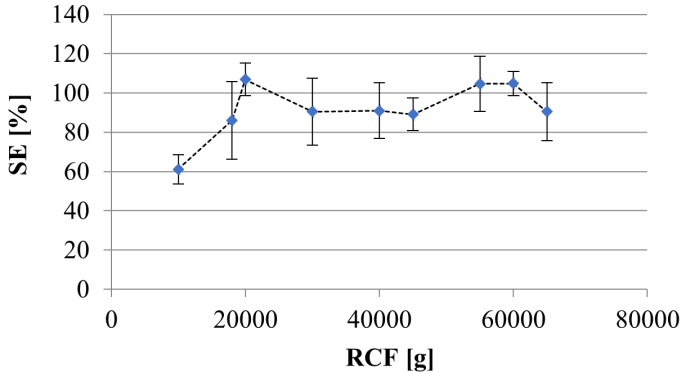

Figure 2.5: The separation efficiency (SE) variation as a function of RCF, along with its corresponding standard deviation.

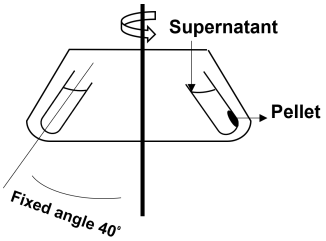

Figure 2.6: Profile of the fixed-angle centrifuge rotor and the pellet location.

that can impact the shape of the pellet at the bottom. Tubes with a smaller angle result in a larger pellet area, while tubes with a larger angle make the pellets stick to the wall more tightly. Knowing this information was imperative for a successful separation operation, as the extend to which the pellets would be disturbed by the pipette tip depends on how close the pipette tip is to the pellet location and how tightly the pellet is attached to the tube.

The rotor used in this centrifugation test had an angle of 40° (rotor No. 221,23 V01), and the approximate position of the pellet was on the side of the tube, as shown in Fig. 2.6.

After centrifugation, the supernatant was carefully removed using a pipette, taking care to avoid the pellet location, and Demi was added to resuspend the pellet. Before sample-taking for qPCR analysis, it is crucial to ensure the homogeneity of the suspended Si-DNA. Usually, vortexing for a few seconds is sufficient for low-concentration particle suspension. However, preliminary tests showed that the pellet strongly adhered to the wall after centrifuging with high RCFs, necessitating an enforced re-suspension scheme. Consequently, the re-suspension scheme used involved a few rack shakes and a 3-minute vortexing at 2700 revolutions per minute using an Eppendorf Mix Mate machine ($\sim$ 1.2 m/s), followed by sonication for 20 seconds (Hielscher UP200St, $\sim$ 12 W/S) to avoid any clumping.

Decantation separation

When dealing with a large number of environmental samples, the pipetting protocol described above can become labor-intensive. In order to streamline the process, an alternative protocol was designed (Fig. 2.7) where the liquid was poured off and the remaining liquid was dried out through dry bath heating at 40 °C for 30 minutes. As shown in Fig. 2.7, to test the efficacy of decantation, an extremely low concentration (i.e., 1.5×10^{-8} mg/mL) and an intermediate concentration (i.e., 1.5×10^{-4} mg/mL) of Si-DNA were used. To up-concentrate the diluted sample, Demi water one-tenth of the initial volume was added to the tube once it had completely dried out. The Si-DNA was then resuspended in the same manner as described earlier.

With a less cautious, but time-saving operation of removing the supernatant, more mass is anticipated to end up in the wash. To compare the performance of the two operations, the overall mass, mass in the wash, and the recovered mass were plotted for two different suspension concentrations (i.e., 1.5×10^{-4} [mg/mL] & 1.5×10^{-8} [mg/mL]) in Fig. 2.8. The results showed that with pipetting, there was less mass in the wash for each concentration, confirming the assumption. However, in the case of higher concentrated samples, there was

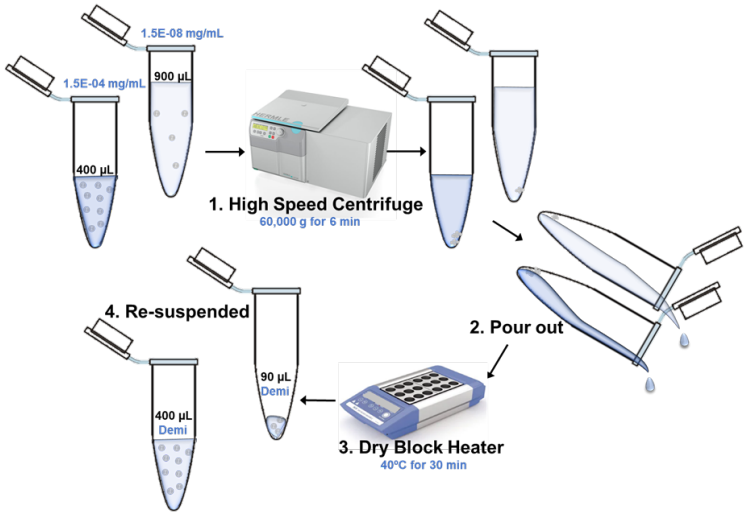

Figure 2.7: Schematic figure for the decantation separation for two different concentrations of Si-DNA suspensions.

more mass in the recovered sample upon pipetting. On the other hand, for samples with lower concentrations, the recovered samples had an equivalent amount of DNA mass.

2.4. Magnetic-separation for SiDNAFe

In the context of up-concentration, centrifugation may not be the sole solution. Easy and fast recovery of magnetic particles and no limitation of sample volume are the major advantages of magnetic separation over centrifugation (Aguilar-Arteaga et al., 2010; Puddu et al., 2014). Especially, centrifuging micro-sized or smaller particles often requires high centrifuging forces (e.g., 60,000 g) which are only applicable for small sample volumes (i.e., 1.5 or 2 mL). Furthermore, in cases of river water with abundant suspended solids, all particles, including SiDNAFe, would be spun down, rendering downstream sample analysis using qPCR a challenging task.

Our internal experimental results have demonstrated that the optimal magnetic separation duration was 30 minutes (unpublished results). Accordingly, a magnetic separation and up-concentration protocol has been developed in this dissertation. Briefly, 1 mL sample tubes were hold against magnets in a 16-Tube SureBeads™ Magnetic Rack (Bio-Rad Laboratories, Inc., USA) for 30 minutes. Following this, 850 μL was pipetted out, carefully avoiding the magnetically drawn particles on the side. The same tube was then replenished with 850 μL of MQ. The SiDNAFe was subsequently resuspended and subjected to a second round of magnetic separation. Following this, a third round of magnetic separation was conducted, with 800 μL being pipetted out to leave 200 μL of the sample in the tube. This process yielded a 5-fold up-concentration (Fig. 2.9).

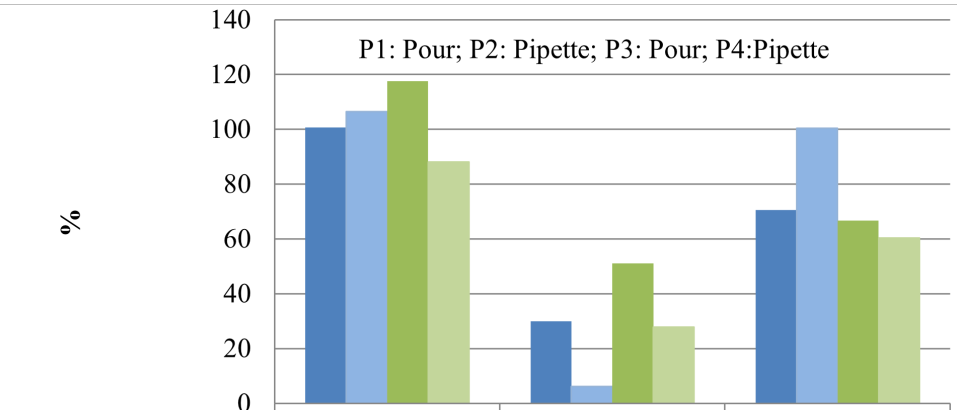

	Overall Mass	Wash	Recovered Mass
P1(1,50E-04mg/mL)	101	30	71
P2(1,50E-04mg/mL)	107	6	100
P3(1,50E-08mg/mL)	118	51	67
P4(1,50E-08mg/mL)	88	28	60

Figure 2.8: Comparison of the recovered mass of two different concentrations of Si-DNA using two different ways for removing supernatant.

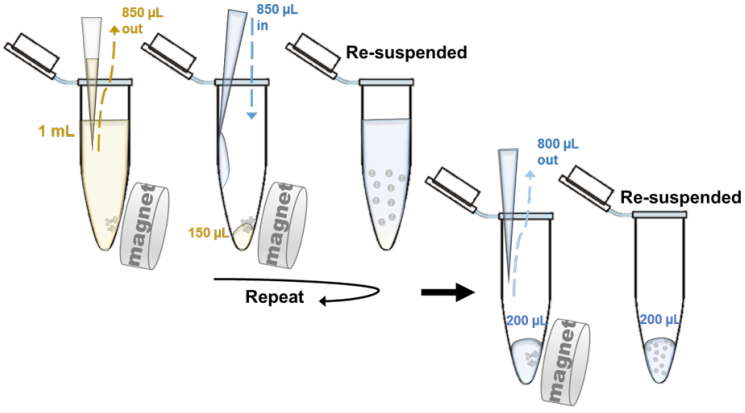

Figure 2.9: Schematic figure of the magnetic separation protocol.

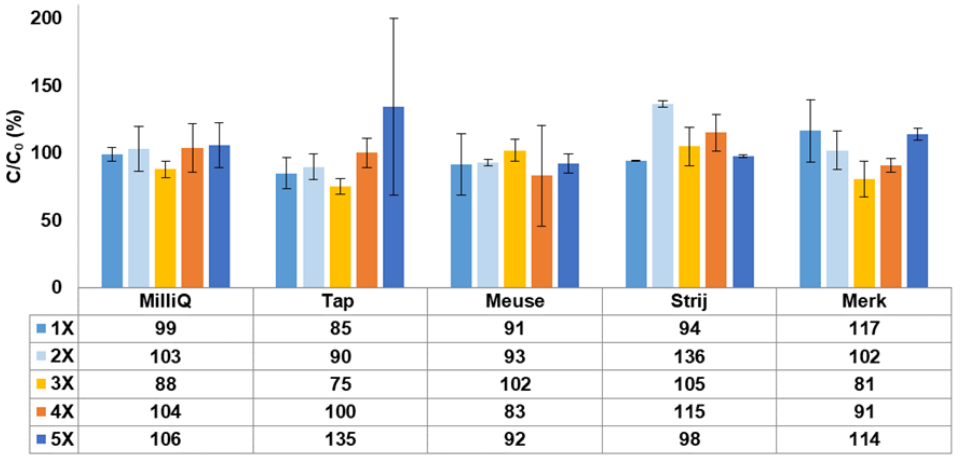

	MilliQ	Tap	Meuse	Strij	Merk
1X	99	85	91	94	117
2X	103	90	93	136	102
3X	88	75	102	105	81
4X	104	100	83	115	91
5X	106	135	92	98	114

Figure 2.10: Change of sample concentrations in five water types after up to five times of magnetic separation.

2.4.1. Effect of magnetic separation times & water quality

To identify the most appropriate magnetic separation times, sample concentrations were assessed before and after up to five rounds of magnetic separation. Furthermore, the impact of different water quality on the efficacy of magnetic separation and subsequent qPCR assays was evaluated. To achieve this, SiDNAFe was initially suspended to attain a final concentration of $\sim 1 \times 10^{-4}$ mg/mL in MQ water, Tap water, and three selected river waters. The river water samples were collected from river Meuse at Keizersveer, the Netherlands (51°43'05.7"N, 4°53'27.5"E), Strijbeek Beek (51°29'58.3"N, 4°47'01.7"E), and Merkske (51°24'57.1"N, 4°50'48.5"E) on the Netherlands-Belgium border (referred to and interchangeably as "Meuse", "Strij", and "Merk", respectively). These river water types were also employed in Chapters 4 and 5 in this dissertation.

Fig. 2.10 showed that, in MQ water, no mass loss was detected after five rounds of magnetic separation, suggesting that repeated magnetic separation would not result in SiDNAFe mass loss. No pattern of mass decline was observed in the other four water types as a function of magnetic separation times. The results of a one-way ANOVA test revealed no significant difference at a 95 % significance level among the five water types in terms of mass recoveries and their corresponding standard deviations (p = 0.4871 and p = 0.5738, respectively). Furthermore, there was no significant difference in mass recoveries and standard deviations when categorized by the number of magnetic separation cycles (p = 0.3375 and p = 0.7480, respectively). Despite this, mass variations and standard deviations in these four water types were visually larger than those observed in MQ, ranging from 75 % to 136 %. This could be due to differences in water quality and potential pipetting errors (e.g., 135 % at the 5th round of separation in Tap water).

2.4.2. Efficacy of magnetic up-concentration

To evaluate the effectiveness of sample up-concentration, magnetic separation and up-concentration were performed across a range of initial SiDNAFe concentrations, from

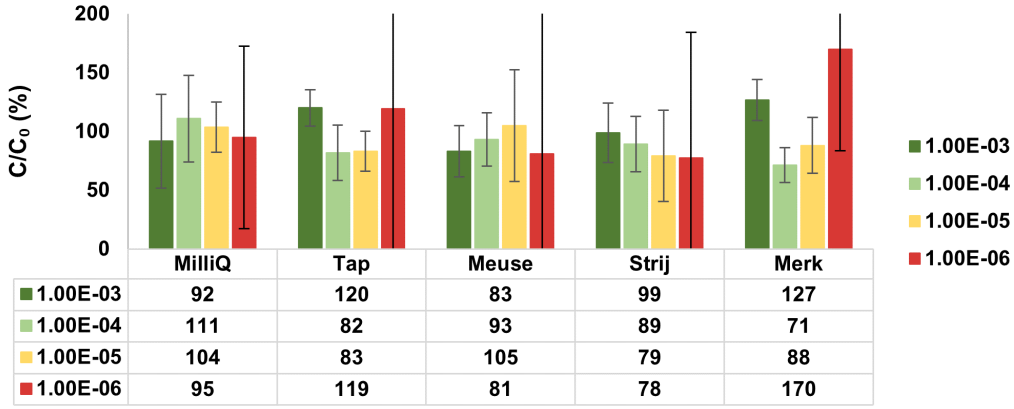

	MilliQ	Tap	Meuse	Strij	Merk
1.00E-03	92	120	83	99	127
1.00E-04	111	82	93	89	71
1.00E-05	104	83	105	79	88
1.00E-06	95	119	81	78	170

Figure 2.11: Mean relative concentration variations of SiDNAFe after up-concentrating five times using the magnetic separation protocol. The concentration ranged from $\sim 1\times10^{-3}$ mg/mL ("1.00E-03") to $\sim 1\times10^{-6}$ mg/mL ("1.00E-06"). Error bars are standard deviations.

$\sim 1\times10^{-3}$ mg/mL to $\sim 1\times10^{-6}$ mg/mL. SiDNAFe was also suspended in five different water types, including MQ, Tap water, Meuse water, Strij water, and Merk water, respectively. After magnetic separation and washing twice with MQ, SiDNAFe was finally suspended in one fifth of the initial sample volume (Fig. 2.11). The resulting concentration was compared to a mathematical five-fold initial concentration (C_0). Mean concentration variations ranged from 71 % to 170 % across the five water types (Fig. 2.11). The mean concentration variations for MQ, Tap, and Meuse were within the acceptable range of 80 % to 120 %. However, for Merk, the mean variation went up to 170 % in the group "1.00E-06". Nevertheless, there was no significant difference found among the mean variations and their standard deviations when categorized by water types (p = 0.8017 and p = 0.9208, respectively).

Notably, the lowest concentration group (i.e., $\sim 1\times10^{-6}$) had the largest standard deviations of all concentration groups, regardless of water types. According to one-way ANOVA at a 95% significance level, the standard deviations in the "1.00E-06" group were significantly larger than those in the other three groups ($p \ll 0.01$). This indicated that the magnetic separation and up-concentration protocol was effective and accurate when the initial sample concentration is within a certain range. Therefore, the most appropriate range of DNA concentrations encountered should be between $\sim 1\times10^{-3}$ and $\sim 1\times10^{-5}$ mg/mL for the batch of SiDNAFe tracers used in this dissertation.

2.5. Conclusions for the up-concentration protocols

To optimize the centrifugation protocol for Si-DNA, a range of centrifuge forces, from 5,000 g to 65,000 g, were tested with varying durations of 4, 6, 12, 18, and 24 minutes to determine the separation efficiencies. The best results were obtained using high centrifuge forces between 40,000 g and 65,000 g, and the lowest variance was obtained at 60,000 g with 6 minutes. To simplify the protocol, decantation by pouring off instead of carefully

pipetting was tested for supernatant removal. Although separation efficiency was inferior to the original design, the results were still acceptable with ~ 70% recovered mass. With less concentrated samples, the results of pouring and pipetting were essentially the same in terms of DNA mass recovery. The centrifugation and decantation protocol is not only time-efficient but also more robust as less delicate work is involved.

For magnetic separation, it was found that repeated magnetic separation of SiDNAFe did not result in mass loss when the sample concentration was within an appropriate range. To ensure accurate quantification, the magnetic-separation and up-concentration protocol is recommended to be applied to SiDNAFe concentrations no less than $\sim 1 \times 10^{-5}$ mg/mL, as below this concentration it becomes difficult to obtain accurate results due to large variations between replicates. Moreover, The mass variations of the SiDNAFe samples that were magnetically separated and up-concentrated did not appear to be related to the selected five water types.

2.6. CRediT author statement

Conceptualization, Y.Tang, J.W.Foppen; Methodology, Y.Tang, A.Abdelrady, J.W.Foppen; Formal analysis, Y.Tang, J.W.Foppen, T.A.Bogaard; Investigation, Y.Tang; Resources, Y.Tang, A.Abdelrady, J.W.Foppen, T.A.Bogaard; Data Curation, Y.Tang; Writing – Original Draft, Y.Tang; Writing – Review & Editing, Y.Tang, J.W.Foppen, T.A.Bogaard; Visualization, Y.Tang; Supervision, J.W.Foppen, T.A.Bogaard; Project administration, Y.Tang, T.A.Bogaard; Funding Acquisition, Y.Tang, J.W.Foppen, T.A.Bogaard.

3

Transport of Si-DNA in controlled instantaneous injection open channel experiments

This chapter is based on Y. Tang et al., 2021: Tang, Y., Foppen, J. W., & Bogaard, T. A. (2021). Transport of silica encapsulated DNA microparticle in controlled instantaneous injection open channel experiments. Journal of Contaminant Hydrology, 242, 103880.

3.1. Introduction

Environmental pollution poses an unprecedented burden over surface water quality and aquatic ecosystems. Between terrestrial and marine ecosystems, rivers are the major dispersal vectors both to distribute nutrient and to transport detrimental contaminants (Nantke et al., 2019). A comprehensive understanding of riverine mass transport is a prerequisite for pollution control. Solute and particle are used in surface water tracing experiments to characterize in-stream transport of solutes and particulates. While solute tracers have been predominantly employed to decipher processes like tracking pollutant sources and pathways, exploring sediment-water interactions, and probing transient storages (Bencala et al., 2011; Haggerty et al., 2008), the use of particle tracers has been comparatively circumscribed, albeit present, in research, exemplified by a select few studies that used micron-sized fluorescent microspheres, bacteriophages/bacteria, and natural clay/sediment particles (Göppert and Goldscheider, 2008; Jamieson et al., 2005; Schiperski et al., 2016; Spencer et al., 2011; Wyer et al., 2010). In these studies, the deployment of particles smaller than ≤ 1 μm is scarce, with only one study known to us, primarily constrained by practical and experimental limitations (Goeppert and Goldscheider (2019)). However, colloids, defined as materials between 10 nm and 10 μm (J. McCarthy and Zachara, 1989, in the aquatic environment are of significant interest due to their sizes, surface charge, surface areas, and mass: as nutrients in phosphorus related colloids (Guo and Macdonald, 2006; Heathwaite and Dils, 2000; Jarvie et al., 2012; Stolpe et al., 2010), as carriers for contaminants (Lead and Wilkinson, 2006; H. Wang et al., 2015), and, when smaller than ~30 nm, their -limited- sizes may cause enhanced biological and chemical reactivities (Auffan et al., 2009; Azimzada et al., 2021). These aquatic colloids include naturally occurring biocolloids (e.g., viruses, bacteria, extracellular polymeric substances, etc.), geocolloids (e.g., clay, metal oxides and hydroxides), anthropogenic engineered nanomaterials (e.g., titanium dioxide nanoparticles and carbon nanotubes) and microplastics (Alimi et al., 2018; H. Wang et al., 2015; L. Xu et al., 2020; X. Zhu et al., 2021). Besides, traditional tracer tests have several disadvantages: 1) a limited number of distinguishable artificial tracers is available, 2) tracer detections often have background noise with dilution limitations, and 3) practical constraints limit the application of a proper tracer (e.g., strict regulations for uranine or rhodamine or being very expensive like fluorobenzoic acid) (Bencala et al., 2011; Choi et al., 2000; Stern et al., 2001; Whitmer et al., 2000; Wilderer, 2010).

In multiplexed tracing experiments in streams and rivers, DNA-tagged microparticles were traceable at greater distances compared to solute tracers and exhibited similar breakthrough behaviour (Garnett et al., 2009; Pang et al., 2020; A. N. Sharma et al., 2012). However, the transport behaviour of these DNA-tagged microparticle tracers has not been rigorously quantified and compared with that of solute tracers.

Therefore, the objective of this chapter was to understand and quantify the transport behaviour of Si-DNA in comparison with solute tracer NaCl in surface water tracing experiments. Our hypothesis was that, when in colloidal stable conditions, Si-DNA has a transport behaviour comparable to solute tracer NaCl in surface water injection experiments. Hereto, we conducted a series of controlled injection experiments in six environmentally representative water types and compared the BTCs and hydrodynamic dispersion coefficient $D_{L\,\text{Si-DNA}}$ of Si-DNA to that of NaCl ($D_{L\,\text{NaCl}}$).

3.2. Materials and Methods

3.2.1. Hydrodynamic diameter and zeta potential of Si-DNA

The hydrodynamic diameter (D_{hDLS}) of Si-DNA in each water type (~ 500 μg/L) was measured by Dynamic Light Scattering (DLS), and ζ of Si-DNA was calculated by using Smoluchowski's equation from its electrophoretic mobility measured on a NanoSizer (Nano Series, Malvern Instrument Ltd., Worcestershire, United Kingdom). To assess if aggregations of Si-DNAtook place within the time frame of the injection experiment, in each water type the D_{hDLS} was measured as a function of time in quiescent and in mixing conditions, respectively. Thereto, in each water type, Si-DNA was suspended to reach a final concentration of ~ 500 μg/L of 2 mL in duplicate. Each sample tube was sonicated to reach a homogenous suspension before the first measurement. After the first measurement of D_{hDLS}, one sample was allowed to stand still while the other sample was mixed at 1500 revolutions per minute until the next measurement in 2 hours.

3.2.2. Injection experiments

Injection experiments of tracers are widely conducted to obtain BTCs to understand transport behaviour because they are simple to carry out and give good and reliable results (Leibundgut and Seibert, 2011). A series of pulse-injection experiments with Si-DNA was performed in six water types in a horizontally-placed PVC box (Fig. 3.1). The channel was 20 cm long, 10 cm wide, and 3 cm deep. Tracers were injected by a peristaltic pump. The injection experiment had a flow rate of ~ 18 mL/min and a duration of approximately 100 minutes (hydraulic retention time was ~ 28.5 minutes). For each experiment, a 10 mL suspension of ~ 5 μg/L Si-DNA was injected. Due to the low flow rate, a magnetic stirrer was set close (~2 cm) to the inlet point to enhance cross-sectional mixing of tracer mass. We assumed that tracer mass was mixed rapidly, but not instantaneous, over the entire cross-section, so that the impact of the mixing in the so-called initial period on the transport in the investigated reach was negligible (Rieckermann et al., 2005), whereby the mixing was not represented by the 1-D advection-dispersion process. A solute fluorescent dye tracer was added once to visualize mixing conditions and the transport pathway of the injected tracer mass in the box (see details in the Appendix A). Sampling was carried out at the outlet. The sampling interval progressively increased from 1 to 5 minutes (see Table A.2 in the Appendix A). From each of the sample bottle, 500 μL of sub-sample was taken (in duplicate) for sample analysis. Sample bottles were vortexed for 1 to 2 minutes before taking sub-samples, ensuring that Si-DNA was homogeneously distributed over the entire sample volume. Each injection experiment was performed three times. The 1st and 2nd injection experiments were sequentially performed with a break of 0.5 hour to rinse the set-up to remove possible residual substances from the previous experiment. The 3rd injection experiment was performed later. After each experiment, extra water samples were analyzed for any residual tracer in the PVC box (see Fig. 3.1).

First, a pulse-injection experiment of NaCl (5.0 mM, EMSURE®, Merck KGaA), a solute tracer, was performed in triplicate for reference. The BTC of NaCl was measured by an electrical conductivity (EC) meter (Multi 3620 IDS, Xylem Analytics Germany GmbH, Germany), and mass recovery was calculated (see the standard curve in Fig. A.2 in the Appendix A). Similarly to the NaCl injection experiment, Si-DNA tests were conducted in

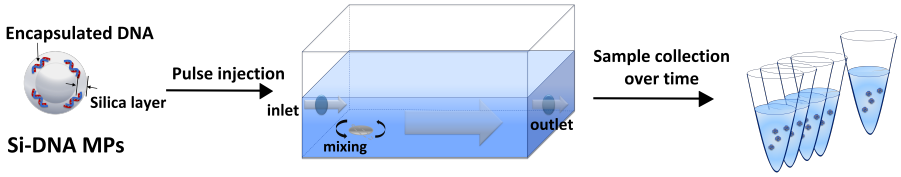

Figure 3.1: Schematic of injection experiments. After a pulse injection of Si-DNA into the PVC box ($20cm \times 10cm \times 3cm$), the particles were transported along with the water flow from left to right.

six representative water types. Demi water was chosen as a 'blank' control. Furthermore, we used a 5.0 mM $NaH_2PO_4 \cdot H_2O$ solution (J.T. Baker), and a 1.67 mM $CaCl_2 \cdot 2H_2O$ (EMSURE®, Merck KGaA) solution to anticipate the effects of monovalent (Dalas and Koutsoukos, 1990; Ji et al., 2020) and divalent cations (Liu et al., 2011). This group of synthetic chemical solutions were prepared in the laboratory. Tap water was used as a transition water type, which was more complex than the synthetic chemical solutions, but less complex than natural water in the sense that various natural or anthropogenic nanoparticles, colloidal particles or particulate matter (> 5 μm) could still be part of that water. Also, two natural surface water samples were collected from a canal in Delft, one of which was filtered (5 μm cellulose nitrate filters; referred to as "Filtered natural water"), and the other was not (referred to as "Natural water"). The canal receives its water from both Rhine River and Meuse River. In this way, we tested for the effect of particulate matter. Concentrations of major cations and anions of Tap water and Natural water samples were measured by ion chromatography (Methrohm AG). When performing the 3rd series of replicate experiments, the organic matter content of the water types was measured as dissolved organic carbon (DOC, in mg-C/L) using the combustion technique with a total organic carbon analyser (TOC-VCPN (TN), Shimadzu, Japan).

Before the injection experiments, to assess if the PVC material could be a possible sink for DNA mass loss during injection experiments, the concentration of Si-DNA in Demi water was determined as a function of time in batch experiments for 7 days (an extended period was designed as an extreme condition). The suspension of Si-DNA in Demi water was kept in PVC containers and protected against daylight at room temperature. No mass loss of Si-DNA was observed (results shown in Fig. A.3 in the Appendix A).

3.2.3. Analysis of breakthrough curves

The physical transport of solutes and Si-DNA in the injection experiments can be described by a one-dimensional advection and dispersion equation with a first-order mass transfer transient storage. We used the One-dimensional Transport with Inflow and Storage model (OTIS) to model the curves (Runkel, 1998). OTIS was chosen because our experimental set-up mimics 1-D steady uniform flow in a main channel with a storage-zone without lateral inflow. Besides, DNA mass was conserved during injection experiments, since no source or sink of DNA mass was observed in our experimental channel. Therefore, no mass-loss term was considered in the OTIS modeling. The goals were to fit the observed BTC and to quantify $D_{L\text{Si-DNA}}$. The fitting was carried out using Nonlinear Least Squares by requiring an input of observed BTC (see details in the Appendix A), which was implemented in OTIS-P. In a modelling case where mass is conserved, the injected mass should equal to

the recovered total mass, which is the area under the observed BTC. In spite of no mass loss, this total recovered DNA mass calculated from the observed BTC can differ from the measured injected DNA mass to some extent. To resolve the imbalance of input/output mass, we scaled the mass recoveries to 100% by linearly correcting the initial injection mass before OTIS modelling. This linear correction of the injected mass has no influence on the characteristics of the BTCs and can be used for dispersion estimation in OTIS-p. The equations underlying the OTIS model are presented as follows,

$$\frac{\partial C}{\partial t} = -\frac{Q}{A}\frac{\partial C}{\partial x} + \frac{1}{A}\frac{\partial \frac{AD\partial C}{\partial x}}{\partial x} + \alpha(C_s - C) \tag{3.1}$$

$$\frac{\partial C_S}{\partial t} = \alpha\frac{A}{A_S}(C - C_S) \tag{3.2}$$

Where A is the main channel cross-sectional area [m^2], A_S the storage zone cross-sectional area [m^2], C the main channel solute concentration [g/m^3], C_S the storage zone solute concentration [g/m^3], D_L the hydrodynamic dispersion coefficient [m^2/s], Q the volumetric flow rate [m^3/s], t time [s], x distance [m], and α the storage zone exchange coefficient [1/s]. In OTIS-P, D_L and α were fitted while other parameters were fixed. Best-fit estimates of $D_{L\text{NaCl}}$ and α_{NaCl} from NaCl injection experiments were used as initial estimates of $D_{L\text{Si-DNA}}$ and $\alpha_{\text{Si-DNA}}$.

3.3. Results and Discussion

3.3.1. Breakthrough curves of Si-DNA & the effect of water quality and hydrodynamics

Water quality (pH, EC, DOC, total suspended solids (TSS) and major chemical compositions) of six water types used for the injection experiments are given in Table 3.1. The mean D_{hDLS} was between ~ 237 ± 81 nm and ~ 299 ± 129 nm (measured before the injection experiments, Table 3.1). In the quiescent condition and as a function of time, the mean D_{hDLS} and PDI of Si-DNA remained constant for each water type (Fig. 3.2a). A one-way ANOVA revealed that there was no significant difference ($p = 0.3$, at 95% significance level) among mean D_{hDLS} and PDI of Si-DNA. However, when mixing, the D_{hDLS} and PDI significantly increased ($p < 0.05$, at 95% significance level) in $CaCl_2$, Tap water, filtered and unfiltered Natural water, while in Demi water and in Phosphate solution the D_{hDLS} and PDI remained constant as a function of time (Fig. 3.2b).

Generally, the BTCs of the Si-DNA in all water types showed a close resemblance to the BTCs of NaCl (Fig. 3.3, Fig. A.4). The C/C_0 (%) of the NaCl BTC demonstrated a sharp increase and then reached a peak of roughly 2% (at ~ 4^{th} minute), which was followed by a slow decline (~ 1% at ~ 24 minute; Fig. 3.3). When compared with Si-DNA, the C/C_0 of Si-DNA were 'noisier' than the NaCl BTCs. Moreover, comparing Si-DNA BTCs within the group of laboratory prepared waters, the BTCs in $CaCl_2$ were slightly 'noisier' than those in Demi and NaH_2PO_4. Also, the Si-DNA BTCs were more scattered in Tap water, Filtered natural water, and Natural water. In other words, the observed relative concentrations of Si-DNA around the peaks were more scattered as compositions of solution became more complex, exhibiting higher peak values than those of NaCl tracers. In particular, the Si-DNA

3

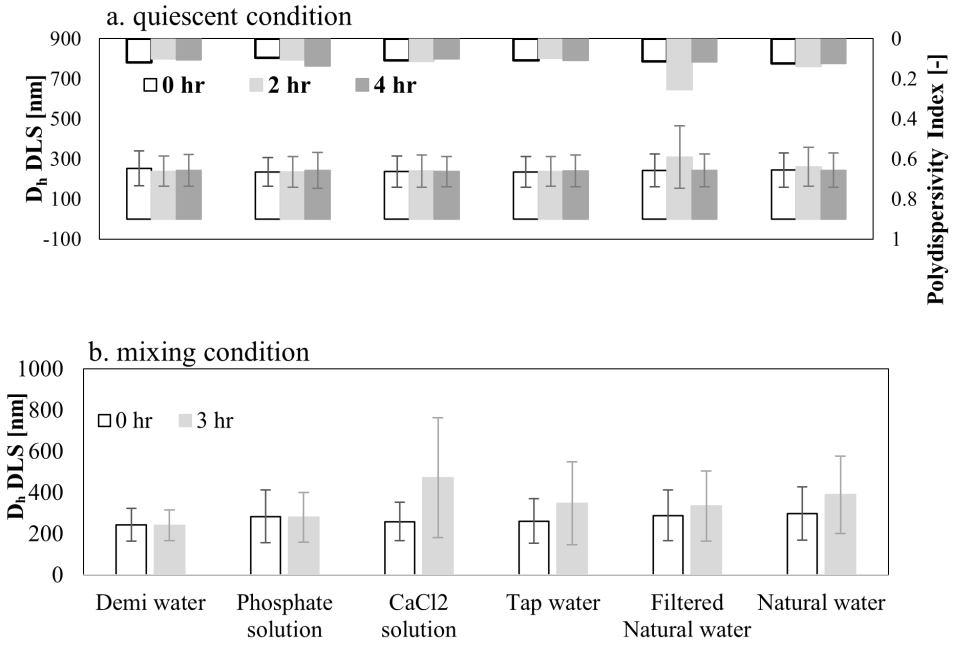

Figure 3.2: Hydrodynamic diameterD_{hDLS} of Si-DNA in six water types as a function of time (a. quiescent condition and b. mixing condition). The error bar represents the standard deviation of the size distribution. Polydispersivity index (PDI) is equal to the square of standard deviation of the size distribution divided by the square of the mean.

BTCs in the Filtered natural water and Natural water were most scattered with the largest discrepancy among the triplicates.

Water quality including ionic strength, NOM content, and suspended solids are important factors determining the fate of engineered nano- and micro-particles in water bodies (Shevlin et al., 2018). In our experiments, the ionic strength of used water types was in the range of 1-25 mM, based on the measured concentrations of known cations and anions (Table 3.1). Note that compared to studies which focused on the effect of ionic strength on colloidal interactions (Ledin et al., 1993; J. F. McCarthy et al., 2002; Nocito-Gobel and Tobiason, 1996; Torkzaban et al., 2008; J. Zhao et al., 2021), the ionic strength of water types used in this paper was in the low range. In such solution chemistry, Si-DNA remained colloidally stable, evidenced by a constant D_{hDLS} over 4 hours (Fig. 3.2.a). The ζ of the Si-DNA was between -17 ± 7.1 mV and -49.8 ± 5.9 mV. This indicated that the solution chemistry alone was unfavorable for aggregation of Si-DNA (Metin et al., 2014). In the classical DLVO (Derjaguin, Landau, Verwey, and Overbeek) theory (Derjaguin and Landau, 1993; Verwey, 1947), energy barriers could be quantified to dictates particle aggregation. Energy barriers refer to the potential energy barriers that particles must overcome to aggregate or coagulate, arising due to the combination of attractive van der Waals forces and repulsive electrostatic forces. Specifically, the calculated total energy barriers based on Classical DLVO theory for Si-DNA in Demi and NaH_2PO_4 solution were relatively high (≥ 50 kT, with negligible secondary minima, see Table A.4 in the Appendix A for the details of DLVO energy calculations). Such high repulsive energy would prevent aggregation of DLVO in the solution chemistry.

In $CaCl_2$, Tap, Filtered natural and Natural waters, the reduction of ζ (Table 3.1) can be explained by the compression of the electric double layer, indicating a likely lower total energy barrier (Elimelech et al., 2013). In contrast to the quiescent condition (no shear force), after 2 hours of mixing, the increase of D_{hDLS} in $CaCl_2$, Phosphate, Tap, filtered and unfiltered natural water (Fig. 3.2 b) indicated shear-induced aggregation (i.e., orthokinetic flocculation) (Barthelmes et al., 2003; Hijnen and Clegg, 2014; Spicer, 1997). Moreover, when a flow field acts on the suspension, the hydrodynamic force (e.g., shear force) is responsible for bringing the particles together and would likely dominate the particle collisions (Elimelech et al., 2013; Frungieri et al., 2020; Zaccone et al., 2009). Thus, it is reasonable to imply that shear-induced aggregation might have taken place during the injection experiments. However, we argue that the effect of aggregation is likely minor, as the coupled effect of shear rate and volume friction (Gregory, 2005) in our experiments was orders of magnitude lower than that in our batch mixing experiments.

The BTCs of Si-DNA in filtered and unfiltered natural water showed similar characteristics with a degree of scatter in the peaks (Fig. 3.3), despite the variations in water quality parameters between the third and the preceding two series of experiments (Table 3.1, there was a time gap between the first two series and the third series). The interactions between natural particulates and nanoparticles were extensively studied in literature (Lead et al., 2018; Oney and Nason, 2021; Peijnenburg et al., 2015; Petosa et al., 2010; Praetorius et al., 2020; Quik et al., 2014; Velzeboer et al., 2014; L. Xu et al., 2020). For example, Quik and co-workers found that natural particulates played a key role in the increased hetero-aggregation and sedimentation of nanomaterials by comparing filtered and unfiltered natural water samples (Quik et al., 2014). However, the effect of particulate matter content (≥ 5

Table 3.1: Water quality, ζ, R_{hDLS}, mass recoveries, and D_L & α of Si-DNA in six water types for injection experiments in triplicate.

Water types	pH	EC	DOC	TSS	Na^+	K^+	Ca^{2+}	Mg^{2+}	Cl^-	NO_3^-	PO_4^{3-}	SO_4^{2-}	ζ	D_{hDLS}[1]	M.R.	α		$D \times 10^{-3}$	
		[µS/cm]	[mg-C/L]					[mg/L]					[mV]	[nm]	[%]	[1/s]	95% C.L. [±]	[m^2/s]	95% C.L. [±]
Demi water	6.4 ±0.25	0.5 ±0.01	0.73 ±0.01	-	-	-	-	-	-	-	-	-	-38 ± 5.3	242 ± 81	91	1.99	1.12	3.96	1.17
															93	1.31	0.56	3.36	1.18
													-30 ± 6.2	243 ± 79	97	1.03	0.18	2.81	0.51
$CaCl_2$	5.8 ±0.01	427 ±7	0.51 ±0.01	-	-	-	68 ±1.5	-	117±0.5	-	-	-	-21 ± 4.5	288 ± 103	102	1.60	0.81	3.91	1.26
															111	1.97	1.20	4.54	1.38
													-22 ± 5.4	259 ± 93	N.D.*	1.29	0.39	2.81	0.76
Pho	7.2 ±0.05	787 ±5	0.57 ±0.01	-	170 ±3	-	-	-	14±0.5	-	478±5	-	-50 ± 5.9	259 ± 111	80	1.66	1.19	4.44	1.88
															84	1.63	0.53	3.48	0.75
													-49 ± 5.6	284 ± 128	98	1.22	0.16	3.10	0.37
Tap water	8.1 ±0.1	522 ±5	-	-	40 ±0.5	46 ±1	49 ±2.5	7 ±0.5	61 ±8	9 ±0.1	-	47 ±5	-24 ± 4.5	237 ± 81	94	3.44	1.41	4.91	0.69
															88	0.96	0.18	2.30	0.54
			2.94 ±0.01										-18 ± 5.4	261 ± 108	N.D.*	1.36	0.72	3.26	1.32
Filtered natural water[2]	8.0 ±0.2	780 ±3	-	-	60 ±2	73 ±1	73 ±2	15 ±1	94±2	2 ±0.5	1 ±0.2	47 ±1	-19 ± 5.2	267 ± 100	103	1.32	0.84	2.69	1.49
															94	1.90	1.20	3.11	1.20
	8.5 ±0.2	1084 ±5	13.32 ±0.02	0.4 ±0.2	69 ±2	10 ±1	127 ±2	18 ±2	101±1	5 ±0.5	1 ±0.3	113 ±2	-21 ± 6.9	288 ± 123	94	1.24	0.46	4.25	1.21
Natural water[2]	7.6 ±0.2	777 ±2	-	-	60 ±2	75 ±1	75 ±2	15 ±1	94±2	2 ±0.4	1 ±0.1	46 ±1	-18 ± 4.7	283 ± 119	97	2.02	2.90	5.46	3.57
															98	2.09	1.76	4.65	1.82
	8.5 ±0.2	1029 ±3	13.05 ±0.1	6.6 ±1.3	69 ±2	10 ±1	127 ±2	18 ±2	101±1	5 ±0.3	1 ±0.1	113 ±2	-17 ± 7.1	299 ± 129	N.D.*	1.52	0.80	3.62	1.31
														Reference 1[3]	98	2.01	0.31	4.07	0.32
														Reference 2	100	1.66	0.15	3.89	0.22
														Reference 3	104	1.38	0.11	3.25	0.20

[1] D_{hDLS} was measured before injection experiments.
[2] For filtered natural water and natural water, all the data are listed in two rows because experiment 3 was conducted 2 years later than experiment 1&2 and natural water quality for experiment 3 differed from the previous 1&2.
[3] Reference 1 - 3 are the simulations of NaCl injection experiments in Demi water.
* N.D. Not determined, due to erroneous initial concentrations (C_0).

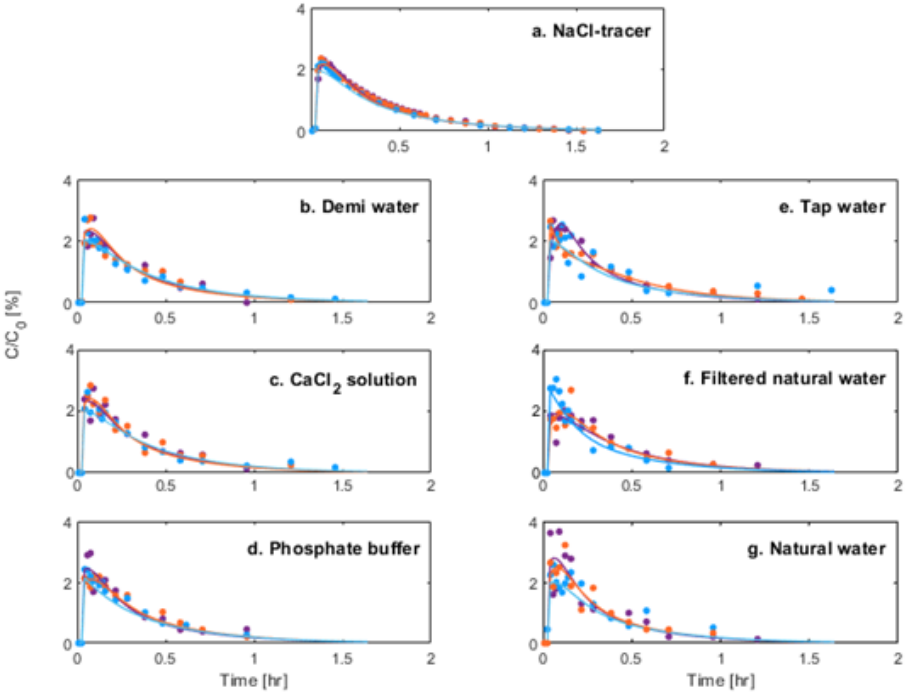

Figure 3.3: Observed and simulated breakthrough curves of Si-DNA in six water types plotted in relative concentration C/C_0 [%].The observed data are shown as solid circles in purple, orange, and blue for the 1st , 2nd, and 3rd replicate experiment, respectively. The corresponding simulated breakthrough curve is shown as line in purple, orange, and blue for 1st, 2nd, and 3rd replicate experiment, respectively. The observed and simulated breakthrough curves of NaCl are shown for reference in plot a.

*mu*m) on the transport characteristics of Si-DNA was not clearly observed in our injection experiments.

3.3.2. D and colloidal stability

After re-scaling mass recoveries to 100% without changing the BTC behaviour, we modelled the BTCs of all injection experiments to determine D_L and α (Fig. 3.4 and Table 3.1). The rising and falling limbs of NaCl BTCs were modelled almost perfectly (Fig. 3.3 panel a, R^2 = 99.8%), and the peaks of NaCl BTCs were slightly underestimated. This showed that the OTIS conceptualization (1D ADE with one transient storage) was well capable of mimicking the experimental set-up even though there was a small discrepancy between the schematisation of OTIS and experimental set-up. In the 1D representation in OTIS the tracer mass is uniformly distributed over the cross-sectional area. We used a stirrer to achieve cross-sectional mixing, and the time required to achieve this was not incorporated in our OTIS modelling. Meanwhile, stirring enhanced the extent of the interaction between

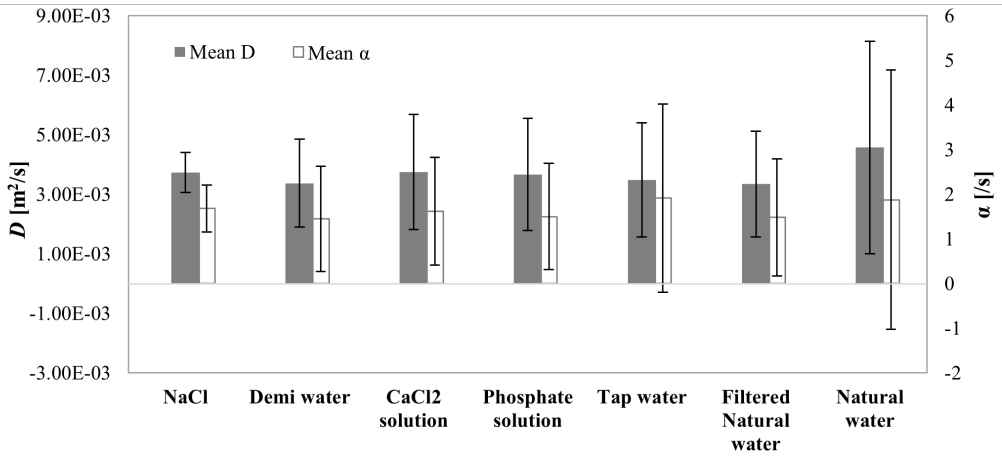

Figure 3.4: Mean estimate of $D_{L\,\text{Si-DNA}}$ & $\alpha_{\text{Si-DNA}}$ in comparison to $D_{L\,\text{NaCl}}$ & α_{NaCl} with error bars showing approximate 95% confidence limits.

tracers and the storage zone, so that tracer spreading caused by storage exchange reached an equilibrium stage soon after tracers entered the channel (Harvey and Wagner, 2000). This storage contribution was visible in the long tail of the BTCs, indicating a diffusion limited steady-state storage. Moreover, the calculated Damkohler number (DaI is ~ 10, see Eq A.4 in the Appendix A) also suggested the dominance of the storage process, caused by enhanced mixing. Thus, fitting the resultant long tail using a higher exchange rate compromised the fitting of the peak (details of OTISs model implementation are provided in the Appendix A). This effect could also be seen in the rest of BTCs of Si-DNAs.

Regardless of solution chemistry and colloidal stability, mean $D_{L\,\text{Si-DNA}}$ was essentially similar across 6 water types and was comparable to D_{NaCl} (Fig. 3.4). The same was observed for the mean $\alpha_{\text{Si-DNA}}$. The size of the confidence intervals of $D_{L\,\text{Si-DNA}}$ and $\alpha_{\text{Si-DNA}}$ were directly related to BTC noisy behaviour. When we plotted the variations against relative concentration, we observed that uncertainties were more associated with tails than peaks of BTCs in all water types, of which natural waters (filtered and non-filtered) had the largest coefficient variations (Fig.A.5). In natural waters, co-transporting with NOM and the likely presence of inorganic particles of various size ranges, Si-DNA microparticles were also subject to more complicated interactions such as steric, acid-base forces, etc. (Grasso* et al., 2002), likely resulting in some random attachment and detachment (e.g., flocculation and breakage due to shear forces). This could possibly contribute to a more "irregular" or noisier Si-DNA BTC, resulting in a larger confidence interval/uncertainty of $D_{L\,\text{Si-DNA}}$ in natural waters.

Likewise, Schiperski et al. (2016) also showed a similar range of dispersion estimations of silica fluorescent particles of micron-size to those of solute tracers in a karst river drainage system, despite differences in the surface properties of the particle tracers (Schiperski et al., 2016). The effect of hydrodynamics on colloidal particle transport in subsurface environments is widely studied (Elimelech et al., 2013; Sasidharan et al., 2014; Torkzaban et al., 2007). However, in surface waters, less research focuses on quantitatively comparing

colloids in the size range of 200 - 400 nm such as Si-DNA microparticles to that of solutes. Recently, DNA-tagged alginate-coated microparticles with a similar negative surface-charge in stream injection experiments showed to behave similarly to solute tracers in rising limb and peak of BTCs (Pang et al., 2020). Besides, amongst the few studies, most used particles of much larger size (such as natural organic/inorganic particulates, fluorescent latex particles, E.coli, and titanium-dioxide particles), and focused on distribution and fate without quantification of dispersion behavior (J. Drummond et al., 2014; Jamieson et al., 2005; Karwan and Saiers, 2009; J. D. Newbold et al., 2005; Phillips et al., 2019; Spencer et al., 2011; Wyer et al., 2010).

3.3.3. Mass recovery and uncertainty of DNA analysis

The mass recovery of each injection experiment is of fundamental importance for quantifying attenuation and transport behaviour of Si-DNA. We analyzed all samples and randomly performed lab duplicates. The mass recovery of Si-DNA with known initial concentration was calculated and ranged between 88% and 118% (Table 3.1). In Demi water, where minimal impurity or interfering ion was present, the mass recoveries of Si-DNA ranged between 91 – 97%. In such case, the Si-DNA mass was considered fully recovered. A mass ambiguity of less than 10% is well within the expected mass ambiguity range ~ ±20% which was mentioned earlier in Chapter 2.we speculate that the discrete nature of such heavier-than-fluid particles with a certain spread of size distribution might be the origin of the fluctuations in BTCs (Won et al., 2019). It would be very convenient if the size distribution was very limited such that every particle is essentially subject to the identical transport characteristics.

3.4. Conclusion

We concluded that the transport behaviour of Si-DNA resembled that of NaCl in surface-water relevant conditions, evidenced by BTCs with a similar range of D_L. With special attention paid to mass balance, the Si-DNA as colloids had overall more erratic BTCs than solute tracers, whereby the scatter increased a function of water quality complexity. The overall larger confidence interval of $D_{L\text{Si-DNA}}$ we contributed to the discrete nature of colloidal particles with a certain particle size distribution and possible minor shear-induced aggregation.

3.5. CRediT author statement

Conceptualization, Y.Tang, J.W.Foppen, T.A.Bogaard; Methodology, Y.Tang, J.W.Foppen, T.A.Bogaard; Software, Y.Tang, J.W.Foppen; Formal analysis, Y.Tang, J.W.Foppen, T.A.Bogaard; Investigation, Y.Tang; Resources, Y.Tang, J.W.Foppen, T.A.Bogaard; Data Curation, Y.Tang; Writing – Original Draft, Y.Tang; Writing – Review & Editing, Y.Tang, J.W.Foppen, T.A.Bogaard; Visualization, Y.Tang; Supervision, J.W.Foppen, T.A.Bogaard; Project administration, Y.Tang, T.A.Bogaard; Funding Acquisition, Y.Tang, J.W.Foppen, T.A.Bogaard.

4

Settling of SiDNAFe in river water

This chapter is based on Y. Tang, Zhang, et al., 2023: Tang, Y., Zhang, F., Bogaard, T., Chassagne, C., Ali, Z., Bandyopadhyay, S., & Foppen, J. W. (2023). Settling of superparamagnetic silica encapsulated DNA microparticles in river water. Hydrological Processes, 37(1), e14801.

4.1. INTRODUCTION

For the past two decades, researchers have been exploring synthetic DNA strands and encapsulated DNA MPs for environmental tracing (e.g.,Dahlke et al., 2015; Foppen et al., 2013; A. N. Sharma et al., 2012). As mentioned before in Chapter 2, superparamagnetic DNA-tagged silica microparticle (SiDNAFe) was designed with a magnetite core in order to facilitate easy harvesting and up-concentration from larger volumes of sample water (Puddu et al., 2014; A. Sharma et al., 2021). SiDNAFe is expected to behave like colloidal particle, whereby DLVO theory can be used to interpret findings (Petosa et al., 2010; Praetorius et al., 2020). Homo-aggregation and hetero-aggregation of nano/micro-particles were studied in the presence and/or the absence of natural organic matter (NOM) and suspended particulate matter (SPM) of varied types and concentrations in relevant freshwater conditions (e.g., Abe et al., 2011; Domingos et al., 2009; Liu et al., 2011; Metin et al., 2014; Oncsik et al., 2014;Ottofuelling et al., 2011; Quik et al., 2014; J. Zhao et al., 2021). Homo-aggregation was shown to be quantitatively unimportant at realistic environmental concentrations and relevant time scales, yet hetero-aggregation was considered as a more important mechanism given the higher concentrations of natural colloids and SPM (Labille et al., 2015; Lead et al., 2018). Overall, driving factors in particle hetero-aggregation in rivers mainly were pH, ionic strength, the presence of divalent ions, and the type and/or the concentration of NOM and SPM (Baalousha et al., 2016; Buffle et al., 1998; Klaine et al., 2008; Lagarde et al., 2016; Y. Zhang et al., 2009).

Particle settling is considered to be an important process in freshwater systems, representing a downward energy/nutrient/contaminant flux from the water column to the benthic environment. Of particular interest are the settling of riverine SPM (e.g., fine and coarse organic particulate matter), engineered nano/micro particles, and potentially their co-settling (Hochella Jr et al., 2019; Hünken and Mutz, 2007; Kumar et al., 2021; Vincent and Hoellein, 2021). Riverine SPM is mainly composed of macro- and micro-aggregates/flocs of inorganic and biogenic colloidal particles, organized by bacterial exopolymeric substances (EPS) (Lartiges et al., 2001; Many et al., 2016). The high surface area to volume ratio and high organic content of SPM is conducive to interactions with other colloids and substances (J. D. Newbold et al., 2005; Ongley et al., 1992). Consequently, SPM settles differently from the settling of its constituent particles. It is difficult to use Stokes' law to predict the settling velocity of SPM, due to the various single-aggregate densities over the spectrum of SPM sizes (Khelifa and Hill, 2006; Larsen et al., 2009). The resultant settling of SPM is a collective of contributing factors, such as structural characteristics, bulk densities, the effect of SPM and thus the flocculation potential (Lee et al., 2019; Zimmermann-Timm, 2002). For example, enhanced SPM flocculation was found in nutrient-rich (e.g., EPS) water conditions, where aggregates were formed with significantly larger sizes (F. H. Tang and Maggi, 2016). Nevertheless, the settling velocities of SPM aggregates were found mostly invariant and ranged between 1 and 4 mm/s in natural river environments across a wide range of density, size and organic matter fraction (Maggi and Tang, 2015).

For engineered nano/micro particles (ENP), given the practical limitations of quantifying aggregation-settling processes in real natural environments, most studies focused on the settling in quiescent conditions, to understand either enhanced or diminished settling as a result of hetero-aggregation or stabilization (Klaine et al., 2008; Lagarde et al., 2016; Petosa et al., 2010; Quik et al., 2014). Results from those static settling experiments could

be used to obtain important parameters (e.g., hetero-aggregation and sedimentation rate) for modelling the exposure concentration of nano/micro particles in large rivers (Besseling et al., 2017; Garner et al., 2017; Praetorius et al., 2012; Quik et al., 2015). Usually, co-settling experiments of ENP with (e.g., EPS) and SPM employ higher than realistic concentrations to observe the co-settling due to strong hetero-aggregation. However, weak hetero-aggregation, such as a small amount of ENP adsorption on cell surfaces, may have detrimental effects on organisms (Ma et al., 2015). SiDNAFe could be an alternative for studies on potential ecotoxicological effects of extremely low concentrations of ENP in natural environment.

Sedimentation could be an important removal mechanism for SiDNAFe which would jeopardize its application as particulate tracer. Encountering naturally occurring material, such as SPM, SiDNAFe would likely undergo aggregation and subsequent settling, which could alter the transport and fate of the SiDNAFe in aqueous conditions. For example, the sedimentation rate of dispersed nano/microparticles in the presence of SPM was found to be significantly higher than those without (Li et al., 2019; Velzeboer et al., 2014). Reduced transport of nano/micro-particles could result from a high attachment efficiency to SPM, where the resultant aggregates are subject to gravitational sedimentation due to increased size and density (Petosa et al., 2010; Shevlin et al., 2018). Thus, the settling potential of SiDNAFe in real river waters in quiescent conditions needs to be investigated before their release in rivers, which is of practical importance when employed in future tracing applications. In this regard, the main objective was to understand and quantify the settling behaviour of SiDNAFe, by conducting a series of settling experiments with filtered and non-filtered natural river waters.

4.2. Materials and Methods

4.2.1. SiDNAFe characterization

As mentioned in Chapter 2, to mitigate inhibition during qPCR, SiDNAFe was magnetically separated from river water, re-dispersed and up-concentrated in MQ (Fig. 4.1). Zeta potential(ζ) of SiDNAFe was measured in filtered river water and in MQ, respectively, by using a Zetasizer (Zetasizer Nano S, Malvern Instr., UK). Hydrodynamic diameter (D_{hDLS}) of SiDNAFe was obtained by dynamic light scattering (DLS). Distribution algorithm (General Purpose) and cumulant analysis were both used to calculated the D_{hDLS} from the measured correlogram. The General Purpose algorithm fitted the exponentially decaying correlogram to a sum over several exponential decay functions that decayed at different rates, achieved by non-negative least squares (Morrison et al., 1985). The results were reported in the displayed size distribution as peaks, each with a characteristic width. In contrast, the cumulant analysis modeled the particle size distribution as a Gaussian, with the average hydrodynamic diameter (Z-Ave) being the mean value and the polydispersity index (PDI) being the variance of the hypothetical Gaussian (Koppel, 1972; Stetefeld et al., 2016). To have good scattered light signals, a SiDNAFe concentration of 10^{-2} mg/mL was used, which was 1000 times higher than the settling experiments (10^{-5} mg/mL). The measurement position was at the center of the cell with 173° backscattering. The particle size distribution (PSD) of SiDNAFe suspended in MQ was characterized based on their sedimentation rate in a centrifugal force field by a centrifugal separation analysis using a LUMiSizer (STEP-Technology, L.U.M

GmbH, Berlin, Germany). Briefly, the apparatus measures light transmission over the total length of the sample cell containing sample suspension, whereby time dependence of the position of the interface particle-free fluid/particle suspension was determined (Lerche, 2002). These transmission profiles were then transformed into velocity distributions and size distributions given the particle density (see details in the Appendix A).

4.2.2. CHARACTERIZATION OF RIVER WATER

As mentioned earlier, three river water types were collected from different sources, each with differing SPM and NOM content (Meuse, Strijbeek, and Merkske). River water sampling was carried out on the same day in winter of 2021 (06/01/2021). Upon collecting water samples, iodide was added to reach a concentration of 1 mg/L to minimize microbial activity during sample storage. Water samples were kept at 4 ºC in polyethylene sample containers and completely filled and tightened with double-sealed plastic caps. The OM content of river water was measured as dissolved organic carbon (DOC, in mg-C/L) using the combustion technique with a total organic carbon analyser (TOC-VCPN (TN), Shimadzu, Japan). EC and pH were measured in situ using an EC meter and pH meter, respectively. The total suspended solids (TSS) in river water samples were calculated by drying the filtrate ($\oint$ 1.2μm) at 105 °C and weighing the dry weight of the filtrate. Main compositions of SPM (> 1.2 μm) in river water samples were identified by using Energy-dispersive X-ray spectroscopy with a Scanning Electron Microscope (JSM-6010A, JEOL, Tokyo, Japan). In addition, high-resolution images of the SPM were taken by the Scanning Electron Microscope operated at 20 kV. As proxies for SPM (Velde, 1977; Velzeboer et al., 2014), total Fe and Al were measured by a PlasmaQuant MS Inductively Coupled Plasma Mass Spectrometry (ICP-MS) (Alanlytik Jena, Jena, Germany). Before ICP-MS measurement, to dissolve ICP-MS completely, river water samples were microwave-digested with 65% HNO_3 using a CEM MARS5 Digestion Oven (CEM corporation, USA).

4.2.3. SETTLING EXPERIMENTS

The settling of the SiDNAFe was recorded by measuring DNA concentration of the supernatant at a fixed depth as a function of time. Filtered (0.45 μm cellulose-acetate filter, MF-Millipore® & 1.2 μm glass microfiber filter (GF/C), Whatman) and unfiltered river water types were used for the settling experiments. The initial concentration (C_0) of the SiDNAFe was 10^{-5} mg/mL, which was prepared by diluting the stock tracer solution (1 mg/mL SiDNAFe suspended in MQ) in filtered, in unfiltered river water, or in MQ (as a control). Subsequently, well-mixed suspensions of SiDNAFe were aliquoted in 15 mL polythene tubes for separate sample-taking and then allowed to quiescently settle at 4°C (in-situ monitored by a micro temperature/pressure gauge, Van Essen) in a refrigerator for 2, 4, 6, 22, 24 and 30 hours. Following the settling for the selected time period, 1 mL of sample was taken with a micropipette from 1 cm (~ ±1 mm) below the water surface for sample analysis (Fig. 4.1). In each water type, settling experiments were performed in duplicate. At each time step, SiDNAFe concentration was quantified in duplicate using qPCR. The SiDNAFe settling curve was based on the averaged relative mass concentration C/C_0 with the standard deviation based on four measurements at each time step.

To assess homo-aggregation of SiDNAFe, D_{hDLS} of SiDNAFe was measured in MQ at 4°C before, during, and after a 4-hour settling experiment, by using DLS in a Zeta-

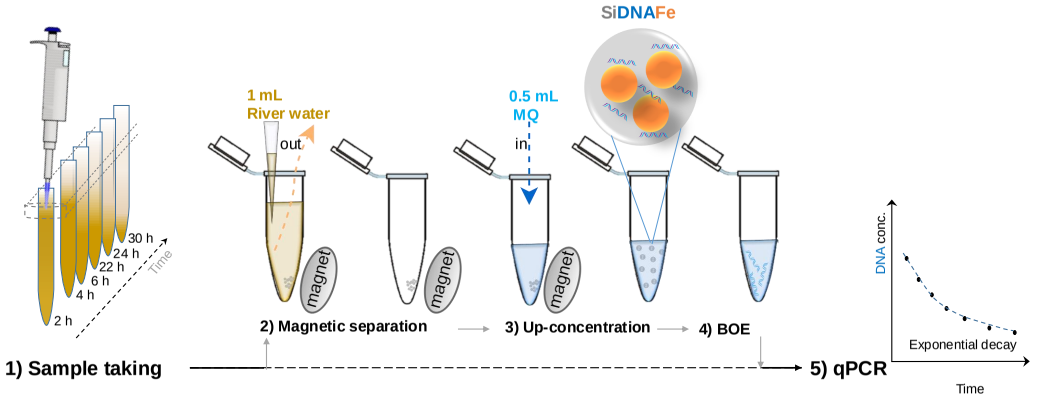

Figure 4.1: A settling experiment including sample analysis. 1) A 1 mL sample was taken from a settling tube; 2) In this sample solution, SiDNAFe was magnetically separated by using an external magnet; 3) SiDNAFe was up-concentrated by adding 0.5 mL MQ ; 4) Encapsulated DNA was released by adding buffered oxide etch solution (BOE); 5) DNA concentration was determined using qPCR.

sizer Nano SZ. Additionally, for comparison, the same settling experiment was conducted with SiDNAFe suspended in 5 mM phosphate buffer (0.77 g/L of $Na_2HPO_4{\cdot}7H_20$ (0.0029 M) (EMSURE®, Merck KgaA, Germany) and 0.29 g/L of $NaH_2PO_4{\cdot}H_20$ (0.0021 M) (J.T.Baker, Spain) dissolved in Demi; pH adjusted to 7.0 – 7.1 using 100 mM NaOH (J.T. Baker, Poland)), in which SiDNAFe was more negatively charged (Chakraborty et al., 2022). To better interpret the DLS measurement results, the same settling experiment was conducted with manually milled silica colloids from silica power of 0.2-0.7 mm (Sigma-Aldrich, Germany, product number: 85356) with an approximate concentration 10 times higher (~ 0.1 mg/mL). As a control, D_{hDLS} was measured right after sample sonication and vortexing prior to the settling experiment. The sample was allowed to settle without disturbance for 4 hours, during which D_{hDLS} was recorded every 0.5 to 1 hour. After that, final measurements were taken after the sample was gently inverted several times.

4

4.2.4. Calculating Settling

In MQ, settling of SiDNAFe can be described by Stokes' law (Stokes et al., 1851), whereby SiDNAFe settled without collision and flocculation in a dilute suspension. The terminal settling velocity of the SiDNAFe with radius i is given by (Stokes et al., 1851):

$$v_i = \frac{2}{9} \times \frac{\rho_p - \rho_f}{\mu} \times g \times i^2 \tag{4.1}$$

With $\rho_p - \rho_f$ being equal to the density difference between particles (p) and fluid (f) [kg/m^3], μ the dynamic viscosity [Pa·s] of the particle-free suspension medium, g the gravitational constant [m/s^2], and i particle radius [m].

From the water surface (depth $h = 0$) down to any given depth (h) at time (t) (Fig. 4.2), the suspension would be devoid of particles with settling velocity greater than $\frac{h}{t}$ and would contain particles with a settling velocity less than $\frac{h}{t}$. The concentration c at a given h and time t would be the sum of the original concentrations of particles which settle slower than $\frac{h}{t}$:

$$c(h,t) = \sum_{alli} (c_i | v_i \iiint \frac{h}{t}) = \sum_{alli} c_{0,i} H_{v_i t} \tag{4.2}$$

where c_i and v_i denote the mass concentration [mg/mL] and the terminal settling velocity [mm/h] of particle size class i, respectively.

At the required time, we took 1 mL of suspension at a fixed depth of the settling column from a slice of water in the settling tube between h_1 and h_2 (Fig. 4.2). Assuming a monodisperse suspension of SiDNAFe with a particle radius i having particle number N_i being in the water column between the water surface 0 and the depth h_2, at any time t, the mass concentration between depth h_1 and h_2, could be described as:

$$c_i(h_1 \sim h_2, t) = \begin{cases} N_i * (h_2 - h_1)/h_2 * V_i * \rho & \text{for} \quad v_i * t \iiint h_1 \\ N_1 * (h_2 - v_i * t)/h_2 * V_i * \rho & \text{for} \quad h_1 \le v_i * t \le h_2 \\ 0 & \text{for} \quad otherwise \end{cases}$$

Where V_i is the spherical volume of a particle with radius i, and ρ is the density of SiDNAFe. Then, the relative mass concentration, C_R, could be described as:

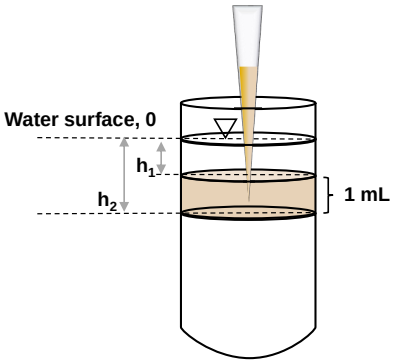

Figure 4.2: Schematic representation of the sampled volume in the numerical simulation.

$$C_R = \sum_{alli} C_i(h_1 \sim h_2, t) / \sum_{alli} N_i * (h_2 - h_1)/h_2 * V_i * \rho \tag{4.3}$$

In addition, the C_R of SiDNAFe was calculated using the measured PSD from the LUMiSizer.

Finally, a best-fit PSD was derived from the observed settling curve, using Genetic Algorithm, available in Python. This algorithm solves an optimization problem based on the mechanics of natural selection, whereby fitting parameters can be automatically improved (Holland, 1992).

4.2.5. STATISTICAL ANALYSIS

Two-sample t-test (p <0.05) was used to determine whether there was a significant difference between the settling of the SiDNAFe in natural waters and in MQ. The null hypothesis was that the observed settling in MQ was not significantly different from the settling in river water types.

4.3. RESULTS

The SPM presented in the three river waters was negatively charged, with ζ ranging between ~ 15.9 mV and ~ 18.6 mV (Table 4.1), with extremely polydisperse size distributions (results not shown). Elemental analysis showed that Si, Fe and Al were dominant (Fig. 4.3, details on elemental data (%) in the Appendix A). In fact, SPM from the Meuse was an assemblage of heterogeneous aggregates and polymer-like material of various shapes and sizes, where Si, Fe, and Al elements were distributed across the entire frame with no particular pattern. Selected as proxies of the SPM, total Fe and total Al in each river water type were also quantified (Fig. 4.4f). Most SPM mass was found in the size classes smaller than 0.45 μm and larger than 1.2 μm in these three river types. The mass concentration of Fe and Al reduced as the filter size reduced, with the largest Fe concentration decrease (more than 50%) from the unfiltered to 1.2 μm filtered sample water. Then, from 1.2 μm to 0.45 μm, Fe and Al concentrations hardly changed. Especially, ~50% of total Fe and Al originated from the size classes smaller than 0.45 μm in case of Strijbeek and Merkske. Conversely,

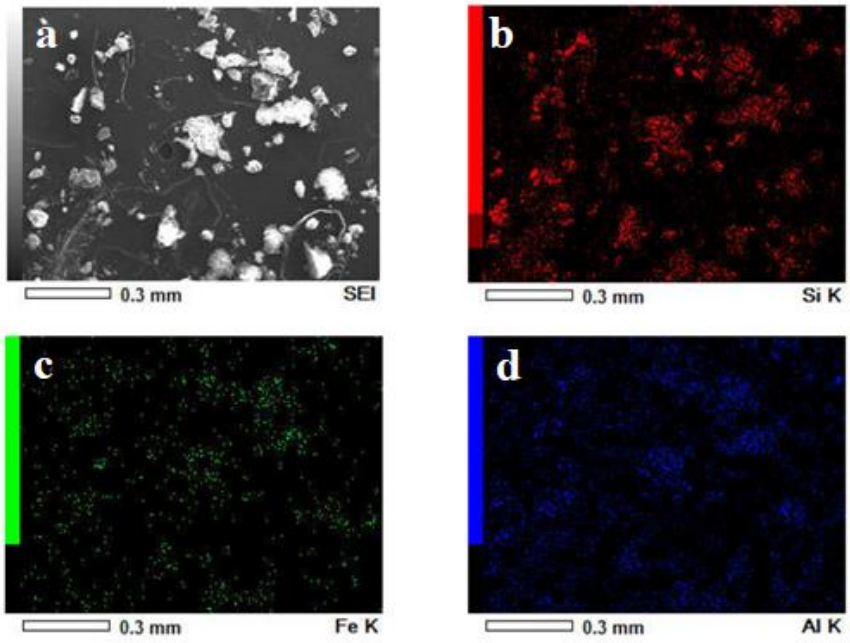

Figure 4.3: Energy-dispersive X-ray spectroscopy (EDS) mapping of dried SPM from Meuse river water, including (a) Scanning Electron Microscope image (x 100 magnification), (b) Si element, (c) Fe element, (d) Al element.

SPM in Meuse was dominant by inorganic particles larger than 1.2 μm.

ζ of SiDNAFe in the three rivers was similar to that in MQ (-22 – -24 mV; Table 4.1), while the electrical conductivity was in a typical fresh water range (371 - 543 μS/cm; Table 4.1). Meuse water had highest TSS (10.4 mg/L) and lowest DOC content (6.0 mg/L), while the other two river water shared similar characteristic with high DOC (~17.0 mg/L) and low TSS (2.0 mg/L).

We observed that in MQ, ~ 40% - 50% of the SiDNAFe mass concentration rapidly settled out in the first 2 to 6 hours (Fig. 4.4; referred to as 'stage 1' hereafter). Then, from 6-30 hours, the SiDNAFe concentration remained almost constant (referred to as 'stage 2') with a significantly ($p < 0.01$) lower settling rate compared to the first 6 hour of settling. The settling behaviour of SiDNAFe in river water resembled that in MQ (Fig. 4.4, Table A.7a), whereby we also observed two distinct stages with a significantly different ($p < 0.01$) settling rate, regardless of river water type or filter size. In fact, there was no statistically significant difference ($p > 0.05$) between the settling in MQ ("MQ-obs." in Table 4.1) and in river waters (Table 4.1). In addition, the difference between the two stages was also clear from the size of the error bars, as these were significantly larger for stage 1 settling than for stage 2 settling ($p < 0.05$; Table A.7b). Furthermore, the observed settling in all water types was statistically significantly larger ($p < 0.05$) than the expected Stokes' settling, which was derived from the PSD measured by LUMiSizer in MQ (Fig. 4.4 and "MQ-sim." in Table 4.1). This discrepancy was likely due to the rapid settling during stage 1. During stage 2, the SiDNAFe generally followed Stokes' settling, as the subtle decline in concentration

	Unit	Meuse	Strijbeek	Merkske	MQ
SiDNAFe ζ	mV	-22.7±3.3	-22.6±3.3	-22.6±3.1	-24.2±3.8
SPM ζ	mV	-16.5±4.4	-18.6±4.4	-15.9±3.5	-
EC	µS/cm	371	491	543	-
DOC	mg/L	6.0	17.0	17.5	0.1
TSS	mg/L	10.4	2.0	2.0	n.a.
pH	mg/L	7.9	7.1	7.3	6.5
p-value (< 0.05)					
MQ-obs.	0.45 µm	0.65	0.11	0.12	-
	1.2 µm	0.21	0.76	0.39	
	Non-filtered	0.57	0.45	0.19	
MQ-sim.	0.45 µm	0.0027	0.0018	0.0043	0.0020
	1.2 µm	0.0099	0.0047	0.0014	
	Non-filtered	0.0038	0.023	0.0012	

Table 4.1: Characteristics of water types, the zeta potential of SiDNAFe and p-value from t-test.

from hour 6 to hour 30 visually concurred well with the descending slope of the expected settling curve. Finally, we found a best-fit PSD with a mean radius of 338 nm by fitting the measured settling data (Fig. 4.4e). This mean radius was three times larger than the measured mean radius (i.e., 101 nm; Table A.6).

The settling experiment of SiDNAFe using a 1000-times concentrated particle suspension in MQ showed that only one peak was visible before settling, while a second peak formed during settling (Fig. 4.5a, upper panel). After the experiment and after inverting the sample, a peak appeared with an almost 8 - 10 times larger diameter than the one before settling (Fig. 4.5a the upper panel). Moreover, PDI showed a positive correlation with Z-Ave, with data points initially clustered at a consistent size and gradually scattered as a function of Z-Ave (Fig. 4.5a the lower panel), indicating aggregation (Malm and Corbett, 2019). For comparison, for SiDNAFe suspended in 5 mM phosphate buffer and SiO_2 colloids suspended in MQ, no hydrodynamic diameter change was observed (Fig. 4.5b – c the upper panel), with well-defined clusters of PDI data indicating colloidal stability (Fig. 4.5b – c the lower panel).

4.4. Discussion

4.4.1. Settling of SiDNAFe in MQ

In MQ, we observed two distinct stages (i.e., the fast and the slow stages) of settling. We interpreted the fast settling during stage 1 due to the presence of relatively large aggregates in suspension. Assuming SiDNAFe was initially completely suspended in MQ with a low volume fraction (a very dilute suspension of ~ 10^{-5} mg/mL), for quiescent conditions, SiDNAFe would have to come close enough to form aggregates through random Brownian motion and/or differential sedimentation, whereby repulsive interparticle and/or hydrodynamic interactions would hinder the approach of colliding particles. Given the small mean diameter of SiDNAFe (i.e., ~ 200 nm), the collision rate derived from Brownian motion was likely more significant than from differential sedimentation (Elimelech et al., 2013). More specifically, the estimated collision efficiency for perikinetic aggregation was extremely low in the presence of an energy barrier of > 30 kBT (See Table A.5 in the Appendix A). Under such unfavourable conditions, only one in every million collisions would occur between particles having sufficient energy to overcome the barrier (Elimelech et al., 2013). Based on this reasoning, we speculate that a small portion of aggregates of SiDNAFe was formed due to increased shear force (Johnson et al., 1996; Van de Ven and Mason, 1977) during the manual mixing when diluting for different water types prior to the actual settling experiments. Shear-induced aggregation of a similar type of DNA-tagged silica microparticle (i.e., Si-DNA in Chapter 3) was also observed and discussed in our previous research (Y. Tang et al., 2021). Moreover, as mentioned before, we observed an increase in the D_{hDLS} of SiDNAFe during a 4-hour settling experiment using a 1000-times concentrated particle suspension (10^{-2} mg/mL) in MQ (Fig. 4.5a the upper panel) compared to the previous settling experiment (10^{-5} mg/mL). From these observations, we inferred that SiDNAFe homo-aggregation had taken place in MQ, whereas no homo-aggregation had taken place when SiDNAFe was more colloidally stable. So, SiDNAFe homo-aggregation was very likely occurring during the sample preparation stage before the settling experiments.

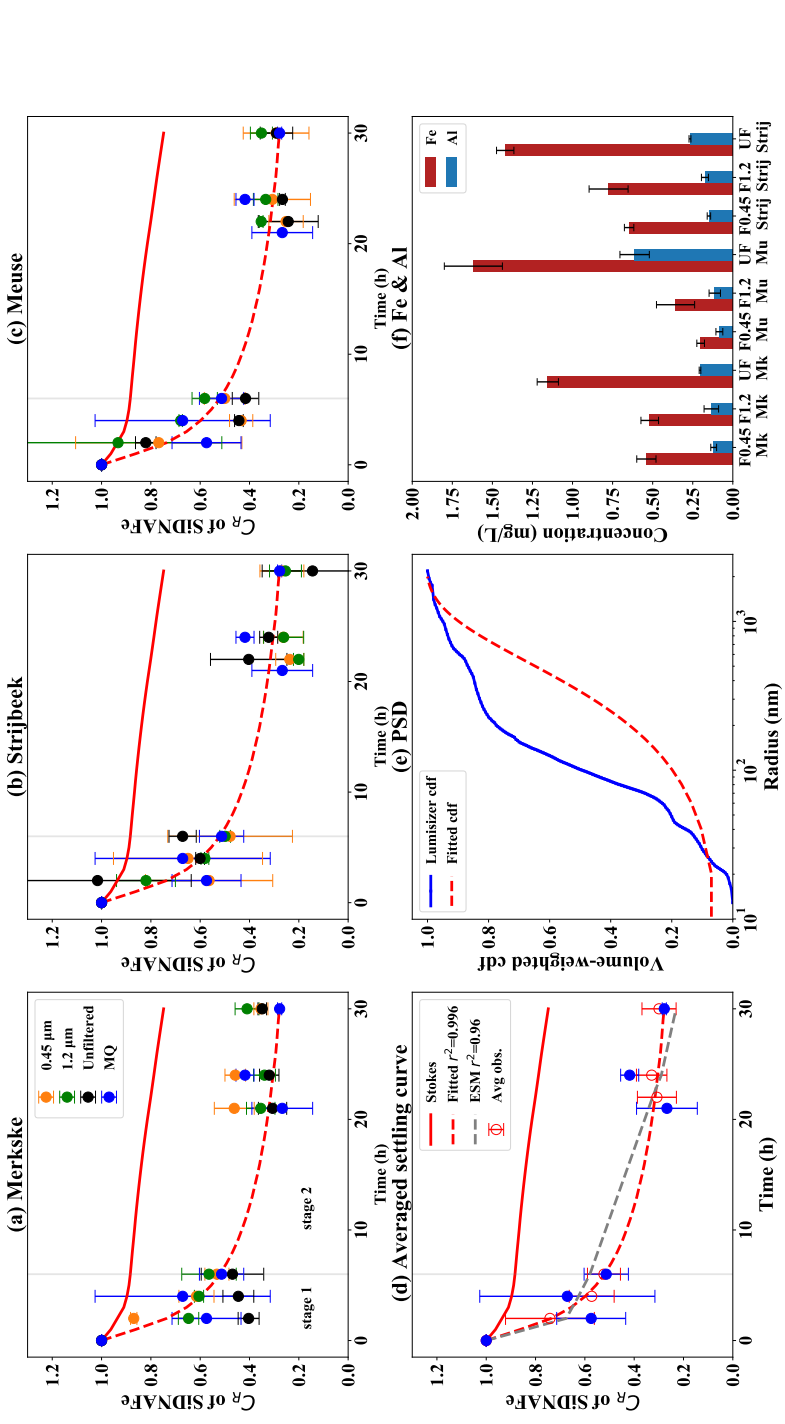

Figure 4.4: a - d Settling of the SiDNAFe in MQ and in filtered and unfiltered river water types. The red solid and the red dashed curves delineate Stokes' settling with a PSD measured by LUMiSizer and with a PSD fitted from the observed curve, respectively, while the grey dashed curve represents settling following an exponential settling model. e Volume-weighted cumulative size distribution function (cdf) of the SiDNAFe measured by LUMiSizer in comparison with the fitted cdf. f Total Fe and total Al as proxies of the SPM in filtered and unfiltered river waters. F0.45, F1.2, and UF: 0.45-μm, 1.2-μm filtered, and unfiltered water; Mk, Mu, and Strij: Merkske, Meuse, and Strijbeek, respectively.

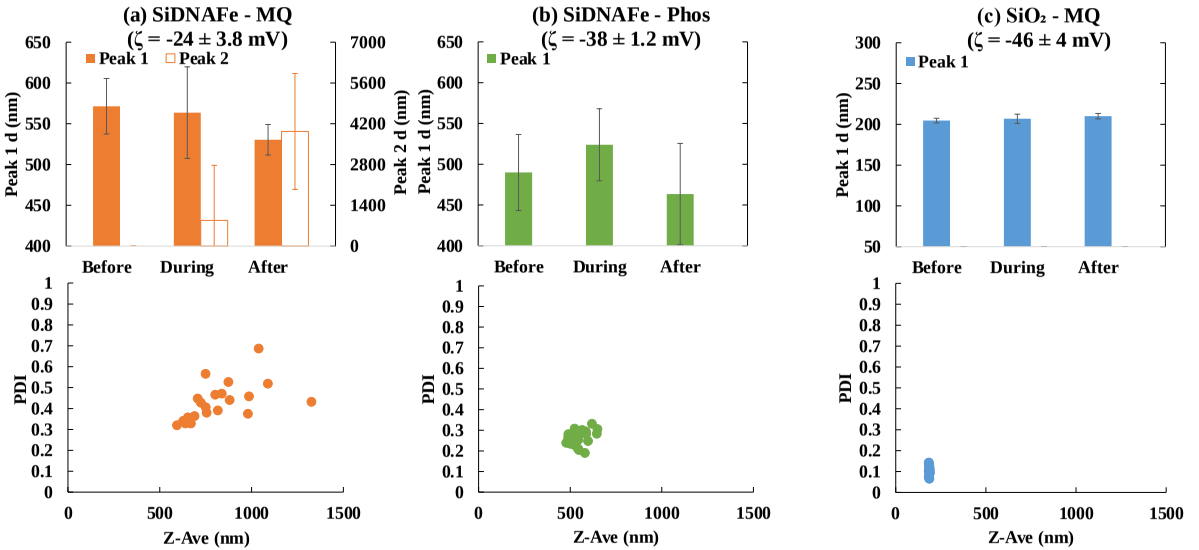

Figure 4.5: Change of mean D_{hDLS} over 4 hours and Z-Ave as a function of PDI in settling experiments performed in a Zetasizer. (a) SiDNAFe suspended in MQ (ζ: -24 ± 3.8 mV); (b) SiDNAFe suspended in a phosphate buffer (ζ: -38 ± 1.2 mV); (c) SiO_2 colloids suspended in MQ (ζ: -46 ± 4 mV). In the upper panel of (a) – (c), peak 1 and 2 were derived from the distribution algorithm- General Purpose. Peak 1 is the main peak, plotted on the primary y-axis; while peak 2 is the minor peak, plotted on the secondary y-axis. The error bars are standard deviations of 15 measurements. "Before", "During", and "After" represent before the settling, during the settling, and gently re-suspended after the settling experiment. In the lower panel of (a) – (c), Z-Ave and PDI were calculated using the cumulant analysis.

4.4.2. Settling in river water

The main elemental compositions of SPM in river waters were Al, Fe and Si, which corresponds to the main inorganic fraction of most riverine SPM aggregates, such as silicate mineral and clay (Slomberg et al., 2016; M. Wilson et al., 2014). The SPM found in our three river waters were likely aggregates of inorganic particles and debris associated with organic materials, as reported by Lartiges et al. (2001). Coexisting with SPM in river waters, SiDNAFe might hetero-aggregate with SPM, resulting in enhanced settling (Velzeboer et al., 2014; B. Zhu et al., 2018). Surprisingly, regardless of the filtered/unfiltered river water, SiDNAFe settled identically to the settling in MQ, where hetero-aggregation was absent. From this observation, we inferred that SiDNAFe did not hetero-aggregate with SPM present in these river waters. Foremost, SiDNAFe was negatively charged with a similar ζ in the three river waters, exhibiting a relatively high energy barrier (with low collision efficiency, as discussed earlier) and a negligible secondary energy minimum (Table A.5). Likewise, SPM found in these three river water types was slightly less negatively charged, which is within the range of ζ reported for most SPM found in freshwater (i.e., -15 mV to -30 mV; Buffle et al., 1998; Jekel, 1986; Ongerth and Pecoraro, 1996; Kim and Sansalone, 2008; Domingos et al., 2009). For solution chemistry conditions like in the case of natural river water, repulsive interactions such as electrostatic repulsion or steric hindrance would dominate and thus likely hinder the approach between SiDNAFe and SPM (Petosa et al., 2010). In our experiments, a rigorous inspection of the composition and structures of the SPM was beyond the scope. However, we would like to speculate that, compared with SiDNAFe, SPM would probably settle much faster and thus rapidly removed itself from the sampling section. Maggi and Tang (2015) found that SPM in freshwater settled with mostly invariant settling velocities, ranging from 1 to 4 mm/s, across a broad spectrum of density, size and organic matter fraction. This was because of the fractal architecture of SPM, which balanced the increase in floc size and the decrease in effective density. In this regard, we may not overlook the chance of differential settling, whereby collisions occurred when rapidly settling SPM overtook and intercepted SiDNAFe settling more slowly (Lick et al., 1993, Zimmermann-Timm, 2002). This could to some extent contribute to the larger error bars detected in the first stage.

4.4.3. From quiescent to turbulent conditions

Compared with the quiescent settling condition, turbulent flows are most likely to be encountered in reality. In real river conditions, inherent properties of microparticles (e.g., density, shape, and size) and hydrodynamic conditions govern the trajectory of nano- and micro-particles (Haberstroh et al., 2021; Hochella Jr et al., 2019; Isachenko, 2020; Vincent and Hoellein, 2021; Waldschläger and Schüttrumpf, 2019). For colloids like SiDNAFe with a larger-than-water density, the sinking rate was likely controlled by the aggregation rates and the shear flow (Quik et al., 2015). Colloidal masses could stay stable in a certain range of shear rates, but could aggregate at higher and lower shear rates (Van de Ven and Mason, 1977). Besides, vertical mixing could also be a significant factor determining the probability of particles hitting each other (McNair et al., 1997). Under turbulent flows where more mixing occurs at higher shear velocities, rapid vertical transport would occur, resulting in a more uniform vertical distribution of particles (Ballent et al., 2012). In this regard, increased mixing and cross-sectional particle exchange would probably delay the

downstream transport or detain microparticles (Frei et al., 2019; Haberstroh et al., 2021). Moreover, microparticles suspended in near-bed flows are affected by the bed geometry (Phillips et al., 2019). Such microparticles could be easily transferred from the near-bed flows into bed sediments due to a local increase in pressure driven flow into and out of the porous bed (Packman et al., 2000). Under laminar flow conditions, SiDNAFe would have a vertical velocity due to the gravity-driven settling in a similar fashion as in quiescent conditions (Hamm et al., 2011). SiDNAFe would likely be transported downstream as the concentration in the water column depleted gradually due to the gravity-driven settling (Kumar et al., 2021).

Experimental studies on settling and deposition in running rivers and streams originally focused on the cycling of particulate nutrients, such as phosphorus (J. D. Newbold et al., 1981; J. Newbold et al., 1983) and fine and coarse particulate organic matter (Paul and Hall Jr, 2002; Wanner and Pusch, 2000). Their findings suggested that as particles move downstream they will decline exponentially with time or longitudinal transport distance. A dimensionless velocity W was defined as the ratio of the effective settling velocity observed in a given flow, to that expected in still water. Thus, values of W >1 indicate 'enhanced' settling, and W < 1 diminished settling (Hamm et al., 2011). The value of W varies according to particle size, and the factors which affect particle deposition in flowing waters can be interpreted according to the relative influence of gravity and particle momentum (Hochella Jr et al., 2019).

Current spatio-temporally explicit transport modelling of nano- and micro-particles in rivers utilised the Stokes' settling velocity in still water to model the sedimentation and/or deposition process (Lazar et al., 2010; Nizzetto et al., 2016). Taking into account the effect of aggregation on the settling, the concentration profiles of environmental nanomaterials were not so different from the one which did not (Quik et al., 2015). In any case of enhanced or diminished settling during transport in real rivers, we think that the longitudinal concentration profile of SiDNAFe would likely remain comparable to what has been measured for quiescent settling, that is, an exponential-like distribution of SiDNAFe for transport times and distances (Battin et al., 2009; McNair and Newbold, 2012). For the sake of applications of such DNA tracers in future field tracing experiments, the implication of such settling experiment lies in understanding to what extent SiDNAFe would interact with the surroundings and thus remain suspended until the sampling point. Since the settling of such heavier-than-water microparticles of DNA tracers is deemed to happen, but -as observed- not substantially, based on our settling results, a pre-defined mass loss rate of first-order should be inserted in the mass transport equation (e.g. advection-dispersion-transient storage), for modelling transport of SiDNAFe in real world tracing experiments. As an example, we used an exponential settling function to fit the averaged settling data (exponential settling model in Fig. 4.4d), and arrived at a decay rate of 0.038 per hour for the best-fit case (R^2 = 0.96). Besides, there is no significant difference between the exponential settling model fitted curve and the observed averaged curve at 95% significance level ($p > 0.05$).

4.4.4. Uncertainty of DNA analysis

The relatively large error bars across all experiments were due to random variations of qPCR readings, differences per sample in effect of inhibitors, and dilution issues. The first can account for ~ ±20% of mass variations, and has been widely recognized and

also discussed in Chapter 2 on DNA-based tracers (Mikutis et al., 2018; Y. Tang et al., 2021). With regard to the second, in our qPCR lab, we optimized the protocol so that the trade-off was minimized between diluting the inhibitors and consuming too much time for the labour-intensive washing and up-concentration. As discussed in Chapter 2, much larger differences existed among replicates when SiDNAFe with lower concentration were exposed to river waters, especially Strijbeek water. Further, the 10-fold dilution series which was used to transform Cq to the mass concentration, was more reliable and reproducible after washing and up-concentrating the SiDNAFe with MQ. Although qPCR theoretically allows the detection of one DNA molecule (Watson et al., 1992), in practice, there is a range of minimal DNA concentrations which is acceptable to be used as initial concentrations to obtain reliable amplifications, as mentioned in Chapter 2. The initial concentration chosen for the settling experiments was the middle point between the highest and the lowest measured concentrations.

4.5. Conclusions

In quiescent conditions, more than 60% of SiDNAFe settled within 30 hours, which started with a rapid settling phase followed by an exponential-like slow settling phase in the three river waters we used (Meuse, Merkske, and Strijbeek) plus MQ water. D_{hDLS} of SiDNAFe increased over time, with its PDI positively correlated with the particle size, in suspensions with a 1000-times higher particle concentration. From these observations, we inferred that the rapid SiDNAFe settling was mainly due to homo-aggregation and not due to hetero-aggregation (e.g. with particulate matter present in these river waters). Incorporating a first-order mass loss term in the order of 0.038 per hour, which mimics the exponential phase of the settling in quiescent conditions seemed an adequate step forward when modelling the transport of SiDNAFe in river injection experiments.

4.6. CRediT author statement

Conceptualization, Y.Tang, J.W.Foppen, T.A.Bogaard; Methodology, Y.Tang, J.W.Foppen, T.A.Bogaard, C.Chassagne; Formal analysis, Y.Tang, F.Zhang, C.Chassagne, J.W.Foppen, T.A.Bogaard; Investigation, Y.Tang, F.Zhang, Z.Ali; Resources, Y.Tang, J.W.Foppen, T.A.Bogaard, S.Bandyopadhyay; Data Curation, Y.Tang, F.Zhang, Z.Ali; Writing – Original Draft, Y.Tang; Writing – Review & Editing, Y.Tang, T.Bogaard, C.Chassagne, S.Bandyopadhyay, J.W.Foppen; Visualization, Y.Tang; Supervision, J.W.Foppen, T.A.Bogaard; Project administration, Y.Tang, T.A.Bogaard; Funding Acquisition, Y. Tang, T.A.Bogaard, J.W.Foppen, S.Bandyopadhyay.

5

Effect of channel bed sediment on the mass loss and transport behaviour of SiDNAFe

This chapter is based on Y. Tang, van Rhijn, et al., 2023: Tang, Y., van Rhijn, F., Abdelrady, A., Foppen, J. W., & Bogaard, T. (2023). Effect of channel bed sediment on the transport behaviour of superparamagnetic silica encapsulated DNA microparticles in open channel injection experiments. Hydrological Processes, 37(9), e14962.

5.1. Introduction

DNA tracers for hydrological investigations have received an increased interest over the past decade (Y. Zhang and Huang, 2022). The micro-sized DNA-tagged tracers seem to have more tracing potential for applications in surface water than in subsurface porous media, mainly because they are subject to filtration removal in porous media (Pang et al., 2020). Nevertheless, DNA-tagged microparticles also experience mass loss of varying degrees compared with conservative tracers in fast-flowing water environments (Kittilä et al., 2019; Pang et al., 2020). To be able to design river tracing experiments with DNA-tagged tracers, quantitative analysis of the microparticle behaviour in river water and upon contact with the riverbed is a prerequisite.

In rivers, transport of waterborne constituents can be divided into two parts, a fast-flowing region where constituents are carried by the average fluid velocity and dispersive mixing, and a low-velocity region where a mass exchange occurs between the fast- and the low-flowing regions (Bencala et al., 2011; Boano et al., 2014; Briggs et al., 2009; Karwan and Saiers, 2009; Kerr et al., 2013; Paul and Hall Jr, 2002; Wagener et al., 2002). Near the riverbed is a low-velocity region and the riverbed acts as a significant sink for particle retention due to a process known as "hyporheic exchange", which traps a wide range of particles, including lightweight plastics (J. D. Drummond et al., 2020; J. D. Drummond et al., 2022; Frei et al., 2019). Complex is the interaction between fluid motion, particulate matter being transported, and the flow within the streambed (Ho and Gelhar, 1973; Ruff and Gelhar, 1972). A shallow hyporheic flow can be induced by hydrodynamic forces when it is triggered by sand ripples, dunes, or grain clusters on a small spatial scale (Käser et al., 2013; Stonedahl et al., 2013), whereas a deeper and larger hyporheic flow is typically caused by hydrostatic forces beneath topographic features, e.g., steps and cascades, riffles, and even larger meanderings (Boano et al., 2006; Revelli et al., 2008; Tonina and Buffington, 2009). Additionally, flow velocity (Elliott and Brooks, 1997; O'Connor et al., 2012), pH, temperature, chemistry of the flowing water (Ren and Packman, 2002; Westhoff et al., 2011), permeability and surface roughness of the streambed (e.g., biofilm) (Battin et al., 2003; Roche et al., 2017), and, finally, bed mobility (Harvey et al., 2012), working in concert, regulate the interfacial interactions where surface water overlies permeable sediments.

Colloidal particles in water columns are subject to advection, dispersion, aggregation, settling, and deposition (Besseling et al., 2017; Kooi et al., 2018; Li et al., 2019; N. Xu et al., 2019). Y. Tang, Zhang, et al. (2023) showed that hetero-aggregation with suspended particulate matter in river waters was an insignificant factor in first-order gravitational settling of SiDNAFe in water columns at a 30-hour time scale. However, rates of fine particle deposition by hyporheic exchange could be up to hundreds of times greater than those for gravitational settling (Roche et al., 2017; Thomas et al., 2001). For example, flat-bed grain-scale flows can induce greater particle deposition than gravity and are comparable to rippled bed particle deposition (Fries and Taghon, 2010).

Therefore, in this chapter, we studied the effect of channel bed sediment on the transport behaviour and mass loss of SiDNAFe in open channel injection experiments using different water qualities. Hereto, a series of laboratory injection experiments were conducted with four channel bed conditions (no sediment, fine sediment, coarse sand, and goethite-coated coarse sand) and two water qualities (tap water and natural river water). This research establishes a methodological foundation for field application of SiDNAFe in river tracing

and characterises the fate and transport of SiDNAFe in riverbeds. This draws a bottom line for applying such DNA-based tracer in future real-world river tracing experiments. With its magnetic properties and the up-concentration scheme, SiDNAFe possess promising potential as a surrogate for multi-tracing micro-contaminants (e.g., microplastics) in rivers, which could be a promising tool for enhancing understanding of hydrological processes.

5.2. MATERIALS & METHODS

5.2.1. SiDNAFe characterization

The zeta potential (ζ) of SiDNAFe was obtained using a ZetaSizer Nano S (Malvern Instr., UK), whereby ζ was calculated using the Smoluchowski equation from the measured electrophoretic mobility of SiDNAFe dispersed in tap water and filtered river water (0.45-μm glassfibre filter), respectively. The hydrodynamic diameter (D_{hDLS}) of SiDNAFe was measured using Dynamic Light Scattering (DLS) method (173° backscattering).

5.2.2. Open channel injection experiments

Open channel setup and the bed sediment characteristics

For the injection experiments, two small, identical, horizontally placed, open channels (PVC gutters with dimension 1.3 meter long × 0.06 meter Width) were used in parallel (Fig. 5.1a). Flow was generated with a peristaltic pump (Watson-Marlow pumps, Falmouth, Cornwall). A rotor was set 7 cm from the inlet to homogenize the cross-sectional concentration of the entering tracer mass with little disturbance to the flow path downstream. Through the outlet point, out-flowing water was caught by sample containers. To investigate the effect of channel bed sediment characteristics on the fate and transport behaviour of SiDNAFe during injection experiments, four types of channel bed were selected (Fig. 5.1a): an impermeable channel bed without sediment (IP) as a control, a clean coarse sand bed (CS), a goethite-coated coarse sand bed (GCS), and a natural fine sediment bed (FS), respectively. The size distribution of the used sand/sediment was obtained through wet sieving (Fig. A.21). The roughness k_s (mm) of the channel bed has been empirically estimated as $k_s \simeq 3.5 \times D_{84}$, where k_s represents the grain size for the 84th percentiles of the grain size distribution (Fig. A.21) (Clifford et al., 1992).

For CS, 1.2-1.5 mm (average 1.36 mm) quartz sand (Table 5.1 and Fig. A.21) was washed sequentially with tap water, nitric acid (10% v/v), and Demi water until an EC of < 2 μS/cm was reached. After that, the wet sand was oven dried at 70 °C overnight. After cooling down, 210 g CS was laid evenly in the open channel to form a visually uniform layer with a thickness of ~ 3 mm (1 to 2 grains, Fig. 5.1a). Retrieved from the CS series of injection experiments, the CS was coated with goethite (GCS) using a coating procedure adapted from Scheidegger et al. (1993) and Schwertmann and Cornell, 2008 (details are in the Appendix A) and used as channel bed sand. To determine iron concentrations, the goethite coating was dissolved by adding 1 g GCS in 50 mL 10% (v/v) HNO_3 with heating for 0.5 hour, the measurements were conducted in triplicate. Total Fe concentration was 0.9 mg/g using ICP-MS) (Analytic Jena, Jena, Germany) (Table 5.1). FS was collected from a top layer (~ 3-5 cm) of the channel bed of Merkske river (51°24'57.1"N, 4°50'48.5"E), which is located on the border of the Netherlands and Belgium. The sediment was very homogeneous. It consisted of 80.6% fine sand (125 μm to 250 μm), 5.0% very fine sand

	A	w	Q	u	Rh	Re	Fr
Unit	cm^2	cm	cm^3/s	cm/s	cm	-	-
	7.75	6	0.83	0.1	0.9	34	3.0E-03

Table 5.1: Characteristics of FS, GCS, and CS and the hydrodynamic condition of the open-channel flume in open-channel injection experiments.

(< 125 μm), and 14.4% medium sand (250 μm to 500 μm). After acid-digestion of FS, the NOM content of FS was measured to be ~ 0.5 mg-C/g, as dissolved organic carbon (DOC, in mg-C/L) using the combustion technique with a total organic carbon analyser (TOC-VCPN (TN), Shimadzu, Japan).

Flume hydrodynamics

The flow rate was set constant by a peristaltic pump (100 series cased pump 120U, Watson-Marlow). The water depth was measured after a steady flow was reached. The mean flume velocity, u, was calculated as follows:

$$u = \frac{Q}{A} \tag{5.1}$$

Where Q is the flow rate (cm^3/s), is the cross-sectional area perpendicular to the flow direction (cm^2). Flume Reynolds number Re was calculated as:

$$Re = \frac{4UR_h}{\nu} \tag{5.2}$$

Where ν is the kinematic viscosity of water (cm^2/s), and R_h is the hydraulic radius of the channel.The Froude number (Fr) was calculated as:

$$Fr = \frac{u}{\sqrt{g\frac{A}{W}}} \tag{5.3}$$

Where w is the flume width (cm), and g is the gravitational constant (cm/s^2).

River water

The river water was collected in March 2021 from the Meuse at Keizersveer, The Netherlands (51°43'05.7"N, 4°53'27.5"E), and was stored at 4∘C in polyethylene sample containers and filled and tightened with double-sealed plastic caps. The river water sample was treated with 1 mg/L iodide to minimize microbial activity during sample storage. The NOM of Meuse water was measured as dissolved organic carbon (DOC, in mg-C/L) using the combustion technique with a total organic carbon analyser (TOC-VCPN (TN), Shimadzu, Japan). EC and pH were measured in situ using an EC meter (Multi 3620 IDS, Xylem Analytics Germany GmbH, Germany) and a pH meter, respectively. The total suspended solids (TSS) in river water samples were calculated by drying the filtrate (>1.2 μm) at 105∘C and weighing the dry weight of the filtrate.

Injection experiments

SiDNAFe injection experiments were performed in duplicate in Tap water and Meuse water, respectively. First, the sand/sediment was laid evenly across the channel. After that, Tap/Meuse water was pumped into the open channel setup until a steady outflow was reached ((the volumetric flow rate, Q = 0.83 cm^3/s; Table 5.1)). At the beginning of an injection experiment, SiDNAFe was suspended in the same water type used for the injection experiment to reach a concentration of ~ 10^{-4} mg/mL. Then, 45 mL of SiDNAFe suspension was pumped into the channel setup at the same flow rate as the inlet flow generated by the pump. After the tracer injection, the inlet source was immediately switched back to the water type used for the injection experiment. Meanwhile, at the outlet point of the open channel, 25 mL samples were taken according to the schedule depicted in Table A.3 in Appendix A. For each 25-mL sample, a sub-sample of 1 mL was taken in duplicate for magnetic separation and up-concentration, and DNA quantification (Fig. 5.1b & c). Before taking the subsample, the sample was vortexed for 1 min to ensure sample homogeneity. BTCs of SiDNAFe were obtained from qPCR data against a standard curve of 10-fold diluted known sample concentrations. Following an injection experiment of SiDNAFe, the sediment from the channel bed was collected and washed with Demi water to quantify any SiDNAFe previously retained. Prior to SiDNAFe injection experiments, for reference, NaCl injection experiments were performed. NaCl concentrations as a function of elapsed time were measured by an EC meter (Multi 3620 IDS, Xylem Analytics Germany GmbH, Germany). The schedule outlining the specific timing for the sequence of injection experiments can be found in Table A.10 in the Appendix A.

5.2.3. Statistical tests

One-way ANOVA and then a post-hoc Tukey's Honestly-Significant Difference (Tukey HSD) test (Tukey, 1949) were performed to assess the effect of the four channel-bed sand types and the two water types on the mass recoveries of SiDNAFe in injection experiments. Data variations across different groups of bed types and in between two water types per bed type were assessed using a one-way ANOVA test and a Student t-test with Welch correction, respectively. The differences were considered significant when $p < 0.05$.

5.2.4. BTC analysis & 1-D transport modeling

One-dimensional advective and dispersive transport in a main channel with transient exchange/first-order mass loss was considered to be the main transport process of SiDNAFe in the open-channel injection experiments. To assess SiDNAFe BTC characteristics, OTIS was used for BTC fitting and transport parameter optimization (Runkel, 1998). The delayed delivery of tracer mass (i.e., the tailing effect/skewness of a BTC) was treated as a first-order transient exchange between a main channel and a lumped transient storage zone. Furthermore, in case of mass loss of SiDNAFe, an additional first-order decay process in the main channel was included in the OTIS simulation. The equations used for the conservative and non-conservative transport in our injection experiments are (Runkel, 1998):

$$\frac{\partial C}{\partial t} = -\frac{Q}{A}\frac{\partial C}{\partial x} + \frac{1}{A}\frac{\partial \frac{AD\partial C}{\partial x}}{\partial x} + \alpha(C_s - C) - \lambda C \tag{5.4}$$

$$\frac{\partial C_S}{\partial t} = \alpha \frac{A}{A_S}(C - C_S) \tag{5.5}$$

Where C and C_S [g/m^3] are the mass concentrations in the main channel and the storage zone, respectively; Q the volumetric flow rate [m^3/s], A and A_S [m^2] the cross-sectional areas in the main channel and the storage zone, respectively; D_L [m^2/s] the longitudinal dispersion coefficient; α [1/s] the storage zone exchange coefficient; t [s] the transport time; x [m] the distance. In case of mass loss with a negligible transient storage exchange, λ [1/s] the first-order decay coefficient in the main channel is included. The hydrodynamic conditions for modelling setup is shown in Table 5.1.

The parameter optimization was automated using the Nonlinear Least Square algorithms of STARPAC (see details in Donaldson and Tryon, 1990), which was implemented in OTIS-P. For the OTIS modeling, we used one master BTC, which was averaged from four individual observed BTCs (2 subsamples × 2 channels) per water type per channel bed type). Four parameters D_L, α, A, and A_S were optimized in case of conservative transport, while one more parameter λ was estimated in case of mass loss. An visual inspection of the BTCs and sensitivity analysis was performed to determine the most appropriate combinations of processes to be considered. When the transient storage parameter set (i.e., A_S and α) showed negligible sensitivity on the BTC fitting, the transient storage process was turned off. Mass recovery was calculated by integrating the area underneath the BTC. Due to the intrinsic variations caused by DNA amplifications in qPCR (as discussed in Chapter 2, measured mass recoveries of SiDNAFe between 80% - 120% were considered full mass recovery and were linearly scaled to 100% to balance the input and the output mass for modeling purposes. Furthermore, a first-order decay term was considered in the case of mass recovery lower than 80%. The optimized parameter sets were presented with 95% confidence intervals, whereby the statistical analyses related to the observed data and the Nonlinear Least Square fitting procedure were conducted by STARPAC (Donaldson and Tryon, 1990).

5.3. Results

5.3.1. SiDNAFe in Tap water and Meuse water

The zeta potential (ζ) of CS, GCS, and FS ranged between -15 mV and -19 mV (Table 5.2) which was determined using a ZetaSizer Nano S (Malvern Instr., UK). To do the analysis, abrasion of the surface of CS, GCS, and FS was done by ultra-sonication. The total porosity of CS, GCS, and FS was determined gravimetrically to be 0.43, 0.46, and 0.5, respectively (Table 5.2).

SiDNAFe was negatively charged in MQ, Tap water, and Meuse water, with a ζ ranging between -22 mV and -24 mV. The hydrodynamic diamter (D_{hDLS}) of SiDNAFe was measured to be ~ 444 - 548 nm (Table 5.2). Table 5.2 shows the water quality characteristics of tap water and Meuse water. With a relatively low particle concentration of ~ 10^{-4} mg/mL, SiDNAFe was well-dispersed at room temperature, given its ζ in the ionic strength and pH of tap water and of Meuse water (Table 5.2 & 5.3).

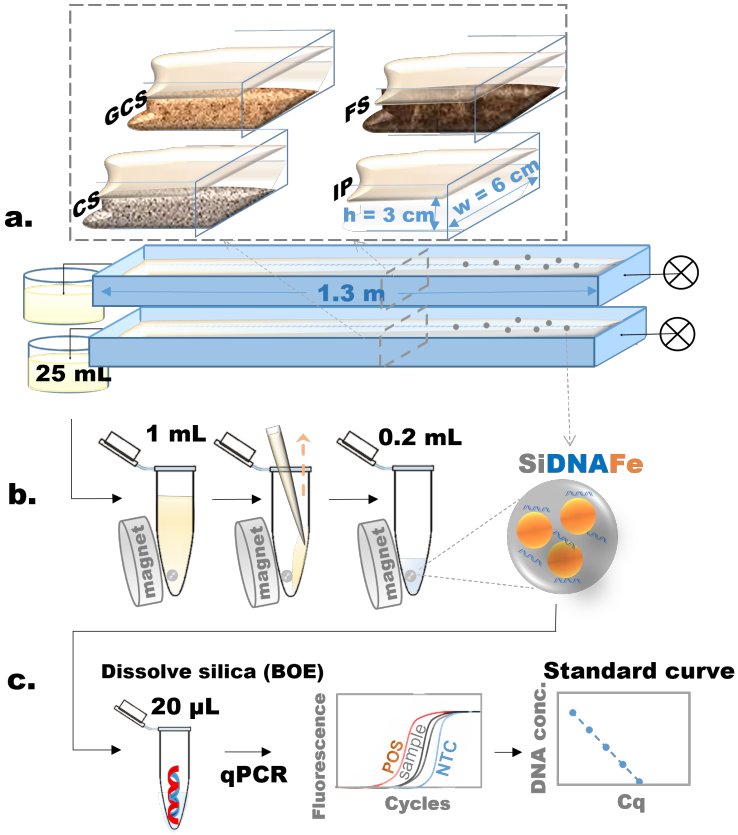

Figure 5.1: Schematic figure of open channel injection experiments and sample analysis. a. Open channel injection experiments in duplicate: four different channel bed were tested: no sediment (IP), coarse sand (CS), goethite-coated coarse sand (GCS), and natural river fine sediment (FS), respectively (see photos in Fig. A.22 in Appendix A). b. Magnetic separation and up-concentration: 1 mL of river water or tap water was gradually diluted and replaced with MQ over two rounds of pipetting, while the SiDNAFe were magnetically attracted to one side of the tube. Finally, 0.2 mL of MQ was left within the tube containing the magnetically separated SiDNAFe (details see Chapter 2). c. DNA analysis and sample quantification: dsDNA was released from SiDNAFe by dissolving the silica shell with BOE, and then dsDNA was amplified and quantified by qPCR with positive controls (POS) and negative controls (NTC) included in each assay. A standard curve of DNA concentrations as a function of Cq was produced in each qPCR assay for sample quantification.

ζ (mV)	-	FS	GCS	CS	SiDNAFe	
	ζ (mV)					D_{hDLS} (nm)
	MQ	-	-	-	-24 ± 3.9	444 ± 133
	Tap	-15	-19	-17	-22 ± 3.1	500 ± 164
	Meuse	-15	-18	-18	-23 ± 3.5	548 ± 138
DOC (mg-C/g)	Tap	0.50	-	-	-	
	Meuse	0.48	-	-	-	
Effective size (mm)		0.18	1.36	1.36	-	
Roughness (mm)		0.77	5.32	5.32	-	
Porosity		0.5	0.46	0.43	-	
Total Fe (acid-digestion) (mg/g)		0.66	0.9	-	-	

Table 5.2: Characteristics of FS, GCS, and CS and SiDNAFe.

5.3.2. NaCl breakthrough curves

NaCl BTC showed an asymmetry, with a flattening tendency from FS to GCS to CS to IP. The first arrival of NaCl was similar among four bed types (Fig. 5.2). After the first arrival, BTCs had sharp rising limbs followed by falling limbs with a similar range of slopes. FS and GCS had the highest peaks followed by CS and IP. Half of the NaCl mass arrived before one-third of the whole BTC period (between 20 minutes and 40 minutes), while the other half of the mass was gradually recovered until the end at 140 minutes, with a total mass recovery ranging from 94% to 99%.

5.3.3. Breakthrough curve comparison between SiDNAFe and NaCl

Fig. 5.3 shows an overview of BTC comparisons between SiDNAFe and NaCl, in four channel bed types and each performed in two water types. SiDNAFe BTCs are shown as master curves, using the average of four observed BTCs (See Fig. A.20 for all observed SiDNAFe BTCs). SiDNAFe traveled at the same rate or faster in comparison with NaCl. SiDNAFe arrived earlier than NaCl in FS series (i.e., both in Tap and in Meuse water), CS series, and IP series. However, in GCS series, SiDNAFe and NaCl arrived at the same time. SiDNAFe had a similar or steeper rising slope than NaCl after arrival. SiDNAFe concentration rose in IP series and CS series with a slope steeper than NaCl, whereas in FS and GCS series, SiDNAFe and NaCl are comparable. In all series except GCS, SiDNAFe reached a peak significantly higher than NaCl. In GCS series, SiDNAFe had a similar peak to NaCl in Tap water, but in Meuse water, SiDNAFe's peak was significantly lower due to mass loss. Additionally, SiDNAFe's peaks were characterised by discrete pulses of data points with relatively larger standard deviations. No generalized pattern was found

Water quality	Unit	Meuse	Tap
pH	-	8.2	8.2
EC	µS/cm	533	511
Ionic Strength	mM	8.5	8.1
DOC	mg-C/L	5.0	2.4
TSS	mg/L	2.3	0.0
Na^{+}	mg/L	28.5	39.8
K^{+}	mg/L	6.6	6.7
Ca^{2+}	mg/L	73.0	51.6
Mg^{2+}	mg/L	7.8	7.4
Cl^{-}	mg/L	38.6	56.7
NO^{3-}	mg/L	17	10
$SO4^{2-}$	mg/L	48.0	48.0
$PO4^{3-}$	mg/L	0.8	0.0

Table 5.3: Water quality characteristics of Meuse water and Tap water.

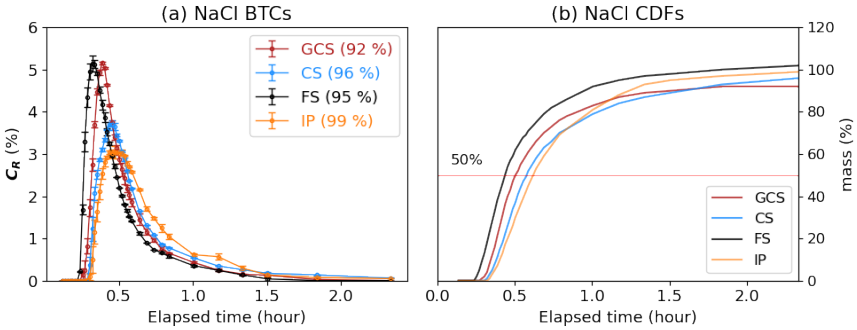

Figure 5.2: Breakthrough curves of NaCl and their corresponding cumulative distribution function (CDFs) in open channel injection experiments with four types of channel bed: natural fine sediment (FS), goethite-coated coarse sand (GCS), coarse sand (CS), and an impermeable channel without sediment (IP). Mass recoveries are shown in brackets. In (b), the red horizontal line denotes 50% of the recovered NaCl mass.

5

for the extent of data scatter as a function of the channel bed types and the water types, respectively (the light blue shades of SiDNAFe BTCs in Fig. 5.3). The falling limbs, which were quite symmetrical to the rising ones, appeared over those scattered points coming after the peak clouds in CS series, FS series, and GCS in Meuse water (hereafter referred to as GCS-Meuse). In IP series, SiDNAFe's tailing effect was evident but less pronounced than NaCl's. Further, in GCS-Tap, SiDNAFe and NaCl had almost overlapped recession curves, despite SiDNAFe having the higher standard deviations. T-test with Welch's correction analysis indicated that there was no statistically significant difference between the BTCs of SiDNAFe and NaCl in GCS-Tap.

5.3.4. Mass recovery of SiDNAFe

Mass recoveries of SiDNAFe ranged between 54% and 135% across all channel bed types and water types (Fig. 5.4). A Tukey post-hoc test revealed that, in Meuse water, three groups of mass recoveries (i.e., FS, GCS, and CS) were significantly different from each other ($p \ll 0.01$). However, in Tap water, mass recoveries of SiDNAFe had no significant difference across four bed types ($p = 0.1525$).

5.3.5. Transport parameter estimation

Fig. 5.5 presents transport parameter estimation for SiDNAFe and NaCl with 95% confidence intervals (parameter values are presented in Table A.9 in the Appendix A). $D_{L\text{NaCl}}$ varied between 1.51×10^{-5} and 2.63×10^{-5} [m^2/s], while α_{NaCl} varied between 4×10^{-4} and 10×10^{-4} [1/s]. A trade-off between $D_{L\text{NaCl}}$ and α_{NaCl} was observed across four bed types, where a higher $D_{L\text{NaCl}}$ was correlated with a lower α_{NaCl} and vice versa. A_S the volume of sand/sediment in the channel increased from a no-sediment to a sediment-laid bed type, main channel cross-sectional area A_{NaCl} decreased from 10×10^{-4} to 7×10^{-4} [m^2]. $A_{S\text{NaCl}}$ remained around half of the A_{NaCl} in all four bed types under the same hydraulic conditions.

$D_{L\text{SiDNAFe}}$ ranged between 1.07×10^{-5} and 7.97×10^{-5} [m^2/s], with FS having the greatest value, followed by GCS and CS with intermediate values, and IP with the lowest value. The transient storage exchange process was included only in the IP series and GCS-

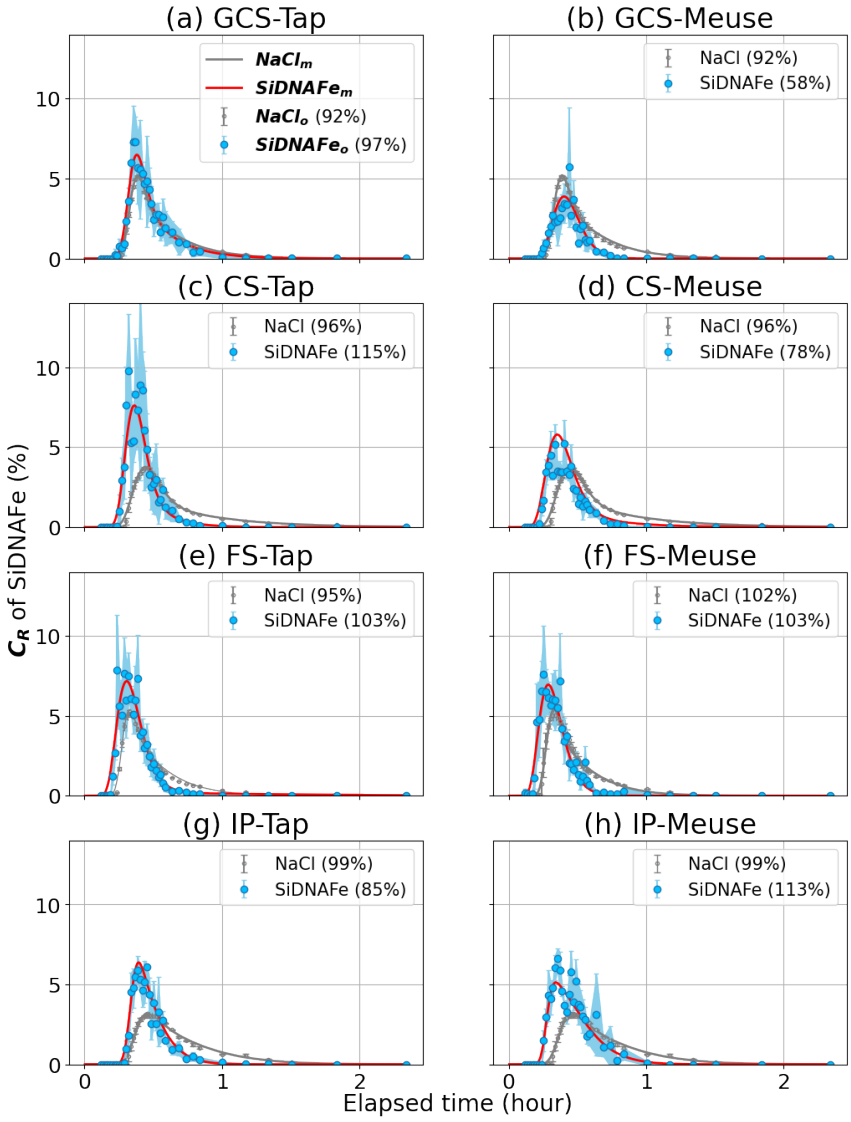

Figure 5.3: SiDNAFe breakthrough curves in comparison with NaCl breakthrough curves in open-channel injection experiments with four types of channel beds and two water types. Breakthrough curves are shown in relative concentrations (C_R: C/C$_0$ in %) over time. GCS represents goethite-coated coarse sand, CS coarse sand, FS fine sediment, and IP impermeable channel without sediment. Observed SiDNAFe breakthrough curves and OTIS-simulated SiDNAFe breakthrough curves are shown in blue closed circles with standard deviations and red solid lines, respectively. NaCl series are shown in grey dots with standard deviations and grey solid lines. Each series of injection experiments were performed in Tap water (the left column) and in Meuse water (the right column), respectively. Mass recovery for each injection experiment is shown in brackets in each subplot. The red solid line in subplot (g) shows the simulated SiDNAFe breakthrough curves fitted with a first-order decay process in OTIS.

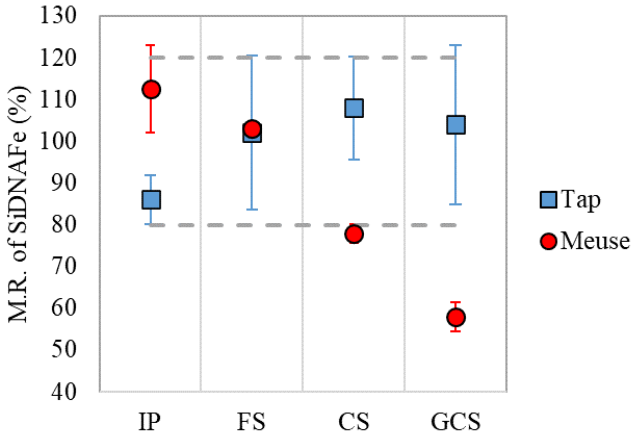

Figure 5.4: Mean mass recoveries of SiDNAFe categorized by four channel bed types: fine sediment (FS), goethite-coated coarse sand (GCS), coarse sand (CS), and an impermeable channel without sediment (IP). Blue squares and red dots denote mean mass recovery, with error bars indicating variation between four values, in Tap water and in Meuse water, respectively. The grey dashed lines delineate mass recoveries lower than 80% and higher than 120%.

5

Tap, with a higher α_{SiDNAFe} in the IP series (11×10^{-4} ~ 20×10^{-4} 1/s) but a lower one (6×10^{-4} 1/s) in GCS-Tap. In four bed types, A_{SiDNAFe} was similar in Tap water (~ 8 to 9×10^{-4} m^2), but, in Meuse water, it ranged from 7×10^{-4} to 10×10^{-4} [m^2], with the highest value in GCS and the lowest value in IP.

$A_{S\,\text{SiDNAFe}}$ was estimated to be half of the A_{SiDNAFe} in IP-Tap but around 30% of the A_{SiDNAFe} in IP-Meuse and GCS-Tap when transient storage was considered. To account for the mass loss in GCS-Meuse and in CS-Meuse, a first-order decay term was included and modelled to be 3.62×10^{-4} and 1.70×10^{-4} (1/s), respectively.

When comparing NaCl and SiDNAFe, $D_{L\,\text{SiDNAFe}}$ was estimated to be significantly higher than $D_{L\,\text{NaCl}}$ in CS, FS, and GCS-Meuse. Notably, in these cases, the transient storage was turned off because the transient storage parameters could not be constrained in inverse simulations (i.e., negligible sensitivity of A_S and α on the BTC fitting, see details in Appendix A). When comparing SiDNAFe and NaCl with transient storage included (i.e., IP and CS series), an equivalent or a smaller portion of A was modelled as A_S to exchange mass at a similar range of α. Additionally, $A_{\text{glssidnafe}}$ was smaller than A_{NaCl} in IP and CS. On the contrary, in GCS and FS, A_{SiDNAFe} was either equivalent or larger than A_{NaCl} (i.e., in FS-Tap and GCS-Meuse). Across two water types, SiDNAFe had similar transport parameters when they were subject to the same transport processes.

5.4. Discussion

5.4.1. The effect of channel beds

SiDNAFe mass recoveries exhibited a wide range, varying from 50% to 120% from sediment-free conditions to fine sediment and to coarse (coated) sediment conditions. SiDNAFe had mass loss in coarse (coated) sediment series, however no mass loss in the IP

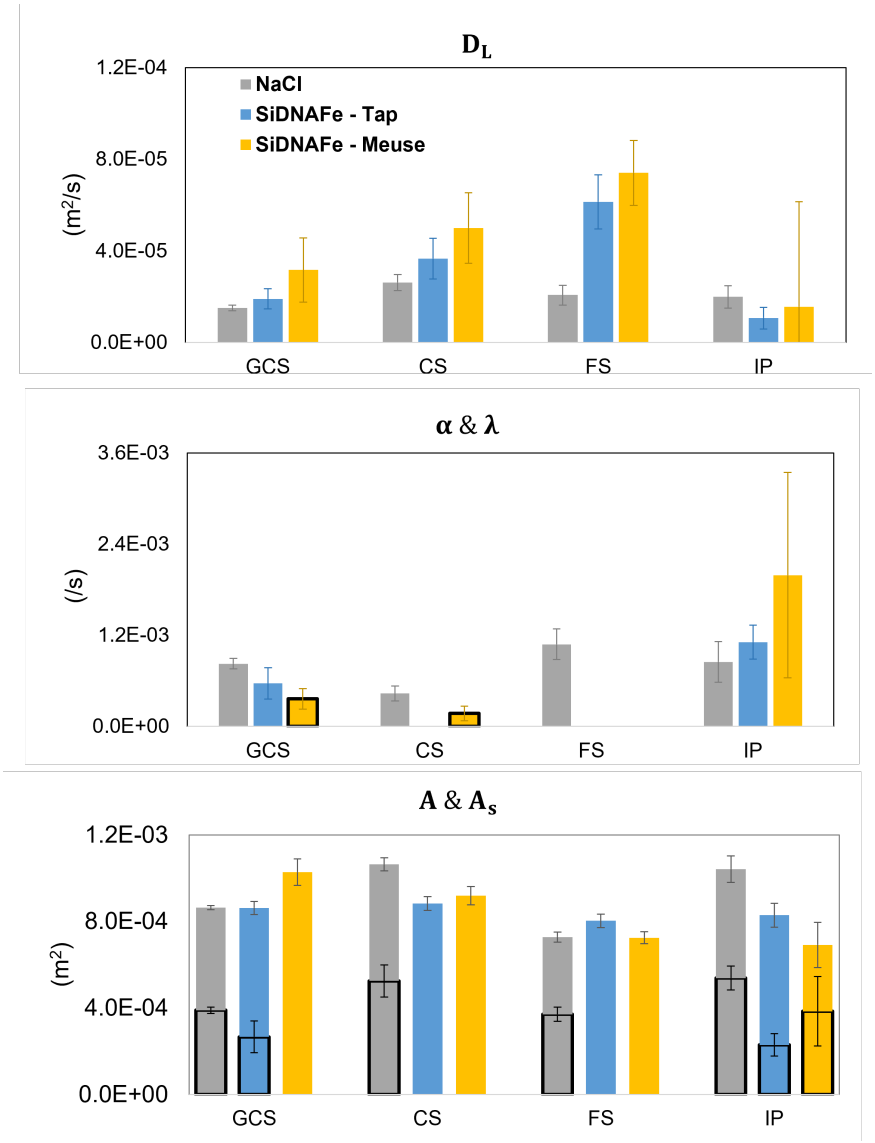

Figure 5.5: Transport parameters estimation with 95% confidence intervals for SiDNAFe and NaCl. SiDNAFe in Tap and in Meuse were shown in blue bars and yellow bars, respectively, while NaCl was shown in grey bars. λ is shown as bars with black borders in the same plot of α, and A_S is shown as a part of A (where applicable) with black borders in the subplot of A & A_S. Missing bars represent no applicable parameters for this category.

series. This indicated that gravitational settling was negligible in the experiments, and the mass loss was likely related to the interactions with the sediment.

For effective particle retention, most studies found that two processes have to work in concert, i.e., the particle delivery from the flow to bed, and the detainment of particles such as filtration (Fries and Taghon, 2010; Packman et al., 2000; Ren and Packman, 2004a; Ren and Packman, 2004b; Ren and Packman, 2005; Thomas et al., 2001; Wörman et al., 2002). However, in our experiments, the effect of filtration was considered minor, due to a relatively thin layer of sediment bed of ~ 3 mm and the low permeability of the bed (Table A.8).

The near-boundary shear Reynolds number for FS, GCS, and CS was calculated to be smaller than 3 (Table A.8), indicating a hydraulically smooth flow condition (Nikaradse, 1933), where the laminar sublayer above the water-sediment interface was thicker than the roughness elements of the bed. Upon approaching the water-sediment interface (i.e., particle delivery), SiDNAFe, which was significantly smaller than the sublayer in size, was supposed to be entirely immersed within this viscous sublayer, where the molecular diffusion should dominate the particle transport (Crawford and Sanford, 2001). The same diffusion responsible for particle delivery also transports momentum into the sediment, driving an interstitial flow. Fries (2002) found that over a flat permeable bed such an interstitial flow can be detected as a velocity slip at the interface. This slip decreases the drag coefficient and generates a negative correlation between drag and deposition over a flat permeable bed. Moreover, the influence of slip in the boundary on the flow profile was most significant at a lower grain Reynolds number (i.e., smaller grain size or smaller shear velocity).

In our experiments, the ratio of void scale to permeability of FS, GCS, and CS was similar, indicating an equivalent open structure of the sediment bed (Table A.8). If a mechanism like the above-mentioned diffusive transport and filtration was in play, SiDNAFe would likely have been more deposited in FS than in CS & GCS, due to a lower grain Reynolds number in FS. From a no-sediment to sediment-laid conditions, we speculated that the retention of SiDNAFe was associated with particle exchange brought by grain-scale hyporheic flows (Packman et al., 2000; Ren and Packman, 2004a; Ren and Packman, 2004b; Ren and Packman, 2005; Wörman et al., 2002) and the nature of the boundary layer over the bed (Hamm et al., 2011; Saffman, 1965).

There was no significant difference in NaCl transport parameters among the four series, except that with the addition of sand/sediment volumes in the channel the effective main channel cross-sectional area was reduced and caused an increase in NaCl BTC peak and an earlier NaCl arrival (Fig. 5.2). The trade-off between $D_{L\,\mathrm{NaCl}}$ and α_{NaCl} indicated that the effect of the transient storage on NaCl transport was on a similar timescale as the hydrodynamic dispersion process in our injection experiments (Briggs et al., 2009). However, there should be a difference in the nature of the transient exchange between with and without channel bed sand. In addition to the exchange between the main channel and surface transient storage where fluid moved slowly or stagnated, a grain-scale hyporheic exchange on the water-sediment interface was likely for the sand-laid cases (Fries and Taghon, 2010).

5.4.2. The coupled effect of water quality & coarse sediment

We observed SiDNAFe mass loss in coarse (coated) sediment bed conditions (i.e., GCS and CS) in Meuse river. Interestingly, this trend was not observed in Tap water under the same

series of bed conditions.

The primary differences of the water quality characteristics lay in the dissolved organic carbon (DOC) and total suspended solids (TSS) content(Table 5.3). Prior research on the settling behaviour of SiDNAFe has demonstrated the insignificance of hetero-aggregation with suspended particulate matter (SPM) in Meuse water (Y. Tang, Zhang, et al., 2023). Furthermore, the pH, ionic strength, and major cations and anions displayed similarities across both water types. Given the current experimental results and water quality measurements, we were unable to conclusively pinpoint the decisive water quality factor that contributed to the observed differences in mass recovery between these two water types. While it is meaningful to delve into the controlling physicochemical characteristics behind the observed mass loss in this particular case, such an investigation requires further research. Nonetheless, our overarching message is that in real world large-scale tracing experiments, SiDNAFe is a promising tracer albeit that in some environmental conditions the particle loss may hinder the measurement.

Specifically, SiDNAFe mass retention in coarse (coated) sediment bed conditions was 1-2 orders of magnitude greater than the estimated first-order decay rate in quiescent settling conditions (Y. Tang, Zhang, et al., 2023). Similarly, Fries and Taghon (2010) found that deposition in excess of gravitational settling could result from the grain-scale deposition process of colloidal particles to permeable sediments regardless of bed roughness. Furthermore, enhanced deposition and retention of particles have been found associated with a greater flow-to-bed flow as a result of a local increase in pressure-driven flows and most likely followed by particle capture. However, this was not the case given the flatbed condition. Thomas et al. (2001) found that A_S/A was most strongly associated with the variation in enhanced deposition rates, which was consistent with interstitial filtration as a significant mechanism of particle deposition. However, in our experiments, transient exchange was negligible in the two cases where enhanced SiDNAFe mass retention occurred. This was additional indirect evidence supporting that filtration did not take place as the main mechanism of enhanced SiDNAFe mass retention in coarse (coated) sediment bed conditions.

It is reasonable to consider that there was a different mechanism than the above-mentioned, driving the enhanced mass loss in coarse (coated) sediment beds with Meuse water. We think that it was related to complex water-sediment-particle interactions. Ren and Packman (2005) found that the colloid mobility could be either enhanced or reduced as a result of general and specific interactions between sorbing solutes and iron oxide particles, and they suggested that the colloidal and contaminant behaviour assessment cannot be separated from each other in surface systems because surface-chemical processes can cause their behaviour to be coupled. In this regard, we speculate that some sort of coupled grain-scale water-sediment-particle interactions, e.g., kinetic attachment between SiDNAFe and goethite-coating in the presence of river waters were the driving mechanism for enhanced SiDNAFe retention. Moreover, kinetic attachment/detachment was concluded to be the driven deposition mechanism in porous media for a similar silica encapsulated DNA microparticles (Kianfar et al., 2022). Another indirect evidence supporting this was the lower mass loss in CS, which was acid-washed and removed from surface impurities. Compared with the surface chemistry of GCS, CS would have weaker particle-particle interactions with SiDNAFe. Likewise, Ren and Packman, 2002 showed a reduced deposition

of silica colloids in a sand bed that was acid- and base-washed. Mechanisms that would otherwise enhance the retention, such as topography and aggregation seemed unlikely, due to a flatbed condition and the constant hydrodynamic diameter of SiDNAFe under similar conditions. Moreover, diffusion across the interface seemed unlikely, as the hydrodynamic dispersion was 10 to 11 orders greater than the diffusion coefficients of SiDNAFe. Only in conditions of quiescent waters with extremely low permeability sediments (clays or silts) does diffusion tend to be the dominant transport process (Huettel and Webster, 2001). In our experiments, SiDNAFe would likely attach to or be deposited on the grain surface. Despite the unfavorable conditions for attachment between SiDNAFe and coarse (coated) sediment, enhanced deposition could occur as a result of grain-scale surface heterogeneity (Ryan and Elimelech, 1996; Schijven et al., 2002). This heterogeneity had been shown to be responsible for a considerable amount of the particle retention, even under conditions characterized by repulsive electrostatic forces (Ren and Packman, 2002).

5.4.3. Comparison between NaCl and SiDNAFe

An evident breakthrough separation was between NaCl and SiDNAFe in IP, CS, and FS, despite the more "chaotic" signals of SiDNAFe. In IP and CS, SiDNAFe arrived significantly earlier than NaCl in both Tap and Meuse water conditions. This indicated that the average velocity of SiDNAFe was higher than that of NaCl. In many surface water tracer experiments, researchers have observed the earlier arrival of the BTC peak by colloids compared to solute tracers (e.g., McCluskey et al., 2021; Göppert and Goldscheider, 2008). This suggests that colloids tend to preferentially travel along faster flow lines in comparison to solutes. However, it is important to note that these differences are generally small, as also observed in our own experiments, and are primarily noticeable at lower average flow velocities (Göppert and Goldscheider, 2008). In FS, despite an earlier arrival of SiDNAFe, A_{SiDNAFe} was estimated to be similar to A_{NaCl}. This was probably because a significantly higher $D_{L\,\text{SiDNAFe}}$ accounted for an earlier arrival in this case. However, we argue that a significantly greater $D_{L\,\text{SiDNAFe}}$ was a result of modelling compensation. OTIS model would tend to increase D_L to compensate for the effect of the transient exchange when the transient storage parameters failed to constrain the simulation (Karwan and Saiers, 2009). This also indicated that the effect of the transient exchange of transport was on a similar time scale as the dispersion process, which corresponds to the trade-off effect shown earlier between $D_{L\,\text{NaCl}}$ and α_{NaCl} in NaCl BTC simulations.

However, in GCS-Tap, SiDNAFe behaved almost identically to NaCl. In addition, SiDNAFe and NaCl arrived at the same time, showing a symmetric BTC in GCS-Meuse. This change indicated that sediment coating and surface heterogeneity could increase the transient interactions with the particles.

5.4.4. Advantages of SiDNAFe and its associated uncertainty

There was no significant difference between standard deviations of SiDNAFe concentrations (σ_{SiDNAFe}) in Tap water and in Meuse water at a 95% significance level (p = 0.5864). In addition, no significant difference was found among σ_{SiDNAFe} grouped by different sediment conditions (i.e., FS, GCS, CS, IP). The 'noise' was more associated with the lower concentrations (rising limbs and tails) rather than the higher concentrations (peaks) (Fig. 5.6). Most of the coefficient of variation (CV) were lower than 0.6. However, when

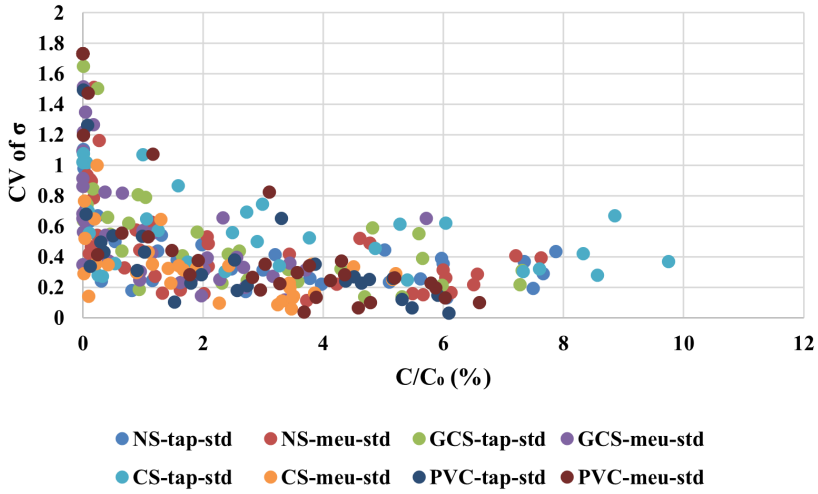

Figure 5.6: Coefficient of variations (CV) of the standard deviation of SiDNAFe concentrations (σ_{SiDNAFe}) as a function of relative concentration C_R C/C$_0$ (%).

5

the C/C$_0$ was below 1%, the CV ranged between 0 – 1.8, indicating a high uncertainty of the concentration value. This high uncertainty of lower concentration was due to having only a few particles/DNA molecules present in the sample for DNA quantification. This range of CVs was consistent with our previous experimental results on the CV of DNA-tagged tracer BTC (Y. Tang et al., 2021). Further, no generic pattern was found for the significant difference of σ_{C_R} and its CV by comparing between groups of channel beds and water types (details in Appendix A). As discussed in Chapter 2 and other DNA-tagged microparticle tracer application experiments (Foppen et al., 2013; Kittilä et al., 2019; Liao et al., 2018), data variation and uncertainty was mostly bound with its discrete nature of colloidal behaviour and qPCR reading uncertainties, water chemistry, etc. As mentioned in Chapter 2, we finalized the up-concentration protocol which was two times of magnetic separation, followed by one time of magnetic separation where one-fifth of the original volume of MQ was left to the sample tube to realize up-concentration. After this magnetic separation and up-concentration procedure, the slopes and R^2 of the 10-fold dilution curves of SiDNAFe, which was originally suspended in Tap water and in Meuse water, revealed that this procedure can be reliably applied to up-concentrate SiDNAFe (see Fig. A.18). This can help to minimize possible inhibition associated with varied river water quality for qPCR quantification.

Our results demonstrated that SiDNAFe could be used in tracing experiments, as evidenced by the complete mass recoveries observed in 6 out of 8 cases. However, apparently, certain combinations of water and sediment can lead to mass loss, as evidenced by our Meuse water-iron coated sand experiments. Here, more detailed research is recommended. Extrapolating our results to tracing experiments in real river experiments, SiDNAFe seems to have the potential to be employed as a tracer also at kilometre scale.

5.5. Conclusions

We investigated the effect of the channel bed characteristics on the transport behaviour and mass loss of SiDNAFe as a colloidal tracer. Natural river fine sediment (FS), coarse sand (CS), Goethite-coated coarse sand (GCS), and no-sediment (IP) were used as four different channel beds. We tested SiDNAFe in two different water qualities (i.e., tap water and river water) and compared SiDNAFe to dissolved NaCl by conducting pulse injection experiments. SiDNAFe BTCs could be adequately described by advection and dispersion with or without a first-order decay process. SiDNAFe mass recoveries exhibited a wide range, varying from 50% to 120% from sediment-free conditions to fine sediment and to coarse (coated) sediment conditions. In 6 out of 8 cases, SiDNAFe mass recovery was complete. Retention of SiDNAFe was 1-2 orders of magnitude greater than gravitational settling rates, as determined in Y. Tang, Zhang, et al. (2023). We reason this was due to grain-scale hyporheic flows and coupled water-sediment-particle interactions. The dispersive behaviour of SiDNAFe generally mimicked that of NaCl tracer. SiDNAFe can be used in tracing experiments. However, water quality and sediment characteristics may affect the fate of SiDNAFe in river environments. With its magnetic properties and the up-concentration scheme, SiDNAFe possess promising potential as a surrogate for multi-tracing micro-contaminants (e.g., microplastics) in rivers, which could be a promising tool for enhancing understanding of hydrological processes.

5.6. CRediT author statement

Conceptualization, Y.Tang, J.W.Foppen, T.A.Bogaard; Methodology, Y.Tang, A.Abdelrady, J.W.Foppen, T.A.Bogaard; Software, Y.Tang; Validation, Y.Tang, F.van Rhijn; Formal analysis, Y.Tang, J.W.Foppen, T.A.Bogaard; Investigation, Y.Tang, F.van Rhijn; Resources, Y.Tang, A.Abdelrady, J.W.Foppen, T.A.Bogaard; Data Curation, Y.Tang, F.van Rhijn; Writing – Original Draft, Y.Tang; Writing – Review & Editing, Y.Tang, A.Abdelrady, J.W.Foppen, T.A.Bogaard; Visualization, Y.Tang; Supervision, A.Abdelrady, J.W.Foppen, T.A.Bogaard; Project administration, Y.Tang, T.A.Bogaard; Funding Acquisition, Y.Tang, J.W.Foppen, T.A.Bogaard.

6

Synthesis and Conclusions

6.1. Main contributions

This dissertation describes the development of a novel technology for tracing particles in surface water using engineered SiDNA(Fe). Synthesised DNA strands are used as unique barcodes tagging the engineered microparticles. These engineered microparticles can be manipulated in various ways and then the microparticles can be tracked for hydrological studies. Accurate sample analysis of DNA quantification is the cornerstone for any further meaningful data interpretation. Chapter 2 outlines the development of a reliable workflow for sample pre-treatment, including sample-taking, sample up-concentration, and sample analysing. This workflow helps to resolve issues with the inconsistent sample size and difficulties in quantifying DNA in environmental waters encountered in practice when combining macroscopic hydrological tracing with microscopic DNA quantification using qPCR.

This dissertation describes the evaluation of the novel tracing technique using SiDNA(Fe) in surface waters. Chapter 3 compares the hydrodynamic dispersion behaviour of Si-DNA with that of a solute tracer NaCl in controlled open channel injection experiments with no mass loss. A series of open channel injection experiments were conducted in six different, environmentally representative water types to obtain tracer breakthrough curves (BTCs). Hereafter, the BTCs were modeled using a 1-D advection-dispersion model with one transient storage zone (OTIS) by calibrating the hydrodynamic dispersion coefficient D_L and a storage zone exchange rate coefficient α. The results showed that when no mass is lost, the Si-DNA dispersed similarly to the NaCl tracer. The hydrodynamic dispersion coefficient (D_L) range for both the Si-DNA and NaCl was similar, indicating that the transport behaivour of Si-DNA was comparable to that of the conventional salt tracer.

In addition to advection-dispersion behaviour, it is important to understand the sinks of the DNA-tagged microparticles in surface waters. SiDNA(Fe) consists of silica (Si-DNA) and/or iron oxides (SiDNAFe) with a specific density larger than water, making them likely to settle and consequently be retained in stream/river bed sediment. Furthermore, hetero-aggregation with natural organic matter and suspended solids may facilitate particle settling which shortens the transport distances of SiDNA(Fe) in streams and rivers. Chapter 4 presents the settling and aggregation behaviour of SiDNAFe in three river waters. Thirty-hour quiescent settling experiments of SiDNAFe were conducted with the presence and absence of various particulate matter in river waters to evaluate the aggregation and settling potential of SiDNAFe. The assessment of the aggregation and settling potential of SiDNAFe microparticle in river waters is a prerequisite for modeling SiDNAFe in future large-scale field tracing applications. The settling of SiDNAFe in filtered/non-filtered river water was not significantly different from SiDNAFe settling in MQ, which could be described by a first-order decay process.

While gravity-driven settling was expected, in-stream cross-sectional mixing brings SiDNA(Fe) to the water-sediment interface, where hyporheic exchange could occur over permeable sediment bed. Physico-chemical interactions with the heterogeneous riverbeds are likely, and in previous research, riverbeds have been found to be significant sinks for colloid alike nano- or microparticles, including light-weighted microplastics. Chapter 5 builds on the previous chapters and further evaluates the effect of bed characteristics on the transport behaviour and especially the mass loss of SiDNAFe in open channel injection experiments. Compared with Chapter 3, a longer channel was used to increase the contact

with the sediment bed. Four channel bed conditions were selected: no sediment, fine river sediment, coarse sand, and goethite-coated coarse sand, with two water qualities: tap water and Meuse river water. Following the conclusion of Chapter 4, which is that the settling could be described as an exponential decay process, the mass loss was accounted for as a first-order process. SiDNAFe BTCsBTCs could be adequately modelled by advection and dispersion with or without a first-order decay. SiDNAFe mass recoveries exhibit a wide range, varying from 50% to 120% from sediment-free conditions to fine sediment and to coarse (coated) sediment conditions. Furthermore, SiDNAFe retention was found to be 1-2 orders of magnitude greater than gravitational settling, as determined in Chapter 4. Grain-scale hyporheic flows and coupled water-sediment-particle interactions might be the reason for the enhanced retention observed. In terms of transport behaviour, SiDNAFe exhibited similar dispersion as solute NaCl, as also concluded in Chapter 3. SiDNAFe can be reliably and reproducibly utilized in tracing experiments, as evidenced by the complete mass recoveries observed in 6 out of 8 cases. With magnetic properties and the up-concentration scheme, SiDNAFe is a promising surrogate tracer for multi-tracing micro-contaminant in streams and rivers. However, caution must be exercised when transitioning from water quality of lower complexity to a more complex water type, as changes in water qualities and sediment characteristics may be coupled to affect the fate of SiDNAFe in streams and river environments.

6.2. Limitations and Challenges

6.2.1. Difficulties related to the laboratory work and DNA analysis

In laboratory settings, the handling and processing of SiDNA(Fe) are delicate tasks that involve the use of various experimental equipment and instruments. Each step of the process requires strict quality control, including material selection to avoid adsorption, accurate pipetting to reduce analytical errors, and an appropriate sonication protocol to ensure thorough mixing without clustering or precipitation while maintaining the integrity and physio-chemical properties of the engineered nano/micro particles(ENP).

For example, the qPCR DNA analysis only requires a small sample size of 4 to 5 microliter, whereas a typical water sample from the field is in the order of 50 to 500 mL. In such cases, determining whether the qPCR sub-sample size contains a statistically representative number of microparticles is critical. When DNA-tagged microparticle content is low (as is to be expected in field experiments), subsampling can introduce a significant error due to over-, or undersampling the microparticles.

Hereto, sample pre-treatment, magnetic separation and up-concentration protocols have been proven important. In this dissertation we developed a pre-treatment protocol that was reproducible and accurate. However, in our explorative studies, pre-treatment was time-consuming, For example, 100 samples using magnetic racks and manual pipetting for subsampling and adding solutions required approximately 2 hours. Prior to magnetic separation, subsampling 100 samples from 20-mL to 1-mL also required approximately 2 hours. Automation of these processes can reduce the time investment.

Inhibitors of the qPCR reactions will likely be enriched during the up-concentration treatment. In our studies we used relatively high concentration of SiDNAFe and only a few mL of sample (up-concentration factor of maximum 10). In future field applications,

sample volumes of e.g., 1 litre can be required, leading to an up-concentration factor of 200 with possible negative effect for the qPCR reactions. Careful sample design and treatment is then required to mitigate possible inhibitor effects in the up-concentrated samples.

Working with DNA-based microtracers requires highly skilled lab support. An automated robot can significantly ease the difficulty of sample analysis and reduce operator involvement in reagent mixing before qPCR analysis. However, a multidisciplinary background remains crucial for personnel engaged in this delicate work. Knowledge in material science, microbiology, and environmental engineering is necessary for various steps of the process.

Challenges related to upscaling SiDNA(Fe) production

Prior to the application of SiDNA(Fe) in hydrological systems, it is essential to estimate the required tracer mass, conduct suitable characterization, and assess the applicability of the freshly synthesized SiDNA(Fe). Our focus lies on the stability assessment of the SiDNA(Fe) in relation to our application protocol, particularly concerning the bleaching step to inactivate any free DNA after the encapsulation, and the required encapsulation thickness of the silica coating to protect DNA against harsh hostile environmental factors, such as, pH variations, enzymatic degradation, ultraviolet radiation, and elevated temperature.

The current production protocol for SiDNAFe at Norwegian University of Science and Technology involves four steps: preparation of magnetite particles, coating of magnetite particles to introduce positive charges, binding of DNA to the positively charged magnetite particles, and silanization of the encapsulated-DNA magnetite particles. However, variations in materials, chemicals, and level of experience of the personnel during these steps can potentially lead to mishaps.

Assuming a successful process, it takes approximately 5-7 days to produce 1 mL of SiDNAFe suspension with a concentration of 1 - 4 mg/mL, resulting in a reasonably high DNA concentration. However, after the bleaching and washing steps with a commercial bleach, the DNA yield drops to about 0.1% of the original concentration. The purpose of the bleaching step is to render any free DNA molecules inactive, as they are poorly protected or not encapsulated by the silica coating. Consequently, a significant portion of DNA is likely to remain unencapsulated at the end of the process.

However, for a field application, more tracer is needed. As an example, we need approximately 4 gram of SiDNAFe to redo the experiment conducted by Foppen et al. (2011) in the Merkske river (see Table A.11 in Appendix A). However, to produce a few grams of SiDNAFe, an up-scaling of the laboratory synthesis of SiDNAFe is required. This is a challenging task. As previously mentioned, the standard protocol produces approximately 0.24 mg of well-protected SiDNAFe per week. To generate a few grams of SiDNAFe, it would be necessary to produce 2500 to 16000 batches, which is currently unfeasible at the current stage of tracer production scale.

Research limitation

In this dissertation, it was observed that SiDNA(Fe) exhibited moderate and above colloidal stability in the selected representative river-water relevant conditions. The colloidal stability of DNA-tagged microparticles should be carefully assessed in different environmental conditions, as the behaviour and fate of the particles are strongly influenced by their interactions with the surroundings, such as, suspended solids, colloidal matter, and solutes in the water

columns. The composition and properties of waterborne substances can vary depending on the geology and hydrochemical conditions of the water body, and anthropogenic factors such as wastewater discharge can also have a significant impact. For instance, water composition conditions can be significantly altered downstream of wastewater treatment plant discharge points (e.g., McCormick et al., 2014; Klein et al., 2015; Hoellein et al., 2017). In addition, hydrochemical parameters such as pH and ionic strength can affect the surface properties and chemical forms of dissolved species that interact with the particles. For instance, particle aggregations are enhanced in the presence of natural organic matter and Ca^{2+} due to bridging (e.g., Chen and Elimelech, 2007; Liu et al., 2011). Therefore, it is important to thoroughly evaluate the colloidal stability of DNA-tagged microparticles in different environmental conditions and to consider potential physio-chemical interactions with suspended/colloidal matter, especially in cases where anthropogenic influences are present.

Additionally, the application of SiDNA(Fe) in real river environments requires a quantification of the mass balance. While it is easy to estimate a mass balance for SiDNA(Fe) in laboratory open channel experiments by comparing the total mass injected with total mass collected, doing so in real river tracing experiments is challenging. The mass loss of SiDNA(Fe) in these experiments could be due to particle settling, which can be estimated from the settling rates observed in Chapter 4, serving as a first estimate when planning field experiments. However, as demonstrated in Chapter 5, an enhanced SiDNAFe mass loss was observed that exceeded the gravitational settling rate. This might be related to grain-scale hyporheic flows and coupled water-sediment-particle interactions. In the real world, kinetic effects, such as kinetic attachment/detachment to the surfaces of grains, advective/diffusive hyporheic exchange due to topographic features of the channel, are likely to be more intricate, introducing additional uncertainty in the mass balance assessment.

Practical issues

The timing of the pandemic was particularly disadvantageous for our research. We had planned to conduct field experiments at the beginning of 2020, when we were 2.5 years into our research and ready to undertake a series of lab and field tests. Unfortunately, the outbreak of COVID-19 severely limited our lab access for over a year, which hindered our ability to conduct experiments and analyze SiDNA(Fe) samples. In addition, the pandemic caused a global shortage of qPCR consumables, which are critical for our routine lab analysis to quantify DNA-tagged microparticle.

Despite SiDNA(Fe) being an environmentally-friendly material with no genetic functionality, ecotoxicological tests must be conducted to evaluate the relevant exposure risks in eco-sensitive freshwaters.

6.3. Perspectives for future research and development of DNA-based tracing system

Environmental ENP is extensively used in daily life and industry. Consequently, these ENP accumulate in the environment, biology, and human bodies due to unregulated environmental discharge. In light of the current societal and environmental protection context, the ongoing and growing usage of ENPs, and the resulting accumulation of ENP waste, concerns about

their eco- and biotoxicity have become paramount in the scientific community.

Within this context, SiDNA(Fe) employed in this research represent a significant breakthrough. Their appropriate design and application in the field of water environment protection contribute to sustainable development and water resource management. They serve as a valuable surrogate for studying the environmental impact of ENPs in water bodies, which are actively and intensively studied by scientists to uncover their eco- and biotoxic properties.

From a hydrologist's perspective, utilizing microscale ENPs as tracers for large-scale hydrological systems presents practical challenges. The process of achieving this objective involves operational steps and procedures that are difficult to both downscale and upscale. Future research and application of such DNA-tagged tracer in surface water hydrology would greatly benefit from further improvement of sample treatment and analysis protocol. For now, in a small scale experiment setting, the routine workflow before sample analysis consists of initial sample-taking, sample mixing, subsampling, and magnetic separation. The ideal way for simplifying these steps would be applying a magnetic field at the desired sample locations where SiDNAFe would be immediately magnetically separated from the fluid on-site upon the arrival. This would also avoid all the potential errors and resulting data uncertainty associated with subsampling. For example, passive sample devices, such as continuous low-level aquatic monitoring, which can be used as field exaction of trace organics in freshwater (Coes et al., 2014), could be evaluated for their feasibility in automatic sampling of DNA tracers. In addition, in environmental monitoring and research, automated sampling stations are commonly used. These stations can be equipped with such magnetic-based/passive samplers to collect samples at predetermined intervals, which can be programmed to collect samples to realize automation for large-river tracing experiments. Furthermore, field application would also benefit from on-site DNA analysis. While quantitative DNA analysis typically requires controlled laboratory conditions, the development of field-deployable PCR and qPCR instruments now offers the potential for quick on-site DNA analysis (Stagg et al., 2018;J. Zhang et al., 2019; Nguyen et al., 2018; Billington et al., 2021). Billington et al. (2021) validated the field-deployable qPCR instrument "Liberty16" against a bench-top laboratory qPCR instrument, demonstrating their comparable sensitivity and repeatability for detecting targets in freshwater samples. This advancement would facilitate more effective and immediate tracking of SiDNA(Fe) tracers within hydrological systems.

From a macro perspective, hydrological conditions play a dominant role in redistribution and transport of mass in streams and rivers. The same holds for DNA-tagged microparticle. In this dissertation, Chapter 4 assessed the settling potential of SiDNAFe in different types of river waters under quiescent conditions and concluded that a pre-defined first-order decay process should be included for the transport modelling of SiDNAFe in large river tracing experiments. While this conclusion stands, we acknowledge that field hydrological conditions are likely to vary, especially for conditions in which high spatial fluctuations flow profiles exist, e.g., bank irregularities and low-velocity river sections which are more likely to be the hotspots of particle accumulation (Nizzetto et al., 2016). In this regard, further research is needed to test the potential effect of different flow conditions on the dispersal, transport, and especially mass loss of SiDNA(Fe) in streams and rivers.

Following the effect of different flow conditions, high flow periods can remobilize the deposited sediment. In this dissertation, river water had a limited amount of suspended

load. For high suspended loads, physico-chemical properties of water, such as density and viscosity, are also influenced by those suspended solids. The co-transport of sediments would likely have an effect on the transport and fate of SiDNA(Fe) in streams and rivers. Therefore, future studies are recommended to consider the cooperative transport of sediment particles with DNA-tagged microparticle.

It is apparent that artificial tracer tests carried out in surface waters need to be rather of a relatively short duration, given the relatively short tracing distances due to the dilution limit and analytical limit of the available tracers. In this dissertation one injection experiment is less than 2 hours. For a field experiment for tracing a few hundreds of meters, the duration, for example, is expected to be less than 8 - 10 hours (depend on stream flow rates). For future large-scale injection experiments, a longer experimental duration could be foreseen. When DNA-tagged microparticle comes into contact with the ecological macromolecules, such as NOM, extracellular polymeric substance (EPS), and proteins, a myriad of substances may adsorb onto the surface of DNA-tagged microparticles, becoming a part of a group of so-called "environmental corona " (L. Xu et al., 2020). Furthermore, this newly formed DNA-tagged environmental corona is strongly dependent on the hydrochemistry of environmental waters and will continue evolve dynamically, subsequently affecting its fate and transport in environments. For instance, the adsorption of humic acid/fulvic acid on SiO_2 particles is size-dependent, where the density of active sites are negatively proportional to the particle size due to their available surface areas (Liang et al., 2011). Ideally, the narrower the PSD, the more identical the behaviour is. Therefore, the PSD of DNA-tagged microparticle should be considered when evaluating these complex interactions. A more clear picture of the mass balance accounting of DNA-tagged microparticle would benefit from researching on the influence of such DNA-tagged environmental corona with some representative ecological macromolecules in streams and rivers.

In conclusion, DNA-tagged tracing poses a great potential in river tracing application. In this dissertation, we establish a solid foundation for understanding the transport and fate of SiDNA(Fe) in river water. For advancing the future large-scale application, we acknowledge practical challenges that require operational steps and procedures. Still, the application of DNA-tagged tracers in surface water hydrology for water resource management represents a significant breakthrough. Future research should focus on a further improvement of sample treatment and analysis protocols, as well as exploring the impact of flow conditions and cooperative transport of sediment particles with SiDNA(Fe). Moreover, the complex interactions between SiDNA(Fe) and environmental corona should be considered, taking into account the influence of the hydrochemistry of environmental waters and the particle size distribution. Such research would contribute to a more comprehensive understanding of the fate and transport of SiDNA(Fe) in the environment and facilitate their application in sustainable water resource management.

Bibliography

Abbott, S., & Holmes, N. (2013). *Nanocoatings: Principles and practice: From research to production*. DEStech Publications, Inc.

Abe, T., Kobayashi, S., & Kobayashi, M. (2011). Aggregation of colloidal silica particles in the presence of fulvic acid, humic acid, or alginate: Effects of ionic composition. *Colloids and Surfaces A: Physicochemical and Engineering Aspects*, *379*(1-3), 21–26.

Aguilar-Arteaga, K., Rodriguez, J., & Barrado, E. (2010). Magnetic solids in analytical chemistry: A review. *Analytica Chimica Acta*, *674*(2), 157–165.

Alimi, O. S., Farner Budarz, J., Hernandez, L. M., & Tufenkji, N. (2018). Microplastics and nanoplastics in aquatic environments: Aggregation, deposition, and enhanced contaminant transport. *Environmental science & technology*, *52*(4), 1704–1724.

Aquilanti, L., Clementi, F., Landolfo, S., Nanni, T., Palpacelli, S., & Tazioli, A. (2013). A dna tracer used in column tests for hydrogeology applications. *Environmental earth sciences*, *70*, 3143–3154.

Aquilanti, L., Clementi, F., Nanni, T., Palpacelli, S., Tazioli, A., & Vivalda, P. M. (2016). Dna and fluorescein tracer tests to study the recharge, groundwater flowpath and hydraulic contact of aquifers in the umbria-marche limestone ridge (central apennines, italy). *Environmental Earth Sciences*, *75*, 1–17.

Auffan, M., Rose, J., Bottero, J.-Y., Lowry, G. V., Jolivet, J.-P., & Wiesner, M. R. (2009). Towards a definition of inorganic nanoparticles from an environmental, health and safety perspective. *Nature nanotechnology*, *4*(10), 634–641.

Azimzada, A., Jreije, I., Hadioui, M., Shaw, P., Farner, J. M., & Wilkinson, K. J. (2021). Quantification and characterization of ti-, ce-, and ag-nanoparticles in global surface waters and precipitation. *Environmental Science & Technology*, *55*(14), 9836–9844.

Baalousha, M., Cornelis, G., Kuhlbusch, T., Lynch, I., Nickel, C., Peijnenburg, W., & Van Den Brink, N. (2016). Modeling nanomaterial fate and uptake in the environment: Current knowledge and future trends. *Environmental Science: Nano*, *3*(2), 323–345.

Ballent, A., Purser, A., de Jesus Mendes, P., Pando, S., & Thomsen, L. (2012). Physical transport properties of marine microplastic pollution. *Biogeosciences Discussions*, *9*(12).

Barthelmes, G., Pratsinis, S. E., & Buggisch, H. (2003). Particle size distributions and viscosity of suspensions undergoing shear-induced coagulation and fragmentation. *Chemical Engineering Science*, *58*(13), 2893–2902.

Battin, T. J., Kammer, F. V., Weilhartner, A., Ottofuelling, S., & Hofmann, T. (2009). Nanostructured tio2: Transport behavior and effects on aquatic microbial communities under environmental conditions. *Environmental science & technology*, *43*(21), 8098–8104.

Battin, T. J., Kaplan, L. A., Denis Newbold, J., & Hansen, C. M. (2003). Contributions of microbial biofilms to ecosystem processes in stream mesocosms. *Nature*, *426*(6965), 439–442.

Becker, M. W., & Coplen, T. B. (2001). Use of deuterated water as a conservative artificial groundwater tracer. *Hydrogeology Journal*, *9*, 512–516.

Bencala, K. E., Gooseff, M. N., & Kimball, B. A. (2011). Rethinking hyporheic flow and transient storage to advance understanding of stream-catchment connections. *Water Resources Research*, *47*(3).

Bergström, L. (1997). Hamaker constants of inorganic materials. *Advances in colloid and interface science*, *70*, 125–169.

Besseling, E., Quik, J. T., Sun, M., & Koelmans, A. A. (2017). Fate of nano-and microplastic in freshwater systems: A modeling study. *Environmental pollution*, *220*, 540–548.

Billington, C., Abeysekera, G., Scholes, P., Pickering, P., & Pang, L. (2021). Utility of a field deployable qpcr instrument for analyzing freshwater quality. *Agrosystems, Geosciences & Environment*, *4*(4), e20223.

Boano, F., Camporeale, C., Revelli, R., & Ridolfi, L. (2006). Sinuosity-driven hyporheic exchange in meandering rivers. *Geophysical Research Letters*, *33*(18).

Boano, F., Harvey, J. W., Marion, A., Packman, A. I., Revelli, R., Ridolfi, L., & Wörman, A. (2014). Hyporheic flow and transport processes: Mechanisms, models, and biogeochemical implications. *Reviews of Geophysics*, *52*(4), 603–679.

Briggs, M. A., Gooseff, M. N., Arp, C. D., & Baker, M. A. (2009). A method for estimating surface transient storage parameters for streams with concurrent hyporheic storage. *Water Resources Research*, *45*(4).

Buffle, J., Wilkinson, K. J., Stoll, S., Filella, M., & Zhang, J. (1998). A generalized description of aquatic colloidal interactions: The three-colloidal component approach. *Environmental Science & Technology*, *32*(19), 2887–2899.

Carman, P. C. (1937). The determination of the specific surface area of powders i. *J. Soc. Chem. Ind.*, *57*, 225–234.

Carman, P. C. (1956). Flow of gases through porous media. *(No Title)*.

Carrier III, W. D. (2003). Goodbye, hazen; hello, kozeny-carman. *Journal of geotechnical and geoenvironmental engineering*, *129*(11), 1054–1056.

Chakraborty, S., Foppen, J. W., & Schijven, J. F. (2022). Effect of concentration of silica encapsulated ds-dna colloidal microparticles on their transport through saturated porous media. *Colloids and Surfaces A: Physicochemical and Engineering Aspects*, *651*, 129625.

Chen, K. L., & Elimelech, M. (2007). Influence of humic acid on the aggregation kinetics of fullerene (c60) nanoparticles in monovalent and divalent electrolyte solutions. *Journal of colloid and interface science*, *309*(1), 126–134.

Choi, J., Harvey, J. W., & Conklin, M. H. (2000). Characterizing multiple timescales of stream and storage zone interaction that affect solute fate and transport in streams. *Water Resources Research*, *36*(6), 1511–1518.

Clifford, N., Robert, A., & Richards, K. (1992). Estimation of flow resistance in gravel-bedded rivers: A physical explanation of the multiplier of roughness length. *Earth Surface Processes and Landforms*, *17*(2), 111–126.

Coes, A. L., Paretti, N. V., Foreman, W. T., Iverson, J. L., & Alvarez, D. A. (2014). Sampling trace organic compounds in water: A comparison of a continuous active sampler to continuous passive and discrete sampling methods. *Science of the total environment*, *473*, 731–741.

Cox, M. H., Mendez, G. O., Kratzer, C. R., & Reichard, E. G. (2003). Evaluation of tracer tests completed in 1999 and 2000 on the upper santa clara river, los angeles and ventura counties, california. *Water-Resources Investigations Report*, *3*, 4277.

Crawford, S. M., & Sanford, L. P. (2001). Boundary shear velocities and fluxes in the meerc experimental ecosystems. *Marine Ecology Progress Series*, *210*, 1–12.

Crowe, C. T., Schwarzkopf, J. D., Sommerfeld, M., & Tsuji, Y. (2011). *Multiphase flows with droplets and particles*. CRC press.

Dahlke, H. E., Williamson, A. G., Georgakakos, C., Leung, S., Sharma, A. N., Lyon, S. W., & Walter, M. T. (2015). Using concurrent dna tracer injections to infer glacial flow pathways. *Hydrological Processes*, *29*(25), 5257–5274.

Dalas, E., & Koutsoukos, P. G. (1990). Phosphate adsorption at the porous glass/water and sio2/water interfaces. *Journal of colloid and interface science*, *134*(2), 299–304.

Derjaguin, B., & Landau, L. (1993). Theory of the stability of strongly charged lyophobic sols and of the adhesion of strongly charged particles in solutions of electrolytes. *Progress in Surface Science*, *43*(1-4), 30–59.

Domingos, R. F., Baalousha, M. A., Ju-Nam, Y., Reid, M. M., Tufenkji, N., Lead, J. R., Leppard, G. G., & Wilkinson, K. J. (2009). Characterizing manufactured nanoparticles in the environment: Multimethod determination of particle sizes. *Environmental science & technology*, *43*(19), 7277–7284.

Donaldson, J. R., & Tryon, T. (1990). *User's guide to starpac* (tech. rep.). NIST internal report, 86-3448.

Drummond, J., Davies-Colley, R., Stott, R., Sukias, J., Nagels, J., Sharp, A., & Packman, A. (2014). Retention and remobilization dynamics of fine particles and microorganisms in pastoral streams. *Water Research*, *66*, 459–472.

Drummond, J. D., Nel, H. A., Packman, A. I., & Krause, S. (2020). Significance of hyporheic exchange for predicting microplastic fate in rivers. *Environmental Science & Technology Letters*, *7*(10), 727–732.

Drummond, J. D., Schneidewind, U., Li, A., Hoellein, T. J., Krause, S., & Packman, A. I. (2022). Microplastic accumulation in riverbed sediment via hyporheic exchange from headwaters to mainstems. *Science Advances*, *8*(2), eabi9305.

Elimelech, M., Gregory, J., & Jia, X. (2013). *Particle deposition and aggregation: Measurement, modelling and simulation*. Butterworth-Heinemann.

Elliott, A. H., & Brooks, N. H. (1997). Transfer of nonsorbing solutes to a streambed with bed forms: Theory. *Water Resources Research*, *33*(1), 123–136.

Foppen, J. W. (2023). Artificial dna in hydrology. *WIREs Water*, *n/a*(n/a), e1681. https://doi.org/https://doi.org/10.1002/wat2.1681

Foppen, J. W., Orup, C., Adell, R., Poulalion, V., & Uhlenbrook, S. (2011). Using multiple artificial dna tracers in hydrology. *Hydrological Processes*, *25*(19), 3101–3106.

Foppen, J. W., Seopa, J., Bakobie, N., & Bogaard, T. (2013). Development of a methodology for the application of synthetic dna in stream tracer injection experiments. *Water resources research*, *49*(9), 5369–5380.

Frei, S., Piehl, S., Gilfedder, B., Löder, M. G., Krutzke, J., Wilhelm, L., & Laforsch, C. (2019). Occurence of microplastics in the hyporheic zone of rivers. *Scientific reports*, *9*(1), 15256.

Fries, J. S., & Taghon, G. L. (2010). Particle fluxes into permeable sediments: Comparison of mechanisms mediating deposition. *Journal of Hydraulic Engineering*, *136*(4), 214–221.

Fries, J. S. (2002). *Enhancement of fine particle deposition to permeable sediments* (tech. rep.). MASSACHUSETTS INST OF TECH CAMBRIDGE.

Frungieri, G., Babler, M. U., & Vanni, M. (2020). Shear-induced heteroaggregation of oppositely charged colloidal particles. *Langmuir*, *36*(36), 10739–10749.

Garner, K. L., Suh, S., & Keller, A. A. (2017). Assessing the risk of engineered nanomaterials in the environment: Development and application of the nanofate model. *Environmental Science & Technology*, *51*(10), 5541–5551.

Garnett, M. C., Ferruti, P., Ranucci, E., Suardi, M. A., Heyde, M., & Sleat, R. (2009). Sterically stabilized self-assembling reversibly cross-linked polyelectrolyte complexes with nucleic acids for environmental and medical applications.

Gibson, K., Schwab, K., Spencer, S., & Borchardt, M. (2012). Measuring and mitigating inhibition during quantitative real time pcr analysis of viral nucleic acid extracts from large-volume environmental water samples. *Water Research*, *46*(13), 4281–4291.

Goeppert, N., & Goldscheider, N. (2019). Improved understanding of particle transport in karst groundwater using natural sediments as tracers. *Water Research*, *166*, 115045.

Gooseff, M. N., Hall Jr, R. O., & Tank, J. L. (2007). Relating transient storage to channel complexity in streams of varying land use in jackson hole, wyoming. *Water Resources Research*, *43*(1).

Gooseff, M. N., Wondzell, S. M., Haggerty, R., & Anderson, J. (2003). Comparing transient storage modeling and residence time distribution (rtd) analysis in geomorphically varied reaches in the lookout creek basin, oregon, usa. *Advances in Water Resources*, *26*(9), 925–937.

Göppert, N., & Goldscheider, N. (2008). Solute and colloid transport in karst conduits under low-and high-flow conditions. *Groundwater*, *46*(1), 61–68.

Grasso*, D., Subramaniam, K., Butkus, M., Strevett, K., & Bergendahl, J. (2002). A review of non-dlvo interactions in environmental colloidal systems. *Reviews in Environmental Science and Biotechnology*, *1*, 17–38.

Gregory, J. (2005). *Particles in water: Properties and processes*. CRC Press.

Guo, L., & Macdonald, R. W. (2006). Source and transport of terrigenous organic matter in the upper yukon river: Evidence from isotope (δ13c, Δ14c, and δ15n) composition of dissolved, colloidal, and particulate phases. *Global Biogeochemical Cycles*, *20*(2).

Haberstroh, C. J., Arias, M. E., Yin, Z., & Wang, M. C. (2021). Effects of hydrodynamics on the cross-sectional distribution and transport of plastic in an urban coastal river. *Water Environment Research*, *93*(2), 186–200.

Haggerty, R., Argerich, A., & Martí, E. (2008). Development of a "smart" tracer for the assessment of microbiological activity and sediment-water interaction in natural waters: The resazurin-resorufin system. *Water Resources Research*, *44*(4).

Haggerty, R., Wondzell, S. M., & Johnson, M. A. (2002). Power-law residence time distribution in the hyporheic zone of a 2nd-order mountain stream. *Geophysical Research Letters*, *29*(13), 18–1.

Hamm, N. T., Dade, W. B., & Renshaw, C. E. (2011). Fine particle deposition to porous beds. *Water resources research*, *47*(11).

Harvey, J. W., Drummond, J. D., Martin, R. L., McPhillips, L. E., Packman, A. I., Jerolmack, D. J., Stonedahl, S. H., Aubeneau, A. F., Sawyer, A. H., Larsen, L. G., et al. (2012). Hydrogeomorphology of the hyporheic zone: Stream solute and fine particle interactions with a dynamic streambed. *Journal of Geophysical Research: Biogeosciences*, *117*(G4).

Harvey, J. W., & Wagner, B. J. (2000). Quantifying hydrologic interactions between streams and their subsurface hyporheic zones.

Harvey, J. W., Wagner, B. J., & Bencala, K. E. (1996). Evaluating the reliability of the stream tracer approach to characterize stream-subsurface water exchange. *Water resources research*, *32*(8), 2441–2451.

Heathwaite, A. L., & Dils, R. M. (2000). Characterising phosphorus loss in surface and subsurface hydrological pathways. *Science of the Total Environment*, *251*, 523–538.

Hijnen, N., & Clegg, P. S. (2014). Colloidal aggregation in mixtures of partially miscible liquids by shear-induced capillary bridges. *Langmuir*, *30*(20), 5763–5770.

Ho, R. T., & Gelhar, L. (1973). Turbulent flow with wavy permeable boundaries. *Journal of Fluid Mechanics*, *58*(2), 403–414.

Hochella Jr, M. F., Mogk, D. W., Ranville, J., Allen, I. C., Luther, G. W., Marr, L. C., McGrail, B. P., Murayama, M., Qafoku, N. P., Rosso, K. M., et al. (2019). Natural, incidental, and engineered nanomaterials and their impacts on the earth system. *Science*, *363*(6434), eaau8299.

Hoellein, T. J., McCormick, A. R., Hittie, J., London, M. G., Scott, J. W., & Kelly, J. J. (2017). Longitudinal patterns of microplastic concentration and bacterial assemblages in surface and benthic habitats of an urban river. *Freshwater Science*, *36*(3), 491–507.

Holland, J. H. (1992). Genetic algorithms. *Scientific american*, *267*(1), 66–73.

Horton, A. A., Walton, A., Spurgeon, D. J., Lahive, E., & Svendsen, C. (2017). Microplastics in freshwater and terrestrial environments: Evaluating the current understanding to identify the knowledge gaps and future research priorities. *Science of the total environment*, *586*, 127–141.

Huettel, M., & Webster, I. T. (2001). Porewater flow in permeable sediments. *The benthic boundary layer: transport processes and biogeochemistry*, *144*, 177.

Hünken, A., & Mutz, M. (2007). Field studies on factors affecting very fine and ultra fine particulate organic matter deposition in low-gradient sand-bed streams. *Hydrological Processes: An International Journal*, *21*(4), 525–533.

Isachenko, I. (2020). Catching the variety: Obtaining the distribution of terminal velocities of microplastics particles in a stagnant fluid by a stochastic simulation. *Marine Pollution Bulletin*, *159*, 111464.

Jamieson, R., Joy, D. M., Lee, H., Kostaschuk, R., & Gordon, R. (2005). Transport and deposition of sediment-associated escherichia coli in natural streams. *Water Research*, *39*(12), 2665–2675.

Jarvie, H., Neal, C., Rowland, A., Neal, M., Morris, P., Lead, J., Lawlor, A., Woods, C., Vincent, C., Guyatt, H., et al. (2012). Role of riverine colloids in macronutrient and metal partitioning and transport, along an upland–lowland land-use continuum, under low-flow conditions. *Science of the Total Environment*, *434*, 171–185.

Jekel, M. R. (1986). The stabilization of dispersed mineral particles by adsorption of humic substances. *Water research*, *20*(12), 1543–1554.

Ji, W., Tang, Q., Shen, Z., Fan, M., & Li, F. (2020). The adsorption of phosphate on hydroxylated alpha-sio2 (0 0 1) surface and influence of typical anions: A theoretical study. *Applied Surface Science*, *501*, 144233.

Johnson, C. P., Li, X., & Logan, B. E. (1996). Settling velocities of fractal aggregates. *Environmental science & technology*, *30*(6), 1911–1918.

Karwan, D. L., & Saiers, J. E. (2009). Influences of seasonal flow regime on the fate and transport of fine particles and a dissolved solute in a new england stream. *Water Resources Research*, *45*(11).

Käser, D., Binley, A., & Heathwaite, A. L. (2013). On the importance of considering channel microforms in groundwater models of hyporheic exchange. *River Research and Applications*, *29*(4), 528–535.

Kerr, P., Gooseff, M., & Bolster, D. (2013). The significance of model structure in one-dimensional stream solute transport models with multiple transient storage zones–competing vs. nested arrangements. *Journal of hydrology*, *497*, 133–144.

Khelifa, A., & Hill, P. S. (2006). Models for effective density and settling velocity of flocs. *Journal of Hydraulic Research*, *44*(3), 390–401.

Kianfar, B., Tian, J., Rozemeijer, J., van der Zaan, B., Bogaard, T. A., & Foppen, J. W. (2022). Transport characteristics of dna-tagged silica colloids as a colloidal tracer in saturated sand columns; role of solution chemistry, flow velocity, and sand grain size. *Journal of Contaminant Hydrology*, *246*, 103954.

Kim, J.-Y., & Sansalone, J. J. (2008). Zeta potential of clay-size particles in urban rainfall–runoff during hydrologic transport. *Journal of Hydrology*, *356*(1-2), 163–173.

Kittilä, A., Jalali, M., Evans, K. F., Willmann, M., Saar, M. O., & Kong, X.-Z. (2019). Field comparison of dna-labeled nanoparticle and solute tracer transport in a fractured crystalline rock. *Water Resources Research*, *55*(8), 6577–6595.

Klaine, S. J., Alvarez, P. J., Batley, G. E., Fernandes, T. F., Handy, R. D., Lyon, D. Y., Mahendra, S., McLaughlin, M. J., & Lead, J. R. (2008). Nanomaterials in the environment: Behavior, fate, bioavailability, and effects. *Environmental Toxicology and Chemistry: An International Journal*, *27*(9), 1825–1851.

Klein, S., Worch, E., & Knepper, T. P. (2015). Occurrence and spatial distribution of microplastics in river shore sediments of the rhine-main area in germany. *Environmental science & technology*, *49*(10), 6070–6076.

Knorr, B., Maloszewski, P., Krämer, F., & Stumpp, C. (2016). Diffusive mass exchange of non-reactive substances in dual-porosity porous systems–column experiments under saturated conditions. *Hydrological Processes*, *30*(6), 914–926.

Kooi, M., Besseling, E., Kroeze, C., Van Wezel, A. P., & Koelmans, A. A. (2018). Modeling the fate and transport of plastic debris in freshwaters: Review and guidance. *Freshwater microplastics: Emerging environmental contaminants?*, 125–152.

Koppel, D. E. (1972). Analysis of macromolecular polydispersity in intensity correlation spectroscopy: The method of cumulants. *The Journal of Chemical Physics*, *57*(11), 4814–4820.

Kumar, R., Sharma, P., Verma, A., Jha, P. K., Singh, P., Gupta, P. K., Chandra, R., & Prasad, P. V. (2021). Effect of physical characteristics and hydrodynamic conditions on transport and deposition of microplastics in riverine ecosystem. *Water*, *13*(19), 2710.

Labille, J., Harns, C., Bottero, J.-Y., & Brant, J. (2015). Heteroaggregation of titanium dioxide nanoparticles with natural clay colloids. *Environmental science & technology*, *49*(11), 6608–6616.

Lagarde, F., Olivier, O., Zanella, M., Daniel, P., Hiard, S., & Caruso, A. (2016). Microplastic interactions with freshwater microalgae: Hetero-aggregation and changes in plastic density appear strongly dependent on polymer type. *Environmental pollution*, *215*, 331–339.

Larsen, L. G., Harvey, J. W., Noe, G. B., & Crimaldi, J. P. (2009). Predicting organic floc transport dynamics in shallow aquatic ecosystems: Insights from the field, the laboratory, and numerical modeling. *Water Resources Research*, *45*(1).

Lartiges, B., Deneux-Mustin, S., Villemin, G., Mustin, C., Barres, O., Chamerois, M., Gerard, B., & Babut, M. (2001). Composition, structure and size distribution of suspended particulates from the rhine river. *Water Research*, *35*(3), 808–816.

Lazar, A. N., Butterfield, D., Futter, M. N., Rankinen, K., Thouvenot-Korppoo, M., Jarritt, N., Lawrence, D. S., Wade, A. J., & Whitehead, P. G. (2010). An assessment of the fine sediment dynamics in an upland river system: Inca-sed modifications and implications for fisheries. *Science of the Total Environment*, *408*(12), 2555–2566.

Lead, J. R., Batley, G. E., Alvarez, P. J., Croteau, M.-N., Handy, R. D., McLaughlin, M. J., Judy, J. D., & Schirmer, K. (2018). Nanomaterials in the environment: Behavior, fate, bioavailability, and effects—an updated review. *Environmental toxicology and chemistry*, *37*(8), 2029–2063.

Lead, J. R., & Wilkinson, K. J. (2006). Aquatic colloids and nanoparticles: Current knowledge and future trends. *Environmental Chemistry*, *3*(3), 159–171.

Ledin, A., Karlsson, S., & Allard, B. (1993). Effects of ph, ionic strength and a fulvic acid on size distribution and surface charge of colloidal quartz and hematite. *Applied Geochemistry*, *8*(4), 409–414.

Lee, B., Kim, J., Hur, J., Choi, I., Toorman, E., Fettweis, M., & Choi, J. (2019). Seasonal dynamics of organic matter composition and its effects on suspended sediment flocculation in river water. *Water Resources Research*, *55*(8), 6968–6985.

Leibundgut, C., & Seibert, J. (2011). 2.09 - tracer hydrology. In P. Wilderer (Ed.), *Treatise on water science* (pp. 215–236). Elsevier.

Leibundgut, C., Maloszewski, P., Külls, C., et al. (2009). *Tracers in hydrology*. Wiley-Blackwell Chichester.

Lerche, D. (2002). Dispersion stability and particle characterization by sedimentation kinetics in a centrifugal field. *Journal of Dispersion Science and Technology*, *23*(5), 699–709.

Li, Y., Wang, X., Fu, W., Xia, X., Liu, C., Min, J., Zhang, W., & Crittenden, J. C. (2019). Interactions between nano/micro plastics and suspended sediment in water: Implications on aggregation and settling. *Water research*, *161*, 486–495.

Liang, L., Luo, L., & Zhang, S. (2011). Adsorption and desorption of humic and fulvic acids on sio2 particles at nano-and micro-scales. *Colloids and Surfaces A: Physicochemical and Engineering Aspects*, *384*(1-3), 126–130.

Liao, R., Yang, P., Wu, W., Luo, D., & Yang, D. (2018). A dna tracer system for hydrological environment investigations. *Environmental science & technology*, *52*(4), 1695–1703.

Liao, R., Zhang, J., Li, T., Luo, D., & Yang, D. (2020). Biopolymer/plasmid dna microspheres as tracers for multiplexed hydrological investigation. *Chemical Engineering Journal*, *401*, 126035.

Lick, W., Huang, H., & Jepsen, R. (1993). Flocculation of fine-grained sediments due to differential settling. *Journal of Geophysical Research: Oceans*, *98*(C6), 10279–10288.

Lindahl, T. (1993). Instability and decay of the primary structure of dna. *nature*, *362*(6422), 709–715.

Liu, X., Wazne, M., Chou, T., Xiao, R., & Xu, S. (2011). Influence of ca2+ and suwannee river humic acid on aggregation of silicon nanoparticles in aqueous media. *Water research*, *45*(1), 105–112.

Ma, S., Zhou, K., Yang, K., & Lin, D. (2015). Heteroagglomeration of oxide nanoparticles with algal cells: Effects of particle type, ionic strength and ph. *Environmental Science & Technology*, *49*(2), 932–939.

Maggi, F., & Tang, F. H. (2015). Analysis of the effect of organic matter content on the architecture and sinking of sediment aggregates. *Marine Geology*, *363*, 102–111.

Mahler, B. J., Winkler, M., Bennett, P., & Hillis, D. M. (1998). Dna-labeled clay: A sensitive new method for tracing particle transport. *Geology*, *26*(9), 831–834.

Malm, A. V., & Corbett, J. C. (2019). Improved dynamic light scattering using an adaptive and statistically driven time resolved treatment of correlation data. *Scientific reports*, *9*(1), 13519.

Many, G., Bourrin, F., de Madron, X. D., Pairaud, I., Gangloff, A., Doxaran, D., Ody, A., Verney, R., Menniti, C., Le Berre, D., et al. (2016). Particle assemblage characterization in the rhone river rofi. *Journal of Marine Systems*, *157*, 39–51.

McCarthy, J., & Zachara, J. (1989). Es&t features: Subsurface transport of contaminants. *Environmental science & technology*, *23*(5), 496–502.

McCarthy, J. F., McKay, L. D., & Bruner, D. D. (2002). Influence of ionic strength and cation charge on transport of colloidal particles in fractured shale saprolite. *Environmental science & technology*, *36*(17), 3735–3743.

McCluskey, J., Flores, M. E., Hinojosa, J., Jafarzadeh, A., Moghadam, S. V., Phan, D. C., Green, R. T., & Kapoor, V. (2021). Tracking water with synthetic dna tracers using droplet digital pcr. *ACS ES&T Water*, *1*(5), 1177–1183.

McCormick, A., Hoellein, T. J., Mason, S. A., Schluep, J., & Kelly, J. J. (2014). Microplastic is an abundant and distinct microbial habitat in an urban river. *Environmental science & technology*, *48*(20), 11863–11871.

McNair, J. N., & Newbold, J. D. (2012). Turbulent particle transport in streams: Can exponential settling be reconciled with fluid mechanics? *Journal of theoretical biology*, *300*, 62–80.

McNair, J. N., Newbold, J. D., & Hart, D. D. (1997). Turbulent transport of suspended particles and dispersing benthic organisms: How long to hit bottom? *Journal of Theoretical Biology*, *188*(1), 29–52.

McNew, C. P., Wang, C., Walter, M. T., & Dahlke, H. E. (2018). Fabrication, detection, and analysis of dna-labeled plga particles for environmental transport studies. *Journal of colloid and interface science*, *526*, 207–219.

Metin, C. O., Bonnecaze, R. T., Lake, L. W., Miranda, C. R., & Nguyen, Q. P. (2014). Aggregation kinetics and shear rheology of aqueous silica suspensions. *Applied Nanoscience*, *4*, 169–178.

Michel, R. (2005). *Tritium in the hydrologic cycle*. Springer.

Mikutis, G., Deuber, C. A., Schmid, L., Kittilä, A., Lobsiger, N., Puddu, M., Asgeirsson, D. O., Grass, R. N., Saar, M. O., & Stark, W. J. (2018). Silica-encapsulated dna-based tracers for aquifer characterization. *Environmental science & technology*, *52*(21), 12142–12152.

Morrison, I. D., Grabowski, E., & Herb, C. (1985). Improved techniques for particle size determination by quasi-elastic light scattering. *Langmuir*, *1*(4), 496–501.

Nagaoka, H., & Ohgaki, S. (1990). Mass transfer mechanism in a porous riverbed. *Water Research*, *24*(4), 417–425.

Nantke, C. K., Frings, P. J., Stadmark, J., Czymzik, M., & Conley, D. J. (2019). Si cycling in transition zones: A study of si isotopes and biogenic silica accumulation in the chesapeake bay through the holocene. *Biogeochemistry*, *146*, 145–170.

Newbold, J. D., Elwood, J. W., O'Neill, R. V., & Winkle, W. V. (1981). Measuring nutrient spiralling in streams. *Canadian Journal of Fisheries and Aquatic Sciences*, *38*(7), 860–863.

Newbold, J. D., Thomas, S. A., Minshall, G. W., Cushing, C. E., & Georgian, T. (2005). Deposition, benthic residence, and resuspension of fine organic particles in a mountain stream. *Limnology and Oceanography*, *50*(5), 1571–1580.

Newbold, J., Elwood, J., O'neill, R., & Sheldon, A. (1983). Phosphorus dynamics in a woodland stream ecosystem: A study of nutrient spiralling. *Ecology*, *64*(5), 1249–1265.

Nguyen, P. L., Sudheesh, P. S., Thomas, A. C., Sinnesael, M., Haman, K., & Cain, K. D. (2018). Rapid detection and monitoring of flavobacterium psychrophilum in water by using a handheld, field-portable quantitative pcr system. *Journal of Aquatic Animal Health*, *30*(4), 302–311.

Nikaradse, J. (1933). Law of flows in rough pipes.

Nizzetto, L., Bussi, G., Futter, M. N., Butterfield, D., & Whitehead, P. G. (2016). A theoretical assessment of microplastic transport in river catchments and their retention by soils and river sediments. *Environmental Science: Processes & Impacts*, *18*(8), 1050–1059.

Nocito-Gobel, J., & Tobiason, J. E. (1996). Effects of ionic strength on colloid deposition and release. *Colloids and Surfaces A: Physicochemical and Engineering Aspects*, *107*, 223–231.

O'Connor, B. L., Harvey, J. W., & McPhillips, L. E. (2012). Thresholds of flow-induced bed disturbances and their effects on stream metabolism in an agricultural river. *Water Resources Research*, *48*(8).

Oncsik, T., Trefalt, G., Csendes, Z., Szilagyi, I., & Borkovec, M. (2014). Aggregation of negatively charged colloidal particles in the presence of multivalent cations. *Langmuir*, *30*(3), 733–741.

Oney, D. M., & Nason, J. A. (2021). Natural organic matter surface coverage as a predictor of heteroaggregation between nanoparticles and colloids. *Environmental Science: Nano*, *8*(3), 687–697.

Ongerth, J. E., & Pecoraro, J. P. (1996). Electrophoretic mobility of cryptosporidium oocysts and giardia cysts. *Journal of Environmental Engineering*, *122*(3), 228–231.

Ongley, E. D., Krishnappan, B., Droppo, G., Rao, S., & Maguire, R. (1992). Cohesive sediment transport: Emerging issues for toxic chemical management. *Hydrobiologia*, *235*, 177–187.

Ottofuelling, S., Von Der Kammer, F., & Hofmann, T. (2011). Commercial titanium dioxide nanoparticles in both natural and synthetic water: Comprehensive multidimensional testing and prediction of aggregation behavior. *Environmental Science & Technology*, *45*(23), 10045–10052.

Packman, A. I., Brooks, N. H., & Morgan, J. J. (2000). A physicochemical model for colloid exchange between a stream and a sand streambed with bed forms. *Water Resources Research*, *36*(8), 2351–2361.

Pang, L., Abeysekera, G., Hanning, K., Premaratne, A., Robson, B., Abraham, P., Sutton, R., Hanson, C., Hadfield, J., Heiligenthal, L., et al. (2020). Water tracking in surface water, groundwater and soils using free and alginate-chitosan encapsulated synthetic dna tracers. *Water Research*, *184*, 116192.

Pang, L., Heiligenthal, L., Premaratne, A., Hanning, K. R., Abraham, P., Sutton, R., Hadfield, J., & Billington, C. (2022). Degradation and adsorption of synthetic dna water tracers in environmental matrices. *Science of The Total Environment*, *844*, 157146.

Pang, L., Robson, B., McGill, E., Varsani, A., Gillot, L., Li, J., & Abraham, P. (2017). Tracking effluent discharges in undisturbed stony soil and alluvial gravel aquifer using synthetic dna tracers. *Science of the Total Environment*, *592*, 144–152.

Paul, M. J., & Hall Jr, R. O. (2002). Particle transport and transient storage along a stream-size gradient in the hubbard brook experimental forest. *Journal of the North American Benthological Society*, *21*(2), 195–205.

Paunescu, D., Puddu, M., Soellner, J. O., Stoessel, P. R., & Grass, R. N. (2013). Reversible dna encapsulation in silica to produce ros-resistant and heat-resistant synthetic dna'fossils'. *Nature protocols*, *8*(12), 2440–2448.

Peijnenburg, W. J., Baalousha, M., Chen, J., Chaudry, Q., Von der kammer, F., Kuhlbusch, T. A., Lead, J., Nickel, C., Quik, J. T., Renker, M., et al. (2015). A review of the properties and processes determining the fate of engineered nanomaterials in the aquatic environment. *Critical Reviews in Environmental Science and Technology*, *45*(19), 2084–2134.

Petosa, A. R., Jaisi, D. P., Quevedo, I. R., Elimelech, M., & Tufenkji, N. (2010). Aggregation and deposition of engineered nanomaterials in aquatic environments: Role of

physicochemical interactions. *Environmental science & technology*, *44*(17), 6532–6549.

Phillips, C. B., Dallmann, J. D., Jerolmack, D. J., & Packman, A. I. (2019). Fine-particle deposition, retention, and resuspension within a sand-bedded stream are determined by streambed morphodynamics. *Water Resources Research*, *55*(12), 10303–10318.

Praetorius, A., Badetti, E., Brunelli, A., Clavier, A., Gallego-Urrea, J. A., Gondikas, A., Hassellöv, M., Hofmann, T., Mackevica, A., Marcomini, A., et al. (2020). Strategies for determining heteroaggregation attachment efficiencies of engineered nanoparticles in aquatic environments. *Environmental Science: Nano*, *7*(2), 351–367.

Praetorius, A., Scheringer, M., & Hungerbühler, K. (2012). Development of environmental fate models for engineered nanoparticles a case study of tio2 nanoparticles in the rhine river. *Environmental science & technology*, *46*(12), 6705–6713.

Puddu, M., Paunescu, D., Stark, W. J., & Grass, R. N. (2014). Magnetically recoverable, thermostable, hydrophobic dna/silica encapsulates and their application as invisible oil tags. *ACS nano*, *8*(3), 2677–2685.

Quik, J. T., de Klein, J. J., & Koelmans, A. A. (2015). Spatially explicit fate modelling of nanomaterials in natural waters. *Water research*, *80*, 200–208.

Quik, J. T., Stuart, M. C., Wouterse, M., Peijnenburg, W., Hendriks, A. J., & van de Meent, D. (2012). Natural colloids are the dominant factor in the sedimentation of nanoparticles. *Environmental Toxicology and Chemistry*, *31*(5), 1019–1022.

Quik, J. T., Velzeboer, I., Wouterse, M., Koelmans, A. A., & Van de Meent, D. (2014). Heteroaggregation and sedimentation rates for nanomaterials in natural waters. *Water research*, *48*, 269–279.

Rådström, P., Knutsson, R., Wolffs, P., Lövenklev, M., & Löfström, C. (2004). Pre-pcr processing: Strategies to generate pcr-compatible samples. *Molecular biotechnology*, *26*, 133–146.

Ren, J., & Packman, A. I. (2002). Effects of background water composition on stream–subsurface exchange of submicron colloids. *Journal of Environmental Engineering*, *128*(7), 624–634.

Ren, J., & Packman, A. I. (2004a). Modeling of simultaneous exchange of colloids and sorbing contaminants between streams and streambeds. *Environmental science & technology*, *38*(10), 2901–2911.

Ren, J., & Packman, A. I. (2004b). Stream-subsurface exchange of zinc in the presence of silica and kaolinite colloids. *Environmental science & technology*, *38*(24), 6571–6581.

Ren, J., & Packman, A. I. (2005). Coupled stream- subsurface exchange of colloidal hematite and dissolved zinc, copper, and phosphate. *Environmental science & technology*, *39*(17), 6387–6394.

Revelli, R., Boano, F., Camporeale, C., & Ridolfi, L. (2008). Intra-meander hyporheic flow in alluvial rivers. *Water Resources Research*, *44*(12).

Rieckermann, J., Neumann, M., Ort, C., Huisman, J. L., & Gujer, W. (2005). Dispersion coefficients of sewers from tracer experiments. *Water Science and Technology*, *52*(5), 123–133.

Rietra, R. P., Hiemstra, T., & van Riemsdijk, W. H. (1999). Sulfate adsorption on goethite. *Journal of colloid and interface science*, *218*(2), 511–521.

Roche, K., Drummond, J. D., Boano, F., Packman, A., Battin, T., & Hunter, W. R. (2017). Benthic biofilm controls on fine particle dynamics in streams. *Water Resources Research*, *53*(1), 222–236.

Ruff, J. F., & Gelhar, L. W. (1972). Turbulent shear flow in porous boundary. *Journal of the Engineering Mechanics Division*, *98*(4), 975–991.

Runkel, R. L. (1998). *One-dimensional transport with inflow and storage (otis): A solute transport model for streams and rivers* (Vol. 98). US Department of the Interior, US Geological Survey.

Runkel, R. L. (2015). On the use of rhodamine wt for the characterization of stream hydrodynamics and transient storage. *Water Resources Research*, *51*(8), 6125–6142.

Ryan, J. N., & Elimelech, M. (1996). Colloid mobilization and transport in groundwater. *Colloids and surfaces A: Physicochemical and engineering aspects*, *107*, 1–56.

Sabir, I. H., Haldorsen, S., Torgersen, J., Alestrom, P., Gaut, S., Colleuille, H., Pedersen, T. S., Kitterod, N.-O., & Alestrom, P. (2000). Synthetic dna tracers: Examples of their application in water related studies. *IAHS Publication(International Association of Hydrological Sciences)*, (262), 159–165.

Saffman, P. G. (1965). The lift on a small sphere in a slow shear flow. *Journal of fluid mechanics*, *22*(2), 385–400.

Sasidharan, S., Torkzaban, S., Bradford, S. A., Dillon, P. J., & Cook, P. G. (2014). Coupled effects of hydrodynamic and solution chemistry on long-term nanoparticle transport and deposition in saturated porous media. *Colloids and Surfaces A: Physicochemical and Engineering Aspects*, *457*, 169–179.

Scheidegger, A., Borkovec, M., & Sticher, H. (1993). Coating of silica sand with goethite: Preparation and analytical identification. *Geoderma*, *58*(1-2), 43–65.

Schijven, J. F., Hassanizadeh, S. M., & De Bruin, R. H. (2002). Two-site kinetic modeling of bacteriophages transport through columns of saturated dune sand. *Journal of Contaminant Hydrology*, *57*(3-4), 259–279.

Schiperski, F., Zirlewagen, J., & Scheytt, T. (2016). Transport and attenuation of particles of different density and surface charge: A karst aquifer field study. *Environmental Science & Technology*, *50*(15), 8028–8035.

Schriewer, A., Wehlmann, A., & Wuertz, S. (2011). Improving qpcr efficiency in environmental samples by selective removal of humic acids with dax-8. *Journal of microbiological methods*, *85*(1), 16–21.

Schwertmann, U., & Cornell, R. M. (2008). *Iron oxides in the laboratory: Preparation and characterization*. John Wiley & Sons.

Sharma, A., Foppen, J. W., Banerjee, A., Sawssen, S., Bachhar, N., Peddis, D., & Bandyopadhyay, S. (2021). Magnetic nanoparticles to unique dna tracers: Effect of functionalization on physico-chemical properties. *Nanoscale research letters*, *16*(1), 1–16.

Sharma, A. N., Luo, D., & Walter, M. T. (2012). Hydrological tracers using nanobiotechnology: Proof of concept. *Environmental science & technology*, *46*(16), 8928–8936.

Shevlin, D., O'Brien, N., & Cummins, E. (2018). Silver engineered nanoparticles in freshwater systems–likely fate and behaviour through natural attenuation processes. *Science of the total environment*, *621*, 1033–1046.

Slomberg, D. L., Ollivier, P., Radakovitch, O., Baran, N., Sani-Kast, N., Miche, H., Borschneck, D., Grauby, O., Bruchet, A., Scheringer, M., et al. (2016). Characterisation of suspended particulate matter in the rhone river: Insights into analogue selection. *Environmental Chemistry*, *13*(5), 804–815.

Smart, P. L., & Laidlaw, I. (1977). An evaluation of some fluorescent dyes for water tracing. *Water resources research*, *13*(1), 15–33.

Spencer, K., Droppo, I., He, C., Grapentine, L., & Exall, K. (2011). A novel tracer technique for the assessment of fine sediment dynamics in urban water management systems. *Water research*, *45*(8), 2595–2606.

Spicer, P. T. (1997). *Shear-induced aggregation-fragmentation: Mixing and aggregate morphology effects*. University of Cincinnati.

Stagg, H., Merino, R., Oladimeji, P., Steiropoulos, N., Munro, E., et al. (2018). Preliminary validation of a portable real-time rt-pcr assay for the detection of salmonid alphavirus. *Bull Euro Assoc Fish Pathol*, *38*, 121–8.

Stern, D. A., Khanbilvardi, R., Alair, J. C., & Richardson, W. (2001). Description of flow through a natural wetland using dye tracer tests. *Ecological Engineering*, *18*(2), 173–184.

Stetefeld, J., McKenna, S. A., & Patel, T. R. (2016). Dynamic light scattering: A practical guide and applications in biomedical sciences. *Biophysical reviews*, *8*, 409–427.

Stokes, G. G., et al. (1851). On the effect of the internal friction of fluids on the motion of pendulums.

Stolpe, B., Guo, L., Shiller, A. M., & Hassellöv, M. (2010). Size and composition of colloidal organic matter and trace elements in the mississippi river, pearl river and the northern gulf of mexico, as characterized by flow field-flow fractionation. *Marine Chemistry*, *118*(3-4), 119–128.

Stonedahl, S. H., Harvey, J. W., & Packman, A. I. (2013). Interactions between hyporheic flow produced by stream meanders, bars, and dunes. *Water Resources Research*, *49*(9), 5450–5461.

Tajadini, M., Panjehpour, M., & Javanmard, S. H. (2014). Comparison of sybr green and taqman methods in quantitative real-time polymerase chain reaction analysis of four adenosine receptor subtypes. *Advanced biomedical research*, *3*.

Tang, F. H., & Maggi, F. (2016). A mesocosm experiment of suspended particulate matter dynamics in nutrient-and biomass-affected waters. *Water Research*, *89*, 76–86.

Tang, Y., Foppen, J. W., & Bogaard, T. A. (2021). Transport of silica encapsulated dna microparticles in controlled instantaneous injection open channel experiments. *Journal of Contaminant Hydrology*, *242*, 103880.

Tang, Y., van Rhijn, F., Abdelrady, A., Foppen, J., & Bogaard, T. (2023). Effect of channel bed sediment on the transport behaviour of superparamagnetic silica encapsulated dna microparticles in open channel injection experiments.

Tang, Y., Zhang, F., Bogaard, T., Chassagne, C., Ali, Z., Bandyopadhyay, S., & Foppen, J. W. (2023). Settling of superparamagnetic silica encapsulated dna microparticles in river water. *Hydrological Processes*, *37*(1), e14801.

Thomas, S. A., Newbold, J. D., Monaghan, M. T., Minshall, G. W., Georgian, T., & Cushing, C. E. (2001). The influence of particle size on seston deposition in streams. *Limnology and Oceanography*, *46*(6), 1415–1424.

Tonina, D., & Buffington, J. M. (2009). Hyporheic exchange in mountain rivers i: Mechanics and environmental effects. *Geography Compass*, *3*(3), 1063–1086.

Torkzaban, S., Bradford, S. A., van Genuchten, M. T., & Walker, S. L. (2008). Colloid transport in unsaturated porous media: The role of water content and ionic strength on particle straining. *Journal of contaminant hydrology*, *96*(1-4), 113–127.

Torkzaban, S., Bradford, S. A., & Walker, S. L. (2007). Resolving the coupled effects of hydrodynamics and dlvo forces on colloid attachment in porous media. *Langmuir*, *23*(19), 9652–9660.

Tukey, J. W. (1949). Comparing individual means in the analysis of variance. *Biometrics*, 99–114.

Van de Ven, T., & Mason, S. (1977). The microrheology of colloidal dispersions vii. orthokinetic doublet formation of spheres. *Colloid and Polymer Science*, *255*, 468–479.

Velde, B. (1977). *Clays and clay minerals in natural and synthetic systems*. Elsevier.

Velzeboer, I., Quik, J. T., van De Meent, D., & Koelmans, A. A. (2014). Rapid settling of nanoparticles due to heteroaggregation with suspended sediment. *Environmental Toxicology and Chemistry*, *33*(8), 1766–1773.

Verwey, E. J. W. (1947). Theory of the stability of lyophobic colloids. *The Journal of Physical Chemistry*, *51*(3), 631–636.

Vincent, A. E., & Hoellein, T. J. (2021). Distribution and transport of microplastic and fine particulate organic matter in urban streams. *Ecological Applications*, *31*(8), e02429.

Wagener, T., Camacho, L. A., & Wheater, H. S. (2002). Dynamic identifiability analysis of the transient storage model for solute transport in rivers. *Journal of Hydroinformatics*, *4*(3), 199–211.

Waldschläger, K., & Schüttrumpf, H. (2019). Effects of particle properties on the settling and rise velocities of microplastics in freshwater under laboratory conditions. *Environmental science & technology*, *53*(4), 1958–1966.

Wang, C., Liu, G., McNew, C. P., Volkmann, T. H. M., Pangle, L., Troch, P. A., Lyon, S. W., Kim, M., Huo, Z., & Dahlke, H. E. (2022). Simulation of experimental synthetic dna tracer transport through the vadose zone. *Water Research*, *223*, 119009.

Wang, H., Adeleye, A. S., Huang, Y., Li, F., & Keller, A. A. (2015). Heteroaggregation of nanoparticles with biocolloids and geocolloids. *Advances in colloid and interface Science*, *226*, 24–36.

Wanner, S. C., & Pusch, M. (2000). Use of fluorescently labeled lycopodium spores as a tracer for suspended particles in a lowland river. *Journal of the North American Benthological Society*, *19*(4), 648–658.

Watson, J. D., Watson, C., Gilman, M., Witkowski, J. A., Zoller, M., & Witkowski, J. (1992). *Recombinant dna*. Macmillan.

Werner, K. (1998). *Tracing technique in geohydrology*. Balkema.

Westhoff, M., Gooseff, M., Bogaard, T., & Savenije, H. (2011). Quantifying hyporheic exchange at high spatial resolution using natural temperature variations along a first-order stream. *Water Resources Research*, *47*(10).

Whitmer, S., Baker, L., & Wass, R. (2000). Loss of bromide in a wetland tracer experiment. *Journal of Environmental Quality*, *29*(6), 2043–2045.

Wilderer, P. A. (2010). *Treatise on water science*. Newnes.

Wilson, I. G. (1997). Inhibition and facilitation of nucleic acid amplification. *Applied and environmental microbiology*, *63*(10), 3741–3751.

Wilson, M., Wilson, L., Patey, I., & Shaw, H. (2014). The influence of individual clay minerals on formation damage of reservoir sandstones: A critical review with some new insights. *Clay Minerals*, *49*(2), 147–164.

Won, J., Lee, D., Pham, K., Lee, H., & Choi, H. (2019). Impact of particle size distribution of colloidal particles on contaminant transport in porous media. *Applied Sciences*, *9*(5), 932.

Workshop, S. S. (1990). Concepts and methods for assessing solute dynamics in stream ecosystems. *Journal of the North American Benthological Society*, *9*(2), 95–119.

Wörman, A., Packman, A. I., Johansson, H., & Jonsson, K. (2002). Effect of flow-induced exchange in hyporheic zones on longitudinal transport of solutes in streams and rivers. *Water Resources Research*, *38*(1), 2–1.

Wyer, M. D., Kay, D., Watkins, J., Davies, C., Kay, C., Thomas, R., Porter, J., Stapleton, C. M., & Moore, H. (2010). Evaluating short-term changes in recreational water quality during a hydrograph event using a combination of microbial tracers, environmental microbiology, microbial source tracking and hydrological techniques: A case study in southwest wales, uk. *water research*, *44*(16), 4783–4795.

Xu, L., Xu, M., Wang, R., Yin, Y., Lynch, I., & Liu, S. (2020). The crucial role of environmental coronas in determining the biological effects of engineered nanomaterials. *Small*, *16*(36), 2003691.

Xu, N., Huangfu, X., Li, Z., Wu, Z., Li, D., & Zhang, M. (2019). Nanoaggregates of silica with kaolinite and montmorillonite: Sedimentation and transport. *Science of the Total Environment*, *669*, 893–902.

Zaccone, A., Wu, H., Gentili, D., & Morbidelli, M. (2009). Theory of activated-rate processes under shear with application to shear-induced aggregation of colloids. *Physical Review E*, *80*(5), 051404.

Zhang, J., Guan, H., Zhao, W., Zhang, H., Wang, W., Ling, X., Xiao, Y., Guo, J., Huang, Z., Xu, Y., et al. (2019). Evaluation of the biofire filmarray gastrointestinal panel and real-time polymerase chain reaction assays for the detection of major diarrheagenic pathogens by a multicenter diarrheal disease surveillance program in china. *Foodborne Pathogens and Disease*, *16*(11), 788–798.

Zhang, Y., Chen, Y., Westerhoff, P., & Crittenden, J. (2009). Impact of natural organic matter and divalent cations on the stability of aqueous nanoparticles. *Water research*, *43*(17), 4249–4257.

Zhang, Y., Hartung, M. B., Hawkins, A. J., Dekas, A. E., Li, K., & Horne, R. N. (2021). Dna tracer transport through porous media—the effect of dna length and adsorption. *Water Resources Research*, *57*(2), 2020WR028382.

Zhang, Y., & Huang, T. (2022). Dna-based tracers for the characterization of hydrogeological systems—recent advances and new frontiers. *Water*, *14*(21), 3545.

Zhao, J., Li, Y., Wang, X., Xia, X., Shang, E., & Ali, J. (2021). Ionic-strength-dependent effect of suspended sediment on the aggregation, dissolution and settling of silver nanoparticles. *Environmental Pollution*, *279*, 116926.

Zhao, S., & Fernald, R. D. (2005). Comprehensive algorithm for quantitative real-time polymerase chain reaction. *Journal of computational biology*, *12*(8), 1047–1064.

Zhu, B., Xia, X., Zhang, S., & Tang, Y. (2018). Attenuation of bacterial cytotoxicity of carbon nanotubes by riverine suspended solids in water. *Environmental pollution*, *234*, 581–589.

Zhu, X., Munno, K., Grbic, J., Werbowski, L. M., Bikker, J., Ho, A., Guo, E., Sedlak, M., Sutton, R., Box, C., et al. (2021). Holistic assessment of microplastics and other anthropogenic microdebris in an urban bay sheds light on their sources and fate. *ACS ES&T Water*, *1*(6), 1401–1410.

Zimmermann-Timm, H. (2002). Characteristics, dynamics and importance of aggregates in rivers–an invited review. *International Review of Hydrobiology*, *87*(2-3), 197–240.

Zipper, H., Buta, C., Lämmle, K., Brunner, H., Bernhagen, J., & Vitzthum, F. (2003). Mechanisms underlying the impact of humic acids on dna quantification by sybr green i and consequences for the analysis of soils and aquatic sediments. *Nucleic acids research*, *31*(7), e39–e39.

A

Supplementary info

A.1. DNA and primer sequences

The DNA sequence of Si-DNA and SiDNAFe presented in this dissertation is artifically randomly generated with lengths of 68 nucleotides (the GC content is 46.2%). The DNA sequence of Si-DNA is designed by ETH Zurich group, and that of SiDNAFe is designed by Biolegio B.V.. Complete DNA sequences and primers are given in the Table A.1.

Table A.1: Si-DNA: DNA and primer sequences

Si-DNA MP	Sequence
Forward DNA	TTATGGGCTCTAAGGATCTCTTCGTTGTCGTTAGGTTCCTGCGTT TTTCGATTCGAGGGTGAGTT
Reverse DNA	AACTCACCCTCGAATCGAAAAACGCAGGAACCTAACGACAACG AAGAGATCCTTAGAGCCCATAA
Forward primer	5'–ATG GGC TCT AAG GAT CTC–3'
Reverse primer	5'–CTC ACC CTC GAA TCG AA–3'
SiDNAFe MP	
Forward DNA	TTCGGACAATCCTTTCCATATTACGCTCTGAAGGCTACTACTCCT TCTTATTAACTGGGTCTCGTTT
Reverse DNA	AAACGAGACCCAGTTAATAAGAAGGAGTAGTAGCCTTCAGAGC GTAATATGGAAAGGATTGTCCGAA
Forward primer	5'–CGG ACA ATC CTT TCC ATA–3'
Reverse primer	5'–ACG AGA CCC AGT TAA TAA G–3'

A.2. Standard curves and mass recovery calculation

The dilution curve (shown in Fig. A.1) was prepared in triplicate, as a representative to show an linear detection of particle concentrations based on Cq values. For each qPCR run a dilution curve in MQ in duplicate was included to extrapolate sample concentrations in the same assay. To the standard curve, a no template control (NTC) was added. The purpose of the NTC was to check for pollution during the process of preparing the mixture

for PCR analysis and to assess the importance of random amplification and the formation of primer-dimers. Since we used SYBR Green, an non-specific dsDNA-binding dye, any non-specific product can make false positive results (Tajadini et al., 2014). We noted random amplification of no template controls at around 35 cycles of amplification. Therefore, in order to distinguish positive samples from negative ones, the lowest reliable detection threshold cycle had to be determined. We applied a difference of 3-5 cycles between the lowest detectable positive sample and random amplification of a negative control sample. Therefore, samples were considered to be positive when the threshold cycle was below 30.

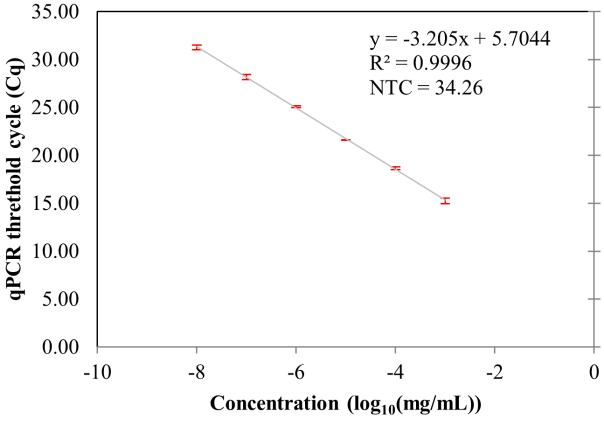

Figure A.1: Standard curves of Si-DNA in MQ. NTC represents no template control.

To convert electrical conductivity into NaCl concentration, a dilution curve was also plotted on the same day of the experiment (Fig. A.2).

Mass recovery (M.R., (%)) was determined using the integral method by calculation of the surface area under the BTC:

$$M.R. = \frac{(\int C_{sample} dt) \times q}{C_{ini} \times V_{ini}} \times 100 \tag{A.1}$$

Where C_{sample} is the concentration of sample Si-DNA/SiDNAFe/NaCl (mg/mL), q is the pump rate (mL/min), $C_{ini} \times V_{ini}$ is the initial DNA/NaCl mass injected (mg).

A.3. BATCH EXPERIMENT: INTERACTIONS BETWEEN SI-DNA WITH PVC

A container of PVC material was filled by a certain dilution of Si-DNA in Demi water reaching ~2 cm water level and was well-mixed by a glass bar, prior to which 100 μL sample was taken as a control for an initial concentration. The container was stored in room temperature shield from daylight. Samples were taken after 30 min, 1 hour, 2 hours, 1 day, 2 days and 7days from the container, and the relative particle concentration was

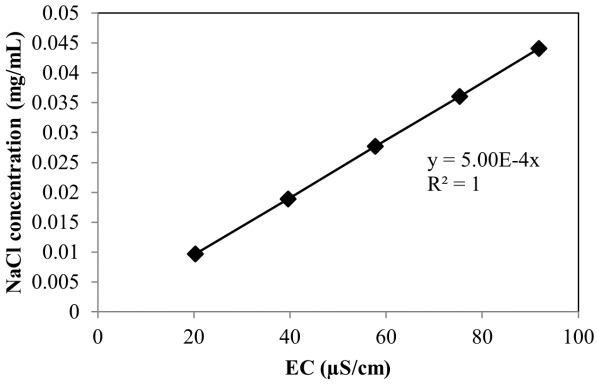

Figure A.2: Standard curve for electrical conductivity versus NaCl concentration.

quantified by measuring DNA concentrations in the samples using qPCR. The relative particle concentration (C/C_0) remained around 1 (±10%) (Figure A.3) throughout the entire experimental duration thus indicated that Si-DNA did not adsorb or interact with the PVC material used for injection experiments.

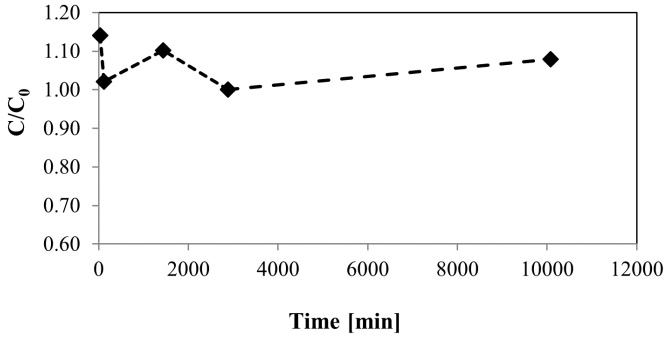

Figure A.3: Relative particle concentration (C/C_0) in contact with PVC over time.

A.4. Dye tracer injection

In the pulse injection experiments in Chapter 3, the injected dye tracer through the length of pump tube arrived at ~1'50" in the storage box, after which it created a coloured zone in the middle of the box between the inlet and sampling outlet. It took 33 seconds to complete the delivery of 10 mL dye tracer (at 2'24" given the pump velocity of ~18 mL/min). The dye tracer was usually fully mixed with water within 30 s since the entering moment.

A

A.5. OTIS MODEL IMPLEMENTATION, NONLINEAR LEAST SQUARES REGRESSION & DAI CACULATION

OTIS uses an inverse solution to equation 3.1 with the spatial derivatives approximated by an implicit Crank-Nicholson finite difference method (Runkel, 1998). OTIS model implementation requires initial estimates of the parameters on the right-hand side of equation 3.1 to constrain the model solution. For our experiments, discharge (Q), main channel cross-section area (A), transient storage parameters (A_s, α), and an estimated longitudinal dispersion (D) were derived. The initial estimates of A and A_s were derived from cross-sectional area of main channel and surface transient storage (cross-sectional area of the box under water level). As parameter reflects all storage including surface transient storage and hyporheic transient storage, and in Chapter 3 measured surface transient storage area was the initial estimate of A_s. Best-fit estimates of D_{NaCl} and α_{NaCl} from NaCl injection experiments were used as initial estimates of D_{Si-DNA} and α_{Si-DNA}. Parameters were optimized by minimizing the weighted sum of squared (RSS in equation A.3) differences between simulated and observed concentrations with objective functions given by:

$$c_i = f(u_i, \sigma) + e_i \tag{A.2}$$

$$RSS = \sum_{i=1}^{N} w_i [c_i - f(u_i, \boldsymbol{\Theta})]^2 = \sum_{i=1}^{N} (w_i {e_i}^2) \tag{A.3}$$

Where N: the number of observations; c_i: ith observation of the dependent variable, the observed main channel solute concentration [g/m^3]; u_i: vector of the time-space location of the ith observation; σ: vector of solute transport model parameters; $\boldsymbol{\Theta}$: the estimated parameters; e_i: random error associated with the ith observation; $f(u_i, \sigma)$: a nonlinear function that simulates the ith observation, the solution of equations 3.1 - 3.2 that provides the simulated main channel concentration; RSS: weighted residual sum of squares; w_i: weighting factor assigned to the ith observation.

Damkohler number was calculated according the equation as follows,

$$DaI = \frac{\alpha \times (1 + \frac{A}{A_s})L}{u} \tag{A.4}$$

Where α, A, and A_s refers to the terms used in equation 3.2; L represents channel length (m), and u reperesnts flow velocity (m/s).

A.6. SAMPLING SCHEME

A.7. DLVO CALCULATIONS AND MAJOR IONS OF THE WATER USED

The DLVO calculation was based on Abbott and Holmes (2013), and a Harmaker constant of 0.6×10^{-20} [J] for SiO_2 (quartz) was used for calculation (Bergström, 1997). The total energy potential V_T is composed of three terms: Hamaker (H) representing van der Waals interactions; Debye (D) representing charge interactions and Steric (S) representing interactions via polymer chains (V_S is omitted in this study):

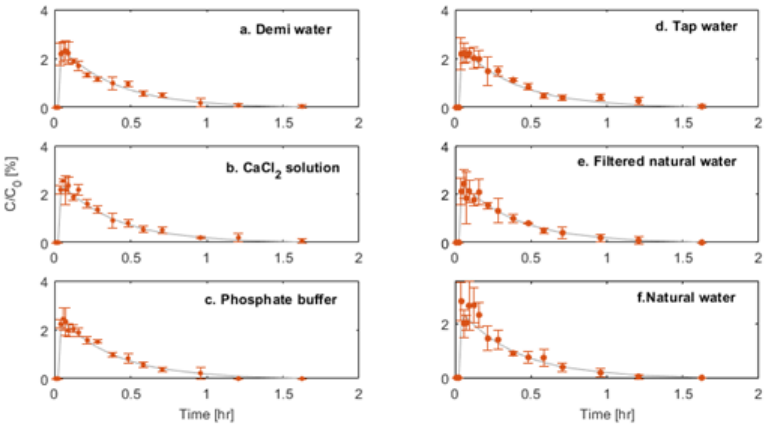

Figure A.4: Averaged observed BTCs of Si-DNA in 6 water types plotted in relative concentration C/C_0 [%]. The error bar represents the standard deviation of 3 data points from 3 replicate experiments. The averaged observed BTC of NaCl in grey line is plotted as a reference per water type.

$$V_T = V_H + V_D + V_S \tag{A.5}$$

For particles of radius r separated by distance h the V_H can be calculated as,

$$V_H = -\frac{A_{12} r}{12 h k T} \tag{A.6}$$

Where $A_1 2$ is the Hamaker constant (0.6×10^{-20} [J]) and kT is the Boltzmann temperature.

$$V_D = \frac{2\pi e_0 \varepsilon r \varphi^2 \ln 1 + e^{-(h/k^{-1})}}{k_B T} \tag{A.7}$$

Where k^{-1} is the Debye length given by :

$$k^{-1} = \sqrt{\frac{e_0 \varepsilon k_B T}{2 N_A e^2 I}} \tag{A.8}$$

N_A is Avogadro's number (6.02E+23 [/mole]), e_0 is permittivity of free space (8.85E-12 [F/m]), e is the electron charge (1.60E-19 [Coulomb]), ε is the dielectric constant (78.2), k_B is the Boltzmann constant (1.38E-23 [J/k]) and I is the ionic strength [mole/m^3]. The electric potential φ can be approximated by the zeta potential ζ [mV].

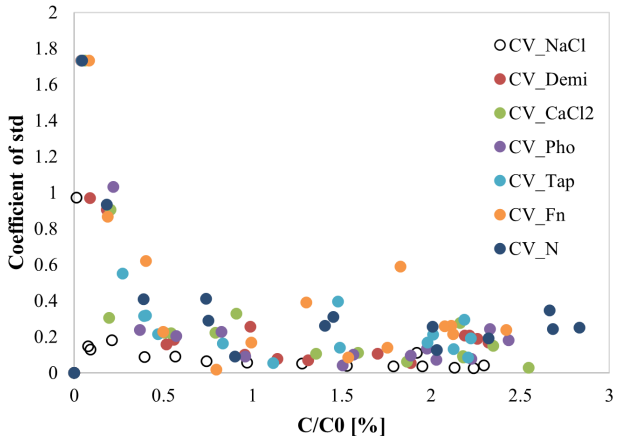

Figure A.5: Coefficient of variations (CV) of Si-DNA in 6 water types plotted as a function of C/C_0 [%].

Table A.2: An overview of the sampling protocol for injection experiments in Chapter 3.

Time	Sample interval	Sample volume	Number of sample
[min]	[min]	[ml]	[-]
0-10	1	18	10
10-40	2	36	15
40-100	5	90	12

A.8. SiDNAFe Lumisizer PSD characterisation and settling rates

PSD characterisation of the SiDNAFe microparticles using LUMiSizer: the kinetics of the transmission profiles were recorded at a wavelength of 410 nm with a time interval of 10 s. The mode "Constant time" was used with an increasing relative centrifuge force (RCF) from 105 g to ~ 2100 g during 64 mins of centrifugation. The density (water 998.4 kg/m^3) and dynamic viscosity of the suspending fluid (water 1.017 mPa·s), and the density (3300 kg/m^3) and refractive index (1.45) of the SiDNAFe microparticles were set to obtain the PSD.

Table A.3: An overview of the sampling protocol for injection experiments in Chapter5.

Elapsed time (min)	Sample interval	Number of samples
7 - 35	1	29
35 - 50	3	5
50 - 90	10	4
90 - 140	20	3

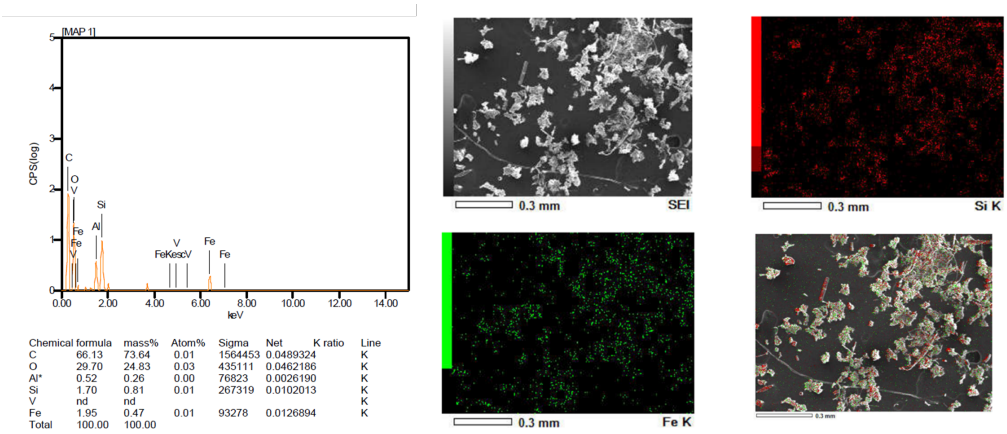

Figure A.6: Main elemental compositions of SPM in Merkske water based on EDS mapping (right, x100 magnification) and high-resolution images of the ion distributions of Fe and Si.

A.9. Main elemental compositions of SPM in 3 river waters

A.10. Sensitivity analysis in Chapter 5

Sensitivity analysis was used to determine the most appropriate combinations of processes to be considered. When the transient storage parameter set showed negligible sensitivity on the BTC fitting, the transient storage process was turned off. Deviations from the best-fit curve were assessed by comparing the coefficient of determination (R^2).

A.10.1. Sensitivity test for model simulated NaCl BTCs

Variation of A & α caused significant deviation (change of $R^2 > 0.1$) from the best-fit curve. Varying the A value greatly impacted the first arrival and the peak concentration, while decreasing the α value greatly diminished the tailing effect. Precisely, a change of ± 10% of the initial value of A lowered R^2 by 20%. A_S had less impact on the BTC shape, where until a 50% reduction of A_S a noticeable deviation of BTC can be reached (i.e., as in the peak concentration and the recession slope). Variation of D_L had the least impact on the BTC shape but caused a minor change in the peak concentration.

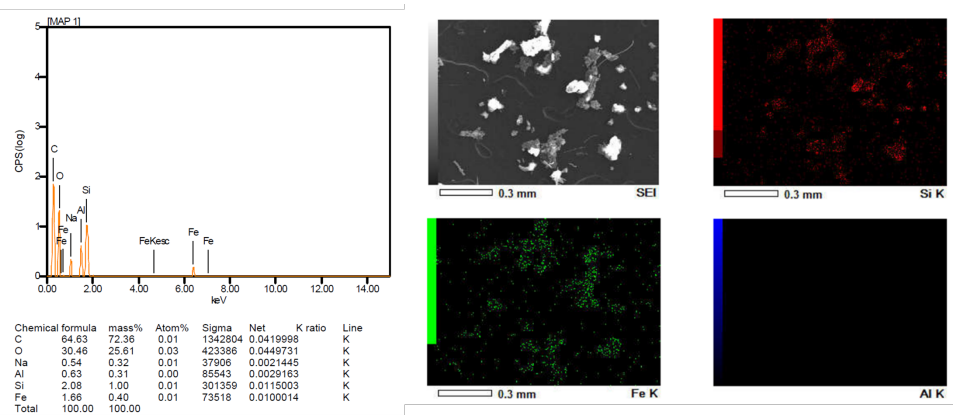

Chemical formula	mass%	Atom%	Sigma	Net	K ratio	Line
C	64.63	72.36	0.01	1342804	0.0419998	K
O	30.46	25.61	0.03	423386	0.0449731	K
Na	0.54	0.32	0.01	37906	0.0021445	K
Al	0.63	0.31	0.00	85543	0.0029163	K
Si	2.08	1.00	0.01	301359	0.0115003	K
Fe	1.66	0.40	0.01	73518	0.0100014	K
Total	100.00	100.00				

Figure A.7: Main elemental compositions of SPM in Strijbeek based on EDS mapping (right, x100 magnification) and high-resolution images of the ion distributions of Si, Fe, and Al.

A.10.2. SENSITIVITY TEST FOR MODEL SIMULATED SIDNAFE BTCS

Four transport parameters of modeled SiDNAFe BTCs responded similarly to that described in NaCl sensitivity tests, that is the sensitivity of $A \oint \alpha \oint A_S \oint D_L$. Inferior to NaCl, SiDNAFe had best-fit R^2 values ranging between 82.48 and 94.65 (Table A.9). Notably, transient storage was turned off when modeling BTCs in CS series, FS series, and GCS-Meuse as a result of the negligible sensitivity of A_S and α. Under these conditions, the sensitivity of A was still greater than that of D_L.

A.11. SIDNAFE BTCS AND THEIR CUMULATIVE DISTRIBUTION FUNCTION IN CHAPTER 5

As shown in Fig. A.19, in both Tap and Meuse water, SiDNAFe arrived significantly earlier in FS than in the other three series, yet with a similar rising limb to those in IP and CS. In Tap, the rising limbs of SiDNAFe BTCs had similar slopes but were separated from each other due to slightly different arrival times of SiDNAFe. In Meuse, GCS had the slowest arrival of SiDNAFe, while CS and IP had rising limbs that overlapped for the first coming 50% of the mass. SiDNAFe was relatively fast recovered from the channel between 0.5 to 1 hour.

A.12. GOETHITE COATING PROCESS IN CHAPTER 5

69.5 g unoxidised crystal of $FeSO_4 \cdot 7H_2O$ was dissolved in 610 mL of distilledwater through which N_2 gas had been bubbled for 30 min prior to the coating in order to create anaerobic conditions. To the solution 450 g sand and 500 mL of 1 M $NaHCO_3$ solution were added. The mixture of sand and solution was stirred and pumped with air continuously for 48 h to allow for the goethite to be formed and attached on the sand surface. After 48 h, the color of the solution turned from green-blue to ochre, which indicated the oxidation of Fe(II) to Fe(III). After the oxidation completion, the mixture of sand and ochre solution was aliquoted into 500 mL plastic bottles (~250 mL of mixture per bottle) and was shook at 220 rpm for

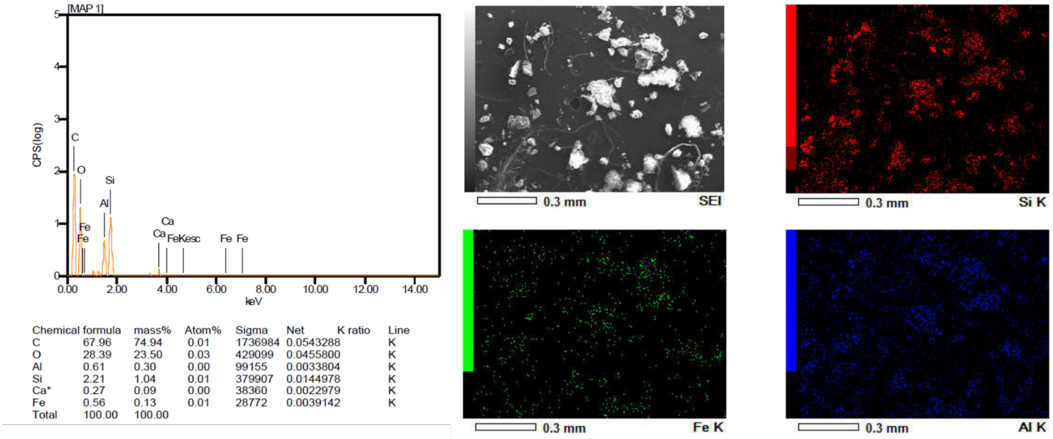

Figure A.8: Main elemental compositions of SPM in Meuse water based on EDS mapping (right, x100 magnification) and high-resolution images of the ion distributions of Fe, Al, and Si.

another 24 h. After that, the mixture of sand and ochre solution was oven dried at 70 °C overnight, washed with deionized water until the solution became colorless with an EC of < 10 μS/cm, and once more oven dried at 70 °C overnight.

The zeta potential of goethite as a function of pH in tap water and in filtered Meuse water (0.45-μm syringe glassfire filter) was determined by pH titration, respectively. Goethite was retrieved from the ochre solution after the oxidation process was complete. Before pH titration, goethite was washed repeatedly with deionized water by centrifugation until EC of the supernatant reached below 10 μS/cm, followed by oven drying at 70 °C overnight. In tap water and in river water, from pH 3 to pH 8 the zeta potential of goethite was found to be between -10 mV to -20 mV. This zeta potential of goethite as a function of pH was different from what was reported for pure goethite in the literature. This negative zeta potential of goethite was probably resulted from the adsorption of sulphate and carbonate to the surface of goethite (Rietra et al., 1999). Even though the goethite was washed multiple times with deionized water by centrifugation, it is known that anions such as sulphate and carbonate, which have a high affinity for the oxide surface, are difficult to remove from the surface of goethite completely (Schwertmann and Cornell, 2008).

A.13. Statistical analysis of data variations in Chapter 5

The significance of the standard deviations of the relative concentrations, σ_{C_R}, and its coefficient of variation, CV, varied across different channel bed and water types. When comparisons were made across four groups of bed types, in Tap water, CS had σ_{C_R} significantly higher than GCS and IP; however, in Meuse water, GCS had significantly larger CV than CS. Between Tap water and Meuse water in each bed type (referred to as pair-wise

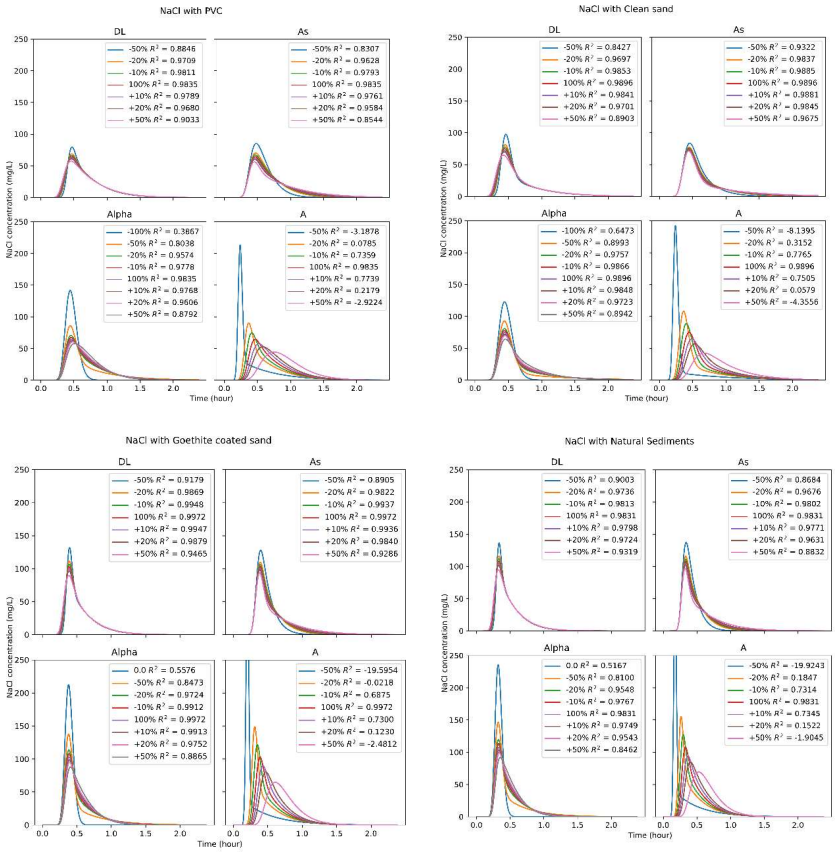

Figure A.9: Sensibility tests for four optimized transport parameters of the modeled NaCl BTCs. For each parameter, the initial best-fit curve was plotted in red (100%) and the resulting curve obtained from varying that parameter (increasing + or decreasing – of parameter value in %).

comparison), no significant difference was found with respect to σ_{C_R} and its CV ($p > 0.05$), except for CS, where σ_{C_R} and its CV were both significantly greater in Tap water than those in Meuse water (σ_{C_R}: $p \ll 0.01$; CV: $p = 0.013$).

Furthermore, for a closer inspection of the patterns of data variations, comparisons were made with respect to a modified version of σ_{C_R} in which those σ_{C_R} having CVs higher than 1 were removed. These σ_{C_R} were all associated with the very beginning and the very end of BTCs. During these periods, SiDNAFe concentrations were low, thus the stochastic effect was at the most for those data points. For pair-wise comparisons in each bed type, a similar result was found to what has been described earlier for the unmodified version of σ_{C_R}. However, for group-wise comparisons across different bed types, in Tap water, σ_{C_R} in CS appeared to be significantly higher than those in the other three bed types ($p \ll 0.01$), yet CV in IP was significantly higher than that in CS ($p < 0.05$). In Meuse water, four groups of channel bed types shared similar ranges of σ_{C_R}, but CV in GCS was significantly higher than that in IP ($p < 0.01$).

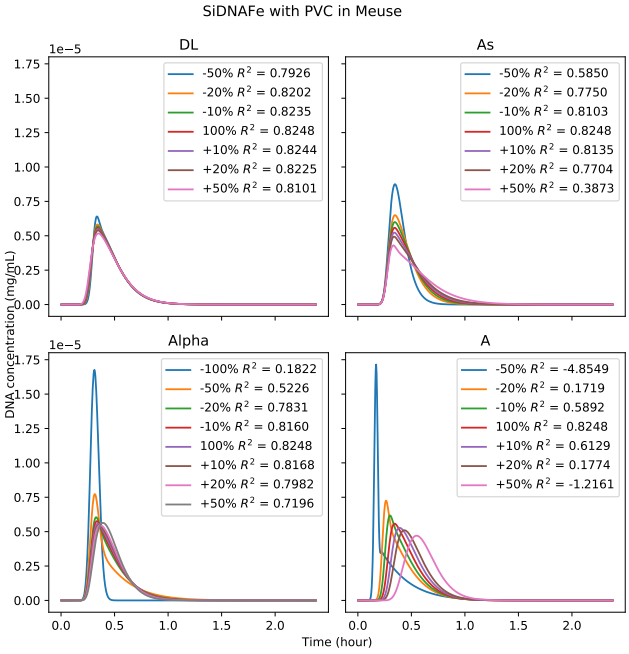

Figure A.10: Sensibility tests for four optimized transport parameters of the modeled SiDNAFe BTCs in IP in Meuse water.

A.14. Near-boundary Reynolds number and the ratio of the void scale to the permeability

Near-boundary shear Reynolds number Re_b can be calculated as:

$$Re_b = \frac{u_\tau \times k_s}{\nu} \tag{A.9}$$

Where u_τ is the shear velocity (m/s), k_s the roughness length (m), and ν the kinematic viscosity of water (m^2/s). When the slope is negligible, the shear velocity can also be approximated as:

$$u_\tau = \sqrt{ghs} = \sqrt{gR_hS} \tag{A.10}$$

where g is the gravitational acceleration of water (m/s^2), h the water depth (m), and S the slope of the channel. According to Clifford et al. (1992), the roughness length can be empirically calculated as:

$$k_s \approx 3.5 \times D_{84} \tag{A.11}$$

where D_{84} represents the grain diameter for the 84th percentiles of the grain size distribution (Fig. A.21). By calculating the near-boundary shear Reynolds number, the flow can be determined as a hydraulically smooth for Re_b <3 or hyraulically rough flow for Re_b > 100 (Nikaradse, 1933).

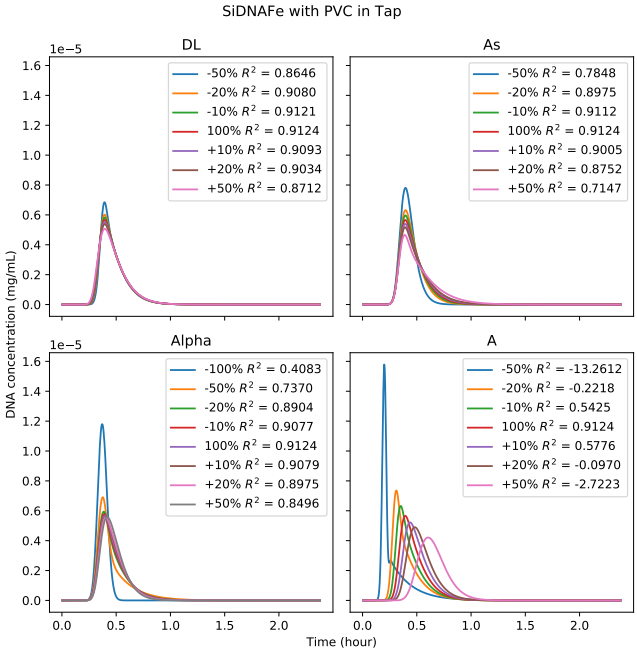

Figure A.11: Sensibility tests for four optimized transport parameters of the modeled SiDNAFe BTCs in IP in Tap water.

For sediment bed, the void scale (B) describes the average pore size, approximated using a geometric relationship by Nagaoka and Ohgaki (1990):

$$B = \frac{2\phi^2}{3(1-\phi)} D_{10} \tag{A.12}$$

Where ϕ the porosity, D_{10} the grain size corresponding to 10% by weight passing (Fig.A.21), also referred to as the effective size (mm).

Carman-Kozeny equation for permeability (cm/s), originally proposed by Kozeny (1927) and modified by Carman (1937) & Carman (1956) (see Carrier III (2003)):

$$K = \frac{\phi^3}{180 \times (1-\phi)^2} \times d_{10}^2 \tag{A.13}$$

To demonstrate the potential application of SiDNAFe in river injection experiments, a hypothetical calculation was performed using a scenario from the injection experiment conducted by Foppen et al. (2011) in the Merkske river. The details of the model parameters and DNA mass required for the tracing experiment were presented in Table A.11. The dispersion coefficient was assumed to be the same as that of NaCl, while a steady and uniform flow was considered. The first-order decay coefficient was assumed to be the same as the gravitational settling rate stated in Chapter 3. To achieve accurate DNA quantification, a minimal range of DNA concentrations should be attained in the collected water samples, without any up-concentration. As mentioned in Chapter 2, a DNA concentration of 1.0×10^{-5}

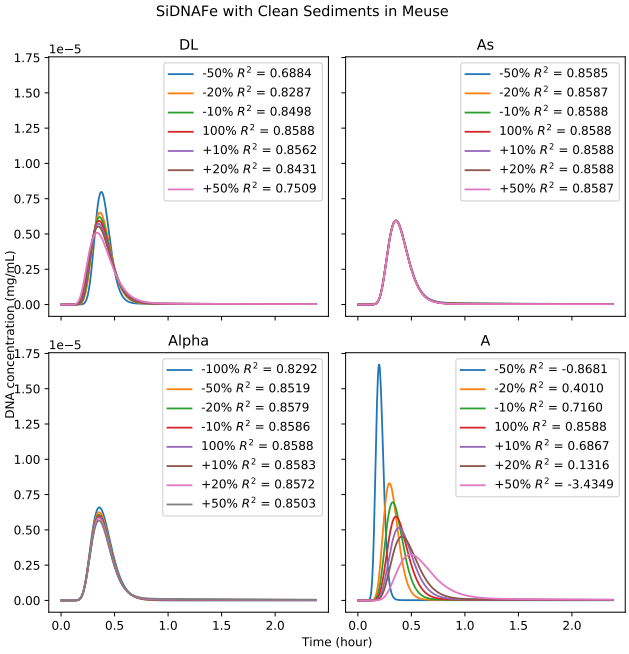

Figure A.12: Sensibility tests for optimized transport parameters of the modeled SiDNAFe BTCs in CS in Meuse water.

mg/mL was considered to be the lower limit for an accurate measurement of the BTC peak. Assuming the sampling location to be 1000 m downstream from the injection point, the minimal SiDNAFe tracer required was ~ 4 g.

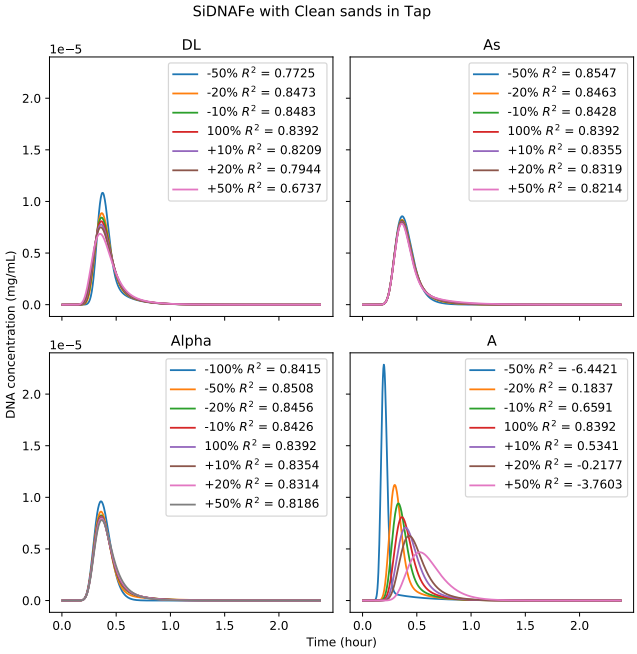

Figure A.13: Sensibility tests for optimized transport parameters of the modeled SiDNAFe BTCs in CS in Tap water.

Table A.4: The estimated ionic strength, average of $\zeta_{\text{Si-DNA}}$, and calculated DLVO interaction parameters in the indicated solution chemistry.

Water type	Ionic Strength (mM)	Zeta potential (SiDNA)(mV)	Energy barrier height (kT)[1]	Secondary minimum depth (kT)
Demi Water	0	-30	50	0
$CaCl_2$ solution	5	-21	21	0
Phosphate solution	25.85	-50	183	-2
Tap water (1^{st} & 2^{nd} exp)	6.39	-24	30	-1
Tap water (3^{rd} exp)	6.39	-18	10	-1.2
Filtered natural (1^{st} & 2^{nd} exp)	9.48	-18.8	9.8	-1.6

[1] The DLVO calculation was based on Abbott & Holmes, 2013, and a Harmaker constant of 0.6 *10^{-20} J for SiO_2 (quartz) was used for calculation (Bergstrom, 1997).

A

Table A.5: Energy barriers of SiDNAFe microparticles in 3 river waters.

	Unit	Meuse	Strijbeek	Merkske	MQ
SiDNAFe ζ	mV	-22.7±3.3	-22.6±3.3	-22.6±3.1	-24.2±3.8
Ionic Strength	mM	5.2	6.9	7.7	-
Energy barrier	k_BT	18.7	16.1	15.4	35.5
Second minimum depth	k_BT	-0.62	-0.65	-0.7	-
Na^+	mg/L	18.3	21.7	23.8	-
K^+	mg/L	4.4	14.8	16.6	-
Ca^{2+}	mg/L	5.8	48.2	60.4	-
Mg^{2+}	mg/L	5.1	11.0	10.2	-
Cl^-	mg/L	24.1	33.3	39.1	-
NO_3^-	mg/L	22.2	69.5	54.4	-
PO_4^{3-}	mg/L	1.2	n.a.	n.a.	-
SO_4^{2-}	mg/L	28.3	74.4	77.6	-

Table A.6: Radius of the measured and fitted PSD and the associated R square of the simulated settling curve.

Radius [nm]	% of the mass distribution		R^2
	50% ≤	90% ≤	
Lumisizer measured	101	615	
Fitted	338	1008	0.996

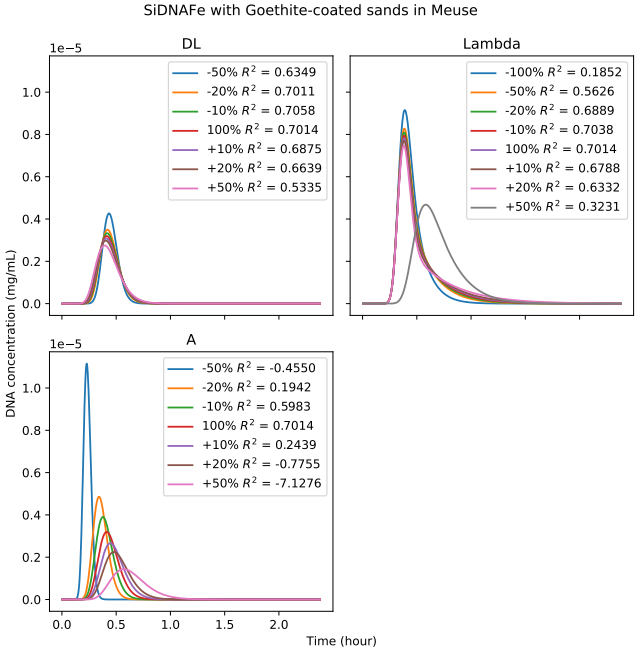

Figure A.14: Sensibility tests for optimized transport parameters of the modeled SiDNAFe BTCs in GCS in Meuse water.

Table A.7: (a). Settling rates of SiDNAFe microparticles during different time periods in all water types. (b) Error bars of the setting data in all water types.

(a)	Settling rate [-/hr] *10^{-2}									
Time period [hr]	MQ	F0.45 Mk	F1.2 Mk	UF Mk	F0.45 Mu	F1.2 Mu	UF Mu	F0.45 Strij	F1.2 Strij	UF Strij
0 – 2	21.28	6.52	17.64	29.82	11.60	3.34	8.96	21.81	9.01	0.81
2 – 4	4.84	12.72	2.12	2.08	16.71	12.70	18.88	4.28	11.95	20.79
4 – 6	7.89	4.15	2.02	1.19	3.33	4.87	1.34	8.53	4.11	3.54
Stage 1 (0 – 6)	8.11	7.80	7.26	8.85	8.32	6.97	9.73	8.69	8.35	5.48
6 – 21	1.64	0.47	1.40	1.08	1.55	1.43	1.08	1.51	1.86	1.67
21 – 24	5.04	0.13	0.50	0.45	2.78	0.91	1.17	1.30	3.04	4.05
24 – 30	2.34	1.73	1.18	0.47	0.25	0.29	0.40	0.10	0.12	2.96
Stage 2 (6 – 30)	0.98	0.74	0.64	0.50	0.87	0.96	0.52	0.88	1.02	2.20

(b)	Error bar [-] *10^{-2}									
Time [hr]	MQ	F0.45 Mk	F1.2 Mk	UF Mk	F0.45 Mu	F1.2 Mu	UF Mu	F0.45 Strij	F1.2 Strij	UF Strij
2	13.99	1.29	4.13	4.25	33.72	42.08	4.17	25.80	11.94	37.99
4	35.52	7.12	1.86	6.26	4.71	0.69	1.76	30.23	1.58	1.78
6	8.98	4.88	11.05	12.67	8.27	5.14	5.37	25.29	2.19	5.53
21	12.32	8.09	5.77	5.73	6.97	0.75	12.15	5.68	2.11	15.50
24	3.66	4.18	4.44	3.94	15.47	4.98	1.16	8.06	8.12	3.66
30	0.84	2.85	4.85	1.74	13.33	4.47	6.59	8.91	6.47	20.42

Table A.8: Calculated empirical parameters of the sediment properties using empirical equations.

	FS	CS/GCS	Equation
Re_b	0.023	0.158	Eq. A.9
B	4.33E-05	3.00E-04	Eq. A.12
K	4.70E-11	2.45E-09	Eq: A.13
$K^{0.5}/B$	0.16	0.16	Eq: A.12 & A.13

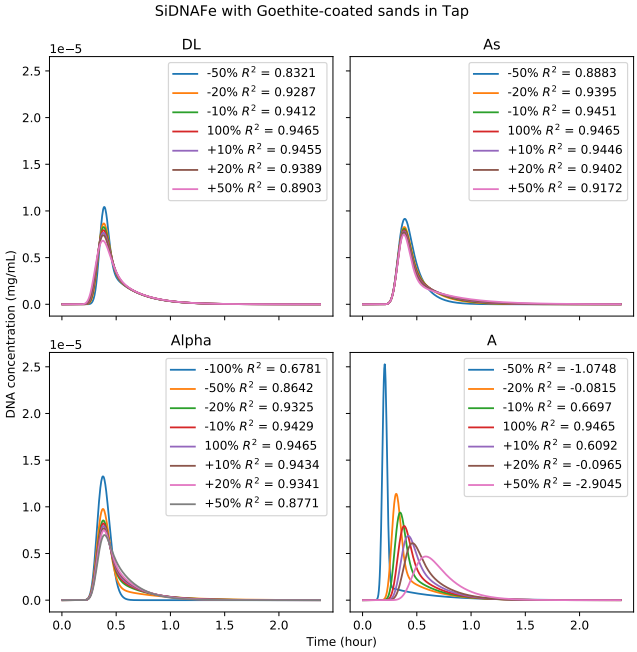

Figure A.15: Sensibility tests for optimized transport parameters of the modeled SiDNAFe BTCs in GCS in Tap water.

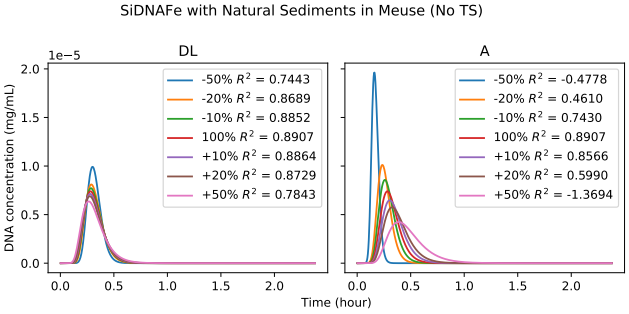

Figure A.16: Sensibility tests for optimized transport parameters of the modeled SiDNAFe BTCs in FS in Meuse water.

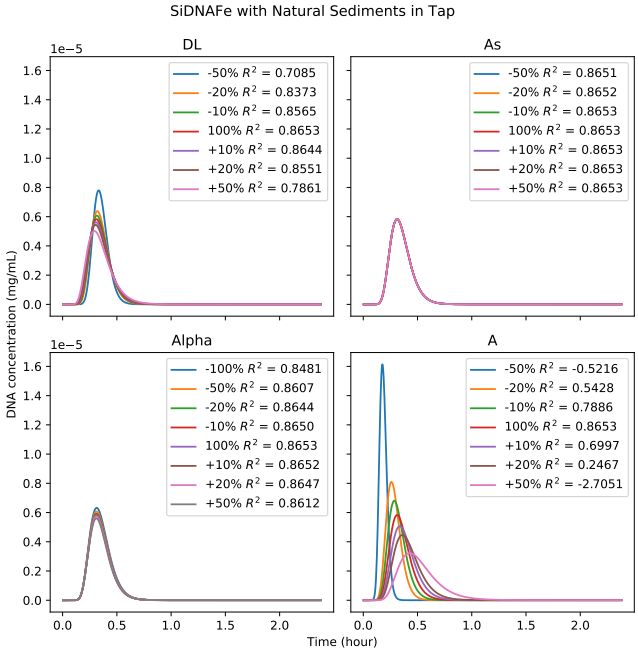

Figure A.17: Sensibility tests for optimized transport parameters of the modeled SiDNAFe BTCs in FS in Tap water.

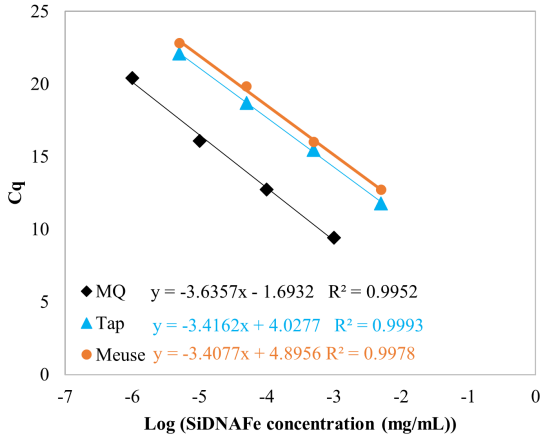

Figure A.18: 10-fold dilution curves of SiDNAFe and their linear regression equations and R^2. MQ in black represents that SiDNAFe was suspended in MQ water. Tap in blue and Meuse in orange denotes that SiDNAFe was originally suspended in Tap water and in Meuse water, respectively, and subsequently magnetic separated, up concentrated 5 times and finally dispersed in MQ.

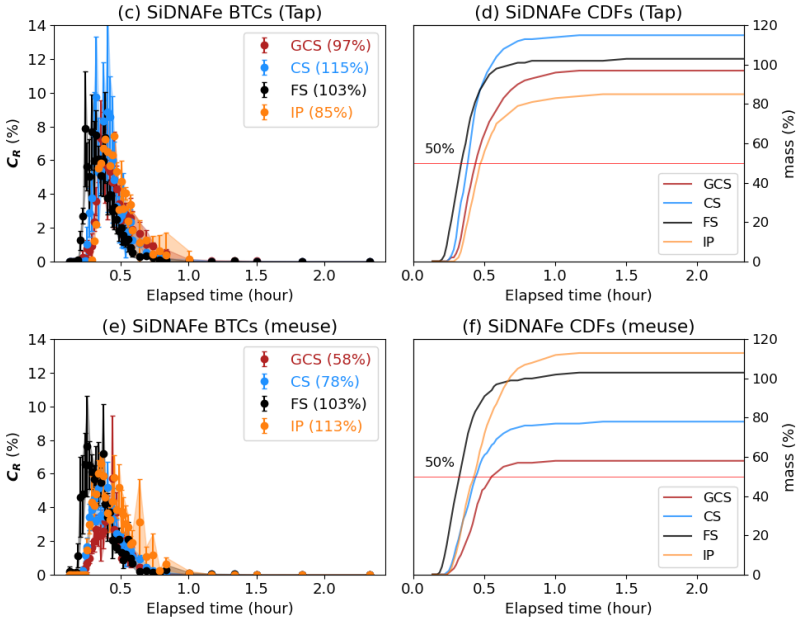

Figure A.19: BTCs of NaCl and SiDNAFe and their cumulative distribution function (CDFs) in open channel injection experiments with four types of channel bed: natural fine sediment (FS), goethite-coated coarse sand (GCS), coarse sand (CS), and an impermeable bed without sediment (IP). Mass recovery is shown in brackets.

Table A.9: The overview of parameters value estimation from OTIS simulation of SiDNAFe BTCs & NaCl BTCs.

Unit	**Mass recovery** (%)		D_L (m^2/s) $\times 10^{-5}$		(m^2) $\times 10^{-4}$		(m^2) $\times 10^{-4}$		α (s^{-1}) $\times 10^{-4}$		λ (s^{-1}) $\times 10^{-4}$		**R^2** (%)	
SiDNAFe	Tap	Meuse	Tap	Meuse	Tap	Meuse	Tap	Meuse	Tap	Meuse	Tap	Meuse	Tap	Meuse
FS	102 ± 18.5	103 ± 1.2	7.68 ± 1.7	7.97 ± 1.26	7.95 ± 0.36	7.38 ± 0.25							84.18	89.07
GCS	104 ± 19.1	58 ± 3.5	1.91 ± 0.44	3.38 ± 1.49	8.62 ± 0.31	10.28 ± 0.61	2.66 ± 0.73		5.65 ± 2.07			3.62 ± 1.35	94.65	82.94
CS	115 ± 12.3	78 ± 2.23	3.66 ± 0.89	5.56 ± 1.54	8.83 ± 0.32	9.19 ± 0.39						1.7 ± 0.95	84.8	85.15
IP	86 ± 5.8	113 ± 10.5	1.07 ± 0.47	1.57 ± 4.58	8.29 ± 0.55	6.91 ± 1.05	2.29 ± 0.52	3.85 ± 2.23	11.1 ± 2.23	19.91 ± 13.52			91.24	82.48
NaCl														
FS	95 ± 0.3		2.07 ± 0.43		7.27 ± 0.23		3.71 ± 0.33		10.8 ± 2.01		-		98.31	
GCS	92 ± 1.1		1.51 ± 0.13		8.64 ± 0.1		3.89 ± 0.15		8.25 ± 0.69		-		99.72	
CS	96 ± 0.2		2.63 ± 0.35		10.64 ± 0.3		5.25 ± 0.75		4.32 ± 1		-		98.96	
IP	99 ± 1		2 ± 0.49		10.42 ± 0.61		5.38 ± 0.55		8.49 ± 2.68		-		98.35	

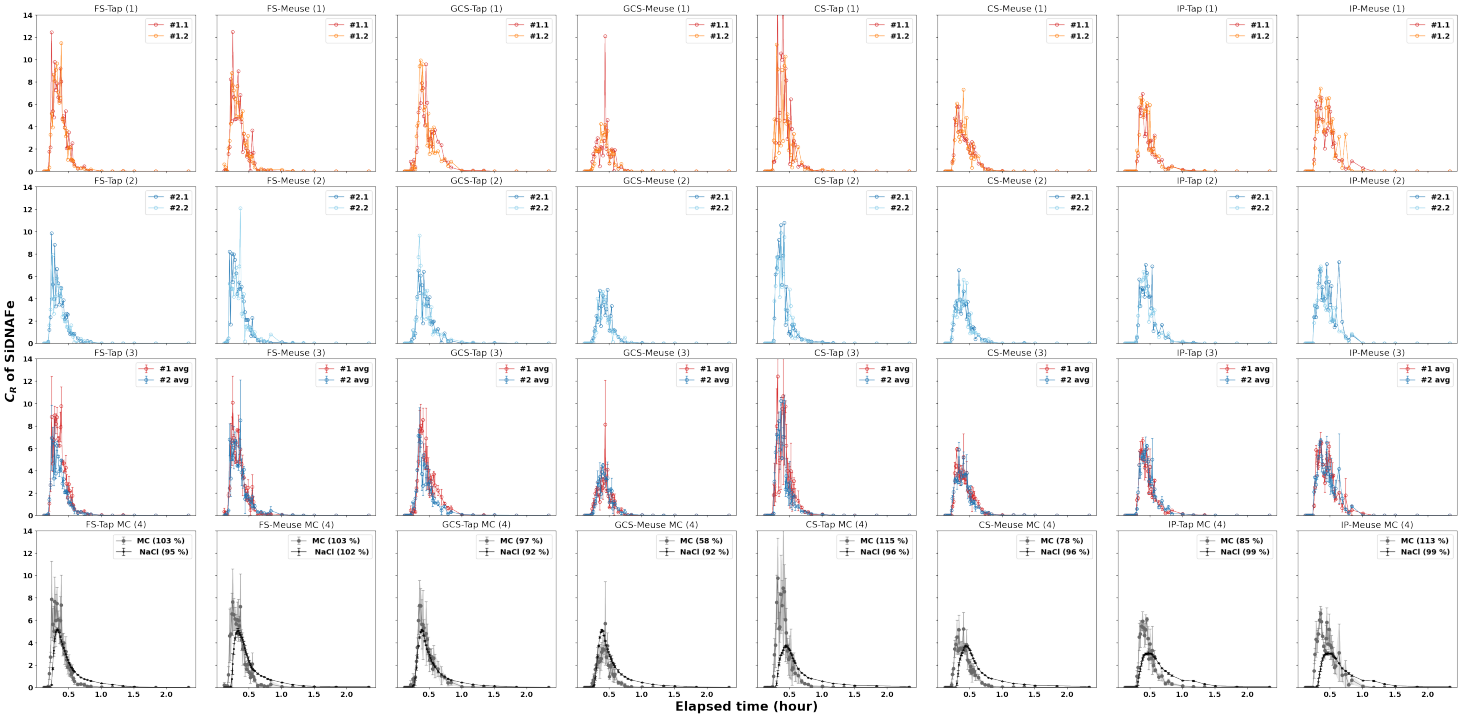

Figure A.20: Master curves (MC) of SiDNAFe BTCs based on 4 single BTCs in 4 types of channel beds with 2 water types. (1)"1.1" and "1.2" in the are two measurements in 1 channel, and (2) the same applies for 2 channel; (3) "1 avg" and "2 avg" represent the averaged BTCs from 1.1 & 1.2 in (1) and 2.1 & 2.2 in (2), respectively; (4) Master curves (MC) of SiDNAFe in comparison with NaCl BTCs.

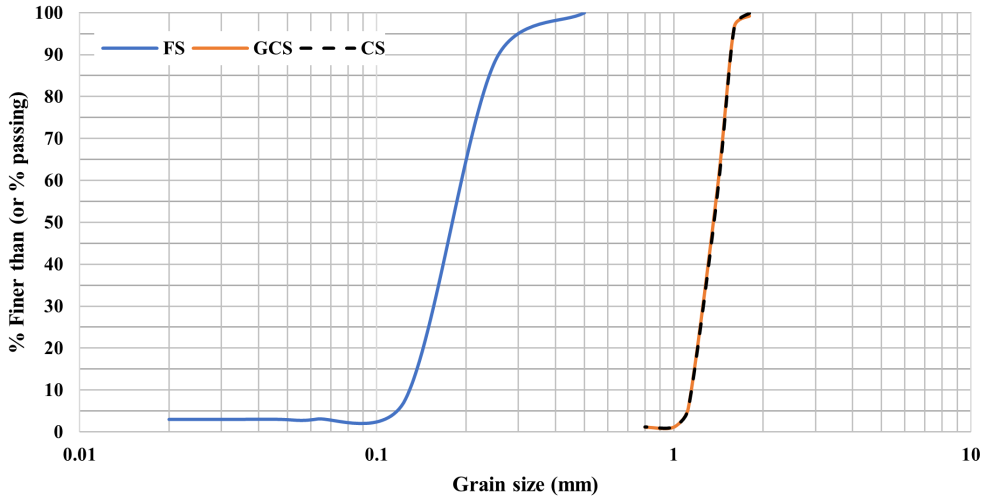

Figure A.21: Grain size distribution curves for FS, GCS, and CS.

Table A.10: Time outline for the sequence of NaCl and SiDNAFe injection experiments in CS, GCS, and FS series.

Time

Step	Action	series
1	Wash the coarse sand (CS) following the sand-washing protocol.	CS series
2	Homoginize the sand before aliquot it into 4 portions.	
3	Take 2 portions and for each channel place 1 portion form a evenly distributed flat bed layer of ~3 mm in the channel.	
4	Fill the channel **#1** and **#2** with Tap water using two calibrated perstaltic pumps.	
5	Turn on the pre-calibrated mixing rotors for both Channel **#1** and **#2**, and monitor the the water flow unitl a steady flow was formed.	
6	Perform NaCl injection experiments in Channel **#1** and **#2** parallely.	
7	Maintain the flow in both channels until the background EC of outflowing water matches the input Tap water.	
8	Perform SiDNAFe injection experimens in Tap water in Channel **#1** and **#2** parallelly.	
9	Drain both the channel and take samples from the darinage water.	
10	Wash the sand with Demi and take samples from the washing fluent for any detained SiDNAFe.	
11	Coat all the coarse sand with Goethite following the Goethite-coating protocol and get GCS.	GCS series
12	Repeat Step 2 to Step 11.	
13	Sample Merkske river sediment (FS).	FS series
14	Characterise FS.	
15	Repeat Step 2 to Step 11 (skipping Step 10).	

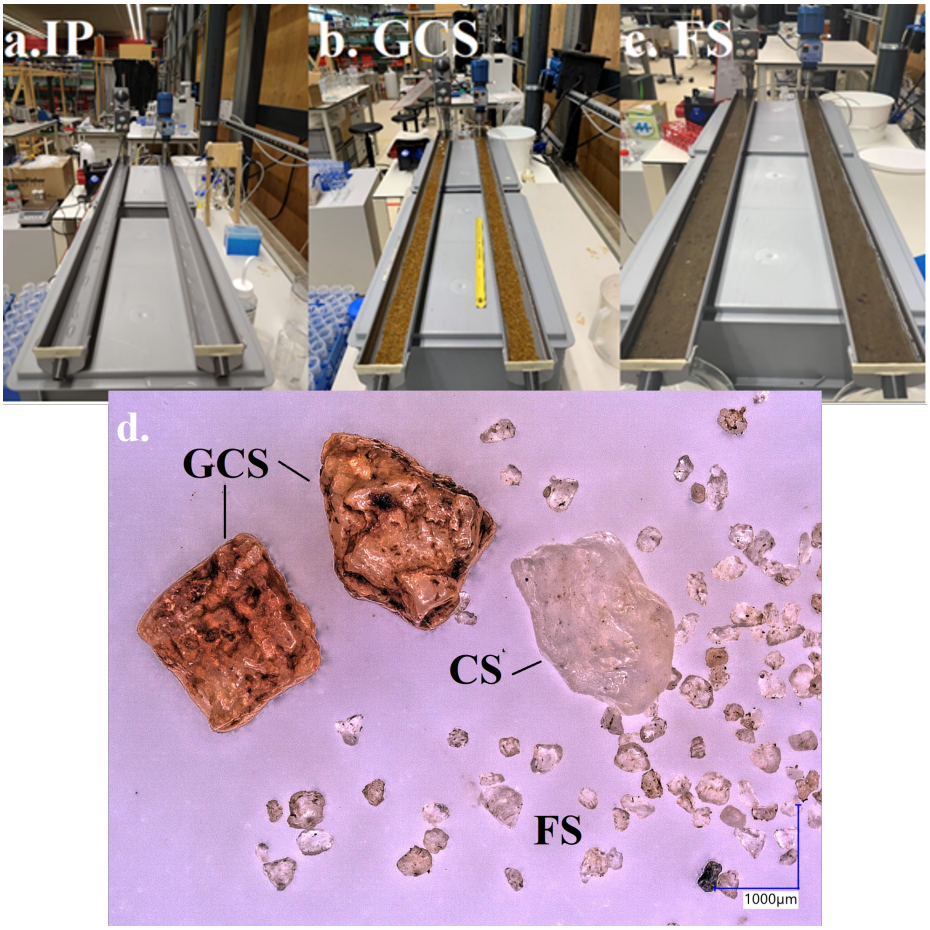

Figure A.22: Experimental photos for the (a) IP, (b) GCS, (c) FS and (d) comparison of three types of bed sediment using a digital microscope (x55 magnification).

Table A.11: OTIS modelling parameters for the case study using the Merkske river injection experiment recorded by Foppen et al. (2011).

Parameters	**Values**
Q [m^3/s]	0.16
A [m^2]	1.02
D_L [m^2/s]	1.5
λ [s^{-1}]	1e-05 [gravitational] – 4e-04 (with sediment)
SiDNAFe mass required	4 - 40

Curriculum Vitæ

Yuchen Tang

07-01-1993	Born in Panzhihua, China.

Education

2011–2015	Bachelor of Science in Environmental Science Beijing Normal University, Beijing, China
2015–2017	Master of Science in Water Environment and Management University of Bristol, Bristol, The United Kingdom
2023	PhD. in Water Management Faculty of Civil Engineering and Geosciences Delft University of Technology, Delft, The Netherlands

Awards

2019	Best Oral Presentation Award Ph.D. Symposium "Innovations for Sustainability"
2017	Excellent Dissertation Award Department of Environmental Science, Beijing Normal University

List of Publications

5. **Tang, Y., van Rhijn, F., Abdelrady, A., Foppen, J. W., & Bogaard, T.**, *Effect of channel bed sediment on the transport behaviour of superparamagnetic silica encapsulated DNA microparticles in open channel injection experiments.*, Hydrological Processes **37(9)**, e14962(2023).

4. **Tang, Y., Zhang, F., Bogaard, T., Chassagne, C., Ali, Z., Bandyopadhyay, S., & Foppen, J. W.**, *Settling of superparamagnetic silica encapsulated DNA microparticles in river water.*, Hydrological Processes **37(1)**, e14801(2023).

3. **Tang, Y., Foppen, J. W., & Bogaard, T. A.** , *Transport of silica encapsulated DNA microparticles in controlled instantaneous injection open channel experiments.*, Journal of Contaminant Hydrology **242**, 103880(2021).

2. **Zhu, B., Xia, X., Zhang, S., & Tang, Y.** , *Attenuation of bacterial cytotoxicity of carbon nanotubes by riverine suspended solids in water.*, Environmental pollution **234**, 581-589(2018).

1. **Liu, G., Yang, Z., Tang, Y., & Ulgiati, S.**, *Spatial correlation model of economy-energy-pollution interactions: The role of river water as a link between production sites and urban areas.*, Renewable and Sustainable Energy Reviews **69**, 1018-1028(2017).

Glossary

A the cross-sectional area in the main channel [m^2] in OTIS model. 33, 62, 66, 68, 69, 71, 72

A_S the cross-sectional area in the storage zone [m^2] in OTIS model. 33, 62, 66, 68, 69, 71

C the mass concentration in the main channel [g/m^3] in OTIS model. 7, 33, 62

C_R the relative concentrations of tracers C/C_0. 67, 73

C_S the mass concentration in the storage zone [g/m^3] in OTIS model. 33, 62

D_L hydrodynamic longitudinal dispersion coefficient [m^2/s]. 7, 11, 30, 32, 33, 36–39, 62, 66, 68, 70, 72, 76

D_{84} represents the grain size for the 84^{th} percentiles of the grain size distribution. 59

D_{hDLS} the hydrodynamic diameter of the microparticle measured by using dynamic light scattering (DLS). 31, 33–35, 43, 50, 52, 55, 59, 62

Fr the Froude number. 60

Q the volumetric flow rate. 33, 62

R_h the hydraulic radius of the channel. 60

Re the flume Reynolds number. 60

α the storage zone exchange coefficient [1/s] in OTIS model. 11, 33, 36–38, 62, 66, 68–70, 72, 76

λ the first-order decay coefficient in the main channel in OTIS model. 62, 69

ν the kinematic viscosity of water. 60

σ the standard deviation. 72, 73

ζ zeta potential. 31, 35, 36, 43, 47, 48, 52, 53, 59, 62

k_s the roughness of the channel bed. 59

u the mean flume velocity. 7, 60

ADE advection-dispersion equation. 7, 37

ANOVA stands for Analysis of Variance, is a statistical test used to analyse the difference between the means of more than two groups. 25, 26, 33, 61

BOE buffered oxide etch solution. 15, 45, 63

BTC breakthrough curve, the concentration-time history of the tracer at one or more downstream sites in a tracer test. 6, 7, 11, 16, 30–33, 35, 37–39, 61, 62, 64, 66, 68, 70, 72–74, 76, 77

cdf Volume-weighted cumulative size distribution function. 51

Cq quantification cycle, Cq, is the cycle number at which the fluorescence first rises above the threshold level in a qPCR assay. 16, 17, 55, 63

CS a clean coarse sand bed in Chapter 5. 59, 60, 62–64, 66–68, 70–72, 74

CV the coefficient of variation. 72, 73

DaI Damkohler number. 38

Demi demineralized water. 18, 19, 22, 32, 33, 35, 39, 46, 59, 61

DLS dynamic light scattering, is a technique for measuring the size and size distribution of molecules and particles in the submicron region. 31, 36, 43, 44, 46, 59

DLVO DLVO theory, named after Boris Derjaguin and Lev Landau, Evert Verwey and Theodoor Overbeek, is a theory describing colloidal stability in aqueous dispersions. 35, 42

DOC dissolved organic carbon. 32, 33, 44, 48, 60, 71

dsDNA double-stranded DNA molecules. 8, 9, 15, 63

EC electrical conductivity, is a measure of the ability of the material (here referred to water samples) to conduct an electrical current (microsiemens per centimeter). 33, 44, 59–61

ENP referred to engineered nano/micro particles. 42, 43, 77, 79, 80

EPS exopolymeric substances, are natural polymers of high molecular weight secreted by microorganisms into the environment. 42, 43, 81

FS a natural fine sediment bed in Chapter 5. 59, 60, 62–64, 66–68, 70, 72, 74

GCS a goethite-coated coarse sand bed in Chapter 5. 59, 60, 62–64, 66–68, 70–72, 74

hetero-aggregation hetero-aggregation is an aggregation process between particles of different types (chemistry, size, shape, surface properties). 10, 42, 43, 53, 55, 76

homo-aggregation homo-aggregation is an aggregation process of particles of the same nature. 42, 44, 50, 55

ICP-MS PlasmaQuant MS Inductively Coupled Plasma Mass Spectrometry. 44, 59

IP an impermeable channel bed without sediment in Chapter 5. 59, 63, 64, 66–68, 72, 74

Merk referred to river water samples collected from river Merkske (51°24'57.1"N, 4°50'48.5"E) on the Netherlands-Belgium border. 25, 26

Meuse referred to river water samples collected from river Meuse at Keizersveer, the Netherlands (51°43'05.7"N, 4°53'27.5"E). 25, 26

MP microparticles. 42

MQ water purified using a Millipore Milli-Q lab water system. 11, 16, 23, 25, 26, 43–48, 50–53, 55, 62, 63, 73, 76

NOM natural organic matter. 10, 35, 38, 42, 44, 60, 81

OTIS a 1-D advection-dispersion model with one transient storage zone, developed by Runkel, 1998. 11, 32, 33, 37, 38, 61, 62, 67, 72, 76

PCR polymerase chain reaction . 14

PDI polydispersivity index. 33, 34, 43, 50, 52, 55

PSD particle size distribution. 43, 47, 48, 50, 51, 81

qPCR quantitative polymerase chain reaction and is a technology used for measuring DNA using PCR. 8, 9, 11, 14–16, 19, 22, 43–45, 54, 55, 61–63, 73, 76, 79, 80

RCF the relative centrifuge force, is the force acting on samples during centrifugation. It is expressed as multiples of the earth's gravitational field (g). 17–22

Si-DNA a non-magnetic silica-encapsulated DNA-tagged microparticle with a silica core used in this dissertation, referred to as Si-DNA. 11, 14, 15, 17, 18, 20–24, 30–39, 50, 76

SiDNA(Fe) Collectively, Si-DNA and SiDNAFe were referred to as SiDNA(Fe) throughout this dissertation. vii, 11, 14–17, 76–81

SiDNAFe a superparamagnetic silica-encapsulated DNA-tagged microparticle with an iron oxide core, referred to as SiDNAFe. 11, 14, 15, 23, 25–27, 42–46, 48–55, 58, 59, 61–64, 66–74, 76–80

SPM suspended particulate matter. 42–44, 47, 48, 51, 53, 71

ssDNA single-stranded DNA molecules. 8, 9

Strij referred to river water samples collected from river Strijbeek Beek (51°29'58.3"N, 4°47'01.7"E) on the Netherlands-Belgium border. 25, 26

TSM transient storage model. 7

TSS total suspended solids. 33, 44, 48, 60, 71

Z-Ave Z-Ave is the intensity weighted mean hydrodynamic size of the ensemble collection of particles measured by dynamic light scattering. 43, 50, 52